Modeling, Stability Analysis, and Control of Distributed Generation in the Context of Microgrids

by

Ehsan Nasr-Azadani

A thesis
presented to the University of Waterloo
in fulfillment of the
thesis requirement for the degree of
Doctor of Philosophy
in
Electrical and Computer Engineering

Waterloo, Ontario, Canada, 2014

I hereby declare that I am the sole author of this thesis. This is a true copy of the thesis, including any required final revisions, as accepted by my examiners.

I understand that my thesis may be made electronically available to the public.

Abstract

One of the consequences of competitive electricity markets and international commitments to green energy is the fast development and increase in the amount of distributed generation (DG) in distribution grids. These DGs are resulting in a change in the nature of distribution systems from being "passive", containing only loads, to "active", including loads and DGs. This will affect the dynamic behavior of both transmission and distribution systems. There are many technical aspects and challenges of DGs that have to be properly understood and addressed. One of them is the need for adequate static and dynamic models for DG units, particularly under unbalanced conditions, to perform proper studies of distribution systems with DGs (e.g., microgrids).

The primary objective of this thesis is the development and implementation of dynamic and static models of various DG technologies for stability analysis. These models allow studying systems with DGs both in the long- and short-term; thus, differential and algebraic equations of various DGs are formulated and discussed in order to integrate these models into existing power system analysis software tools. The presented and discussed models are generally based on dynamic models of different DGs for stability studies considering the dynamics of the primary governor, generators, and their interfaces and controls.

A new comprehensive investigation is also presented of the effects of system unbalance on the stability of distribution grids with DG units based on synchronous generator (SG) and doubly-fed induction generator (DFIG) at different loading levels. Detailed steady-state and dynamic analyses of the system are performed. Based on voltage and angle stability studies, it is demonstrated that load unbalance can significantly affect the distribution system dynamic performance. Novel, simple, and effective control strategies based on an Unbalanced Voltage Stabilizer (UVS) are also proposed to improve the system control and the stability of unbalanced distribution systems with SG- and DFIG-based DGs.

Acknowledgements

I would like to express my sincere gratitude to Professor Claudio A. Cañizares for his guidance, patience, and support throughout my Ph.D studies. His contribution to my life is simply priceless. I also offer special thanks to Professor Kankar Bhattacharya for all his guidance and motivation.

I would like to acknowledge the following members of my comprehensive or examination committees for their valuable comments and input: Professor Mehrdad Kazerani from the Electrical and Computer Engineering Department at the University of Waterloo; Professor Michael Fowler from the Chemical Engineering Department at the University of Waterloo; and Professor Reza Iravani from the Electrical and Computer Engineering Department at the University of Toronto.

I wish to acknowledge ABB Corporate Research USA , MITACS Canada, and the NSERC Strategic Network on Smart Microgrids (NSMG-Net) for providing the funding necessary to carry out this research.

I will always be grateful for the love and support of my family and friends through the happy and sad moments of my life. Special thanks to Behnam Tamimi, Saman Nasirahmadi, and Keyvan Kasiri for being great friends for all great moments during these years. I also acknowledge my officemates for their friendship in the EMSOL lab: Mehrdad Pirnia, Amir Mosaddegh, Mostafa Farrokhabadi, Mohammad Chehreghani, Amirhossein Hajimiragha, Sumit Paudyal, Felipe Ramos, Edris Pouresmaeil, Daniel Olivares, Juan Carlos Munoz, Isha Sharma, Indrajit Das, Nafeesa Mehboob, Jose Daniel Lara, Mariano Arriago, Mauricio Restrepo, and Professor Alfredo Vaccaro. It was such a pleasure to learn many things from them. My warm thanks also extends to my friends: Bahador Bigrari, Amir Ostadi, Hadi Zarkoob, Sasan Asiaee, Saeed Movahed, and Amirjalal Jalali.

I would like to thank my beloved mother, father, and brothers for their unconditional love and support through all these years. A very special word of thanks to my wife Azam for her understanding and endless love.

Finally, I would like to thank God, who is the source of all, for making this thesis possible.

Table of Contents

List of Tables

List of Figures

List of Acronyms

AFC Alkaline Fuel Cell

AVR Automatic Voltage Regulator

BESS Batteries Energy Storage System

CCT Critical Clearing Time

CIGRE Council on Large Electricity Systems

CPF Continuation Power Flow

CSC Current-Sourced Converter

DAE Differential Algebraic Equation

DBFC Demand Based Frequency Control

DFIG Doubly Fed Induction Generator

DFCR Demand Frequency Controlled Reserve

DG Distributed Generation

DLM Dynamic Loading Margin

DOC Depth-Of-Charge

DSTATCOM Distribution Static Synchronous COMpensator

ESS Energy Storage System

FC Fuel Cell

FVSI Fast Voltage Stability Index

LIB Limit-Induced Bifurcation

LPF Low Pass Filter

MCFC Molten Carbonate Fuel Cell

MG Microgrid

ML Maximum Loading

MT Micro Turbine

ODE Ordinary Differential Equation

OPF Optimal Power Flows

PAFC Phosphoric Acid Fuel Cell

PCC Point of Common Coupling

PEMFC Proton Exchange Membrane Fuel Cell

PF Power Factor

PFC Membrane Fuel Cell

PI Proportional-Integral

PQ constant active power P and constant reactive power Q

PV constant active power P and constant voltage V

PWM Pulse Width Modulation

PZ constant active power P and constant impedance Z

SG Synchronous Generator

SLM Static Loading Margin

SNB Saddle-Node Bifurcation

SOC State-Of-Charge

UVS Unbalanced Voltage Stabilizer

VSC Voltage-Sourced Converter

Chapter 1

Introduction

1.1 Research Motivation

In the coming decades, the demand for energy is expected to drastically increase leading to widespread environmental problems. In response to these issues, international movements are pushing for fossil fuels to be replaced with "green" energy sources. Furthermore, competitive electricity markets and international commitments to green energy (e.g., Kyoto Protocol) are motivating the rapid development of decentralized or distributed generation (DG). These DGs connected in distribution systems make these active rather than passive grids, which can affect the dynamics of the entire power system, especially the distribution grid.

Although DG-enhanced systems may be beneficial, numerous technical aspects and challenges still need to be properly understood and addressed. For example, there is a lack of suitable control strategies for networks with significant penetration of DG when interactions between the transmission and distribution systems are taken into consideration [1]. To address these issues, studies have to be carried out based on simulations, which require adequate static and dynamic models for DG units and related interfaces and controls. These models should satisfy certain criteria to allow investigating relevant system stability and control issues from both local and integrated system perspectives.

Among the numerous issues associated with distribution systems with DGs, stability analysis is of particular interest (e.g., [1, 2, 3]). Although some stability studies of distribution systems with DGs have been reported in the literature, a detailed and systematic analysis considering distribution systems under unbalanced conditions has not been adequately addressed. The majority of stability studies reported in the literature are based on

approaches similar to those used in transmission systems, and thus several simplifications, in particular the assumption of balanced conditions, are applied; however, distribution systems cannot be considered to be balanced three-phase systems, since these are inherently unbalanced in steady-state. A full characterization of unbalanced systems with DG in stability studies would allow for a better understanding of the system and DG dynamic behavior.

This thesis aims to model and investigate DGs from the perspective of stability and control, taking into account various DG technologies. Thus, comprehensive DG models and voltage, small-perturbation, and transient stability studies of balanced and unbalanced distribution system with DGs are presented in this work. Furthermore, control strategies based on simple and easy-to-implement voltage stabilizers are proposed to improve the stability of unbalanced distribution systems with DGs.

1.2 Literature Review

In this section, the relevant research papers on the impact of DGs on the stability and control of transmission and distribution systems are reviewed.

1.2.1 DG Stability and Control in Balanced Systems

Generally, the effects of DGs on voltage stability are related to the capability of the DG to provide reactive power. Accordingly, the behavior of the system in response to small or large disturbances may be different for induction generators, synchronous generators (SGs), and electronically interfaced distributed resources. Thus, in the case of induction generators, depending on the operating point of the generator, the voltage stability margin may decrease due to lack of reactive power support. On the other hand, if DGs are SG-based or controllable DG inverter-based (e.g., Fuel Cells or FCs), they can improve voltage stability. For example, small-disturbance stability studies of a distribution system with induction generations are investigated in [4], [5], and [6]. In these papers, models of these types of DGs are presented, and are used to show that the voltage stability margin based on P-V curves may decrease with induction generators. The impacts of an SG-based DG on steady-state voltage profiles, losses, and voltage stability of power systems with different levels of penetration are reported in [7], where it is shown that the utilization of SG-based DG improves voltage profiles and voltage stability margins, while decreasing active power losses in a power system; this study also addresses voltage stability in power systems with high penetration of DGs.

Other issues such as transformer impedances, voltage controllers, and control operations can affect voltage stability [8, 9, 10, 11]. The authors in [8] indicate that the size of a new SG connected to already existing low voltage networks may have to be limited in order to ensure correct voltage control; they also show that an opposite relationship exists between generator excitation voltage and controlled voltage when the transmission network is heavily loaded. However, this result is based on an assumption that there is no remedial action for voltage control. Multiple strategies by executing appropriate control operations (e.g., coordinated generator controls, load tap changers, and load shedding) are proposed in [9], [10], and [11]. These studies are aimed at providing a means of saving a distribution system from voltage collapse due to contingencies occurring in the transmission or distribution system. This work is based on digital signal processing technology for the determination of correct stability controls, as well as the application of modern computer networking technology for real-time monitoring of the distribution system operating states, data transmission, and stability control commands.

Other works in the literature address optimization methods for allocating and sizing DGs to improve voltage stability margin and voltage profiles. For example, the authors in [12], [13], and [14] use genetic algorithms for these purposes. In [15], the authors use the most sensitive buses for DG placement by using the P-V curves. In [16], a static model for a Proton Exchange Membrane Fuel Cell (PEMFC) DG system in power flow analysis is used; different DG placements are compared in terms of power loss, loadability, and a voltage stability index, and a Fast Voltage Stability Index (FVSI) and Line Stability Factor (LSF) for voltage stability contingency analysis are also presented. In [17], optimal allocation and sizing of DGs are formulated, using mix-integer non-linear programming, to improve the voltage stability margin. In [18], a modal analysis and continuation power flow (CPF) are used for determining DG placement candidates in a distribution system.

Other types of studies concentrate on the impacts of selected DGs on power system stability [2, 19, 20, 21]. Thus, the impacts of selected DG units, namely, FCs and micro turbines (MTs), on power system stability for various penetration levels are investigated in [2]. The voltage stability of the investigated network is tested by applying some disturbances in the network, and by analyzing the voltage response to the fault for constant load demand with different contributions from DGs; there is no static analysis of voltage stability margins in the long-term. The authors in [19] investigate the impacts of wind power plants on power system stability, while [20] looks into the effect of doubly-fed induction generators (DFIGs) on the transient behavior of distribution systems. In [21], the impacts of large-scale DGs on voltage stability are studied; the static voltage stability studies based on CPF show that the optimal allocation of DGs can improve system stability.

A variety of storage technologies are available that are capable of smoothing out fluc-

tuating power and voltage, such as superconducting magnetic energy storage, super capacitors, flywheels, compressed air energy storage, hydro-pumped storage, and battery energy storage systems (BESS) [22, 23, 24, 25]. The main issues with these technologies are cost, operation, and maintenance requirements. A successful experiment using a BESS within an existing wind farm to mitigate short-term fluctuation is reported in [26]. In [27], a controller for a BESS is proposed as an outer controller by assigning a current reference for the inverter. The goal of this study is to use the BESS to smooth the net power of a wind farm to be supplied to the system over a given time period; the authors employ this control scheme for the sizing of BESS. The authors in [28] offer a control strategy to manage the flow of power within a full converter wind turbine generator, a BESS, and the grid. Here, the BESS is used as a storage device in the dc link of a full converter wind turbine; however, since the cost of employing a small-scale BESS is relatively high, adopting a control strategy for optimal use of a BESS is an issue.

Generally, eigenvalue analysis provides a proper tool for investigating small-perturbation stability studies that have been widely used both in transmission and distribution systems [2, 29, 30]. Small-perturbation stability analysis based on critical eigenvalues for various penetration levels of selected DGs is investigated in [2]. It is assumed that the load demand is constant and the power system decreases both active and reactive powers with the increase of DG penetration. Also, the DGs are considered to make a constant contribution to the network and that their output powers do not change; this may not be correct, however, because of the presence of different DGs with various control technologies. Nonetheless, further penetration levels of DGs can improve the damping factor and thus increase angle stability. The impact of positive feedback anti-islanding methods on small-perturbation stability of grid-connected inverter-based DG is presented in [31]. Positive-feedback schemes always attempt to destabilize generators; thus, if the positive-feedback gain is too high, the distribution system may become unstable, even when it is connected to the main source. The authors in [32] show that high penetration of selected DGs will not be feasible if the installed DGs are too closed to each other, since this may lead to signal and frequency instabilities. Hence, an optimal location of DGs in view of small-perturbation stability is proposed.

Custom power devices have been adopted to improve power quality and system reliability. Thus, a stability study of the influence of induction and synchronous generators and distribution static synchronous compensator (DSTATCOM) devices on the dynamic behavior of small distribution systems is presented in [33]. This paper shows that the stability performance of induction generators can be significantly improved by a DSTATCOM voltage controller, and a DSTATCOM power factor controller may adversely affect the stability performance of SGs. The installation of an induction generator combined with

a DSTATCOM voltage controller is proposed for distribution systems in this paper as an alternative for SGs; however, economic and technical issues pose a challenge in this case.

In [34] and [35], the impacts of induction generators on transient stability are studied, and [1] addresses the impact of DG penetration levels on transmission systems transient stability. In the latter, an increase in DG penetration level is matched by a reduction in centralized power generation, which consequently results in a reduction in a total amount of rotating mass and reactive power support in the system. In some cases, it is shown that high penetration of DGs (e.g., more than 50%) leads to transient instability. Several solutions are proposed to mitigate this problem, such as rescheduling centralized generators and optimizing power flows. The impact of large-scale DG penetration on the transient stability of transmission systems with different control strategies for a portion of the grid serving Eastern Ontario in Canada is investigated in [36]. Different scenarios for contingencies in the transmission side and the DG side are studied using time-domain simulations. The DG technologies modeled and used in this report are limited to inverter-based DGs and SGs. A hybrid method for fast transient stability assessment based on transient energy functions is presented in [37].

Not many publications analyze transient stability of distribution systems with DGs. A brief study on the transient stability analysis of a distribution system with wind generators, MTs, and combined heat and power (CHP) plants is presented in [38], based on critical clearing time (CCT) calculations. Small-perturbation stability modeling of an SG as a direct-connected DG, and the dynamics of the voltage-sourced converter (VSC) as an indirect-connected DG in a distribution system is presented in [39]. Small-signal behavior of an n-DG chain microgrid (MG) is studied in [40], and sufficient conditions are proposed to guarantee their small-perturbation stability; however, in a real distribution system with DGs, the system tends to be more complex than an n-DG chain MG. The main contribution presented in [41] is a reduced model for distribution systems with selected DGs, and an investigation of small-perturbation and transient stability on these systems; techniques are used for the reduction of the distribution system order (e.g., balanced truncation, Hankel norm approximation, and Krylov); although these techniques are useful tools for reducing computational time, using the full dynamic model of DGs in the context of relatively small size distribution systems is not an issue in most practical studies.

High penetration levels of DGs can affect frequency stability in both transmission and distribution systems. Most of the published research only takes into account selected DGs for these types of studies. Thus, the author in [2] shows that a high penetration of selected DGs (i.e., FCs and MTs) leads to increased frequency deviation. In [42], a reciprocating engine-generator set model is developed, and the small-perturbation and frequency stability of these generators are investigated and validated by experimental testing. An example of

DG impact on frequency stability in a distribution system in Bornholm Island, Denmark, where there is a high penetration of wind power (i.e., 32.4% of its demand) is discussed in [43]. Thus, on December 22, 2005, this distribution system was forced to be islanded for 51 days due to the breakdown of the high voltage sea cable interconnection to the transmission system; local power units were not able to regulate generation fast enough to mitigate the frequency fluctuations caused by the wind turbines. To improve frequency control, different technologies, such as load shedding, droop control among power plants, wind turbine frequency control, and demand frequency controlled reserve are proposed in [43] and [44]. A control mechanism that can improve frequency control for intentional islanding transition is also proposed in [45]. Another method to control frequency is Demand-Based Frequency Control (DBFC), which shifts load by turning off/on the machine in response to frequency deviations [46]; since some devices, such as heating and cooling systems, refrigeration units and industrial melt pots, rely upon energy rather than power consumption, they are considered as potential candidates for DBFC.

MGs which are viewed as subsystems of "small" generators and loads, present different challenges with respect to stability and control [47]. Two control approaches can be used to control MGs: a centralized control and a decentralized control [47, 48, 49, 50, 51]. Power-sharing for different DGs and regulation of voltage and frequency are the basic control objectives in an MG. Sharing active and reactive power in the centralized control of an MG relies on sharing control information among generators. In this technique, the terminal information of each generator and load are sent to the master control via a communication system. One of the major drawbacks of the centralized-based approach is reliability issues, since sending the primary control signals reduces the reliability of MGs, where the control information is critical for operation; furthermore, a master primary control could fail [50].

Fully decentralized-based control relies on a decentralized communication approach, in which DGs can share active and reactive powers and regulate voltage and frequency locally. Simple decentralized power sharing is introduced by frequency and voltage droop control, which follows the same concept for frequency droop control in conventional power systems with multiple generators [47]. In this paper, the controllers use real-time values for active and reactive powers, frequency, and the ac voltage to generate the desired signal at the DG terminals using droop concepts. This allows each DG to change its active power with respect to the frequency droop characteristic; hence, the frequency of the system is the communication signal for power sharing between multiple DGs. Similarly, a voltage droop plays the same role for sharing reactive power. Also, a simple frequency and voltage droop controller is proposed in [48] and [49] for active and reactive power sharing. To improve active and reactive power decoupling, power controllers with virtual impedances are proposed in [52] and [53]. In [50], an adaptive decentralized droop controller

is proposed to preserve the stability of multi-inverters; this controller is based on static droop characteristics combined with an adaptive transient droop function. This is proposed because power-sharing control implies low frequency dynamics of the inverter that can affect the small-signal response of the controller; hence, if the demand power of each inverter is changed, the low-frequency modes of the power-sharing dynamics will move to new locations, which will affect the stability of the system.

Similar to the conventional power system, the hierarchical control method can be applied to an MG with different levels of control [54]. These control levels differ in speed of response, time-frame of operation, and infrastructure requirements (e.g., need for communication) [55, 56]. In [55], the basic concept of the hierarchical control of an MG is introduced. In [56], secondary voltage controllers based on the potential function method are proposed in the context of centralized controllers. In all these papers, the dynamic behavior of prime movers is not taken into account, and only inverter-based MGs are considered.

1.2.2 DG Stability and Control in Unbalanced Systems

Although controls of inverter-based DGs under unbalanced conditions have been extensively studied (e.g., [57, 58, 59]), there are very few reported studies consider the characteristics of distribution systems with DGs in stability analyses while taking into account unbalanced conditions. In [60], a continuation three-phase power flow approach in polar coordinates is presented for voltage stability analysis under unbalanced conditions; this approach is based on static power flow equations of a three-phase model to obtain P-V curves. In [61], voltage stability studies are presented using a three-phase constrained optimal power flow that seeks to maximize the loading factor; since these studies are based on static power flows, the impact of system dynamics on voltage stability is not fully investigated.

Some recent studies examine the effect of unbalanced conditions on small-perturbation stability of SGs. Thus, in [62] and [63], effects of unbalanced conditions on damping factors and frequency are investigated. In [62], a model-based approach in the phasor domain for small-perturbation stability analysis of unbalanced distribution systems is presented, and a model identification technique for small-perturbation stability studies is presented in [63]. However, in these papers, the effects of unbalanced conditions under high loading levels, which would typically lead to instability, are not studied.

Simplified models of synchronous and induction machines have been developed for transient stability studies of unbalanced power systems [64, 65, 66, 67]; these models represent

the fundamental frequency component of machine behavior and neglect the harmonic components. However, the impact of load unbalancing on transient stability studies has not been extensively studied. For example, control and stability studies of DFIG have been discussed in the past for balanced operation [68, 69, 70, 71, 72]; however, if voltage unbalance is not appropriately compensated by system control, the stator current can be highly unbalanced, even with a small unbalanced stator voltage; in this case, the main problem is that high current, torque, and power oscillations appear at double the electrical frequency due to the negative sequence components, resulting in a disconnection [73, 74, 75]. Techniques have been proposed to mitigate these oscillations, based on the injection of negative sequence components, considering rotor-side [74] or grid-side converters [73, 75]. In [76], an approach based on a disturbance rejection controller is presented to compensate oscillations using a feed-forward component of the current controllers. In [77], a stand-alone DFIG under unbalanced conditions is studied, with the grid converter supplying reactive power to compensate the unbalanced grid voltage. A small-perturbation stability analysis of a DFIG wind turbine is presented in [78]. Nevertheless, the effects of unbalanced conditions under high loading levels, which would typically lead to instability, are not studied in any of these papers.

1.3 Research Objectives

Based on the aforementioned review of the current technical literature, the following are the main objectives of this thesis:

- Develop and implement adequate dynamic models of different types of DG technologies that are not overly complex to study the impacts of different DGs on the stability and control of balanced distribution systems in both short- and long-term.
- Investigate for the first time in a comprehensive manner, the influence on voltage, transient, and small-perturbation stability and control of different DG technologies in balanced distribution systems.
- Investigate the stability of unbalanced distribution systems with SG- and DFIG-based DGs, and propose easy-to-implement control strategies to improve the stability of unbalanced distribution systems with DGs.

This work is applied specifically to MGs in grid-connected mode with local DG controls, which are one of the applications of DGs in distribution systems.

1.4 Thesis Outline

This thesis is organized into six chapters and one appendix, as follows:

- Chapter 2 provides a background on stability analysis, including voltage, angle and transient stability. Also, several DG technologies and MGs are presented and discussed.
- In Chapter 3, a first modeling approach for DGs is explained and formulated. The developed models of several DG technologies and associated controls are then used for stability analyses of two test systems.
- In Chapter 4, a model and the methodology used for stability analysis of an SG under unbalanced conditions are presented, along with a novel Unbalanced Voltage Stabilizer (UVS) control to improve system stability. Comprehensive numerical results with different scenarios for a DG-load-grid system are also presented and discussed.
- In Chapter 5, the model and control of DFIG under unbalanced conditions are presented, followed by the description of a novel UVS control for stability improvement. Numerical results with various scenarios for a DG-load-grid system are also presented.
- Chapter 6 summarizes the conclusions and main contributions of this thesis and discusses possible future work. Finally, the Appendix provides the data of the DG models and test systems used in this thesis.

Chapter 2

Background Review and Tools

2.1 Introduction

This chapter presents a review of the concepts, models, and tools related to this research work. The definitions and types of power system stability as well as the model of the system are first discussed; dynamic and static tools for stability studies are then presented. Continuation power flows, eigenvalue analyses, transient stability study tools, and identification approaches used in stability analysis are also briefly discussed, and overviews of MG and different DG technologies are provided.

2.2 Power System Stability Definitions

Power system stability is defined as the ability of a system to maintain a normal operating equilibrium after being subjected to a disturbance for a given initial operating point [79]. The normal operating equilibrium point means that the main system variables (angle, voltage, and frequency) after being subjected to a disturbance are within acceptable ranges, as defined by system operators.

A power system is continually subjected to changes in the operating point because of the variation of load and generation. Therefore, the stability of a system depends on the initial equilibrium point. Moreover, it can be subjected to a wide range of disturbances that can be classified into small disturbances (e.g., small variation of loads or generations) and large disturbances (e.g., faults), depending on their nature and magnitude. The types

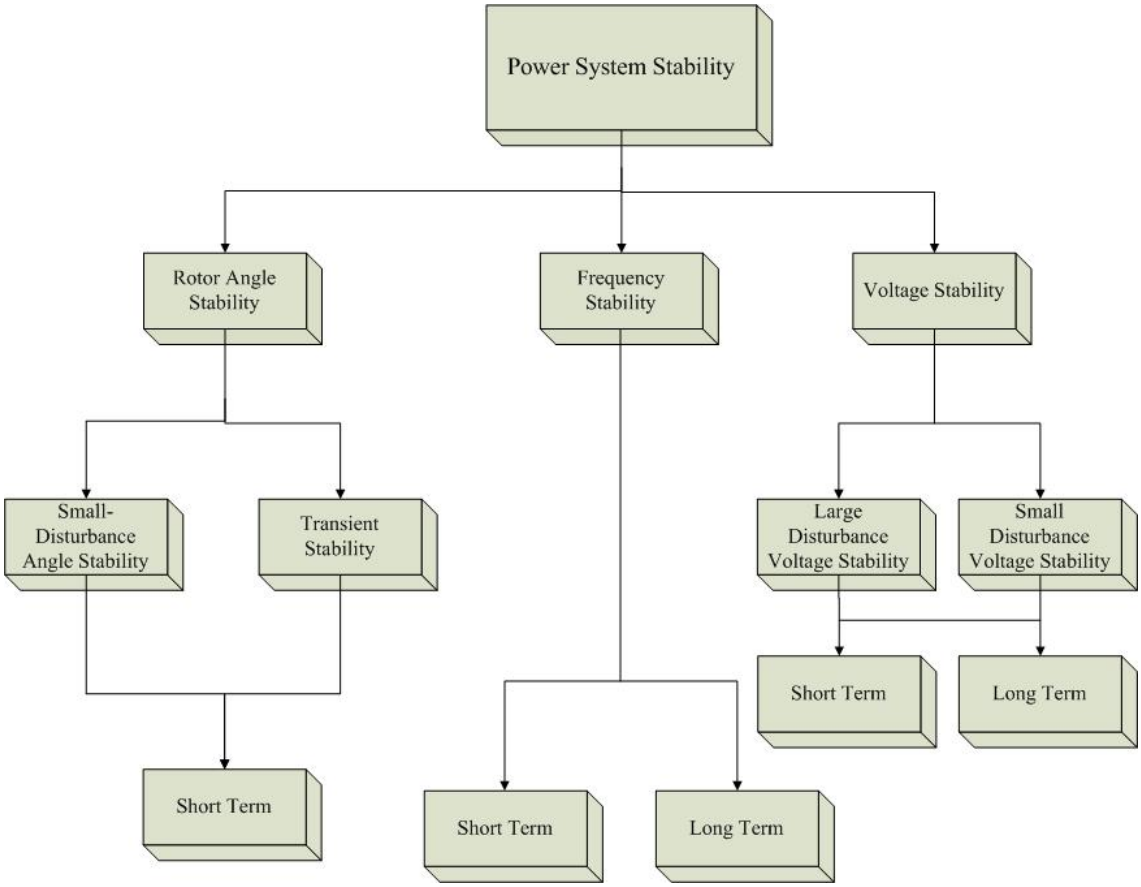

Figure 2.1: Power system stability classification [79].

of disturbances and the resulting system response affect the tools used to assess system stability.

Power system stability is classified as illustrated in Figure 2.1. Rotor angle stability is defined as the capability of synchronous machines in a power system to remain in synchronism under normal operating conditions after being subjected to disturbances [79]. The angle stability depends on the ability to maintain or restore equilibrium between electromagnetic torques of each synchronous machine in the system. In this case, the problem becomes apparent through angular or frequency swings in some generators, which may lead to the loss of synchronism. Maintaining synchronism of the system depends on synchronizing toque and damping torque. Lack of sufficient synchronizing torque leads to non-oscillatory instability, while lack of damping torque leads to oscillatory instability

[79, 80].

Angle stability is divided into small-perturbation stability (small disturbances) and transient stability (large disturbances). Small-perturbation angle stability is defined as the capability of a system to maintain angle stability for small disturbances. The time-frame of small-perturbation stability is in the order of 10-20 seconds after the disturbances. As mentioned previously, lack of damping torque leads to oscillatory instabilities associated with Hopf bifurcations, as discussed in [81, 82, 83]. This type of stability is analyzed using a linearized set of system equations. Transient stability refers to the system's ability to maintain angle stability under severe disturbances. Typically, this phenomenon is due to the lack of synchronizing torque, which may result in first swing instabilities. The time-frame of transient stability is in the order of 1-10 seconds after disturbances. Nonlinear power-angle relationships affect the response of the system to the disturbances.

Frequency stability is defined as a system's ability to maintain a steady frequency following a severe system change that results in a significant imbalance between generation and load [79]. Frequency stability analysis concentrates on studying overall system stability for sudden changes in generation-load balance. Because of the difference of time-frames for various devices, frequency stability is divided into short and long terms. Short-term stability is affected by factors such as load shedding, generator controls, and protection devices with time-frames in the order of several seconds following a disturbance. Long-term stability is affected by other factors such as prime movers; the time-frame in this case is in the order of several minutes following a disturbance.

The voltage stability of a power system is defined as the ability of a system to maintain steady voltage at all buses following a disturbance from an initial condition [79]. It is a well-established fact that voltage collapse is associated with a lack of reactive power support due to insufficient generation and transmission reactive power injection, as well as significant system loading. Two types of bifurcations lead to voltage collapse: saddle-node bifurcations and limit-induced bifurcations [84]. A saddle-node bifurcation (SNB) corresponds to a singularity of the system Jacobian or state matrix that leads to the "disappearance" of steady-state solutions. A limit-induced bifurcation (LIB) is associated with the disappearance of a steady-state solution due to system control limits (e.g., generator reactive power limits). Voltage stability is also classified into long-term and short-term types, depending on the time-frame from several seconds, which involves the dynamics of fast-acting system components, to several minutes, which involves slow-acting system components.

The aforementioned power system classification can be applied to distribution systems with DGs such as MGs. In this context, stability is referred to regaining operating equilibrium with respect to voltage, frequency, and power after being subjected to a disturbance

of a given initial stable operating point.

2.3 Power System Stability Tools

In this section, the system stability tools used in this thesis are briefly described. Although stability issues of DGs in the context of MGs may not be identical to those observed in power system, the discussed system stability tools are general, and basically apply to any kind of non-linear system.

2.3.1 P-V Curves

It is common practice to carry out loadability studies using P-V curves [84], similar to the one illustrated in Figure 2.2, and thus determine the static loading margin (SLM) of the system (nose point) associated with a voltage collapse point. Figure 2.2 also shows the dynamic loading margin (DLM) of a system, which is associated with an angle instability happening before the nose point.

The CPF can be used to obtain P-V curves for voltage stability assessment by increasing the system loading level up to the maximum loadability, at which point the system becomes unstable. This method considers a set of power flow equations, including a load scaling parameter $\lambda \in \Re^{n_\lambda}$, from an initial point and a given generation and load dispatch direction.

A predictor-corrector scheme is employed to solve power flow equations as λ changes, from an initial condition to a maximum loadability point. Figure 2.3 shows the CPF process, where, from a known initial point A that is associated with the power flow solution at a loading level λ_0, a tangent predictor step is used to estimate a solution point B that corresponds to an increase in the value of λ. A "corrector" is used to determine the exact solution point C through a Newton-Raphson algorithm [85]. This technique traces the voltage profile of a system.

2.3.2 Eigenvalue Analysis

There are two approaches for small-perturbation stability studies, as follows:

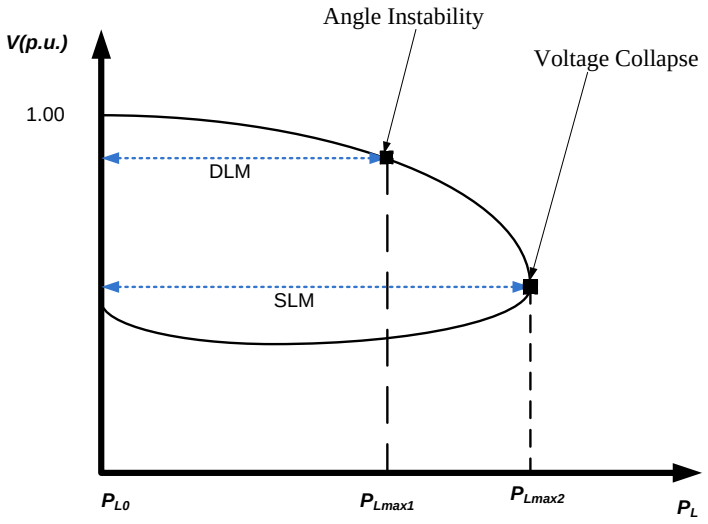

Figure 2.2: A typical P-V curve and corresponding SLM and DLM.

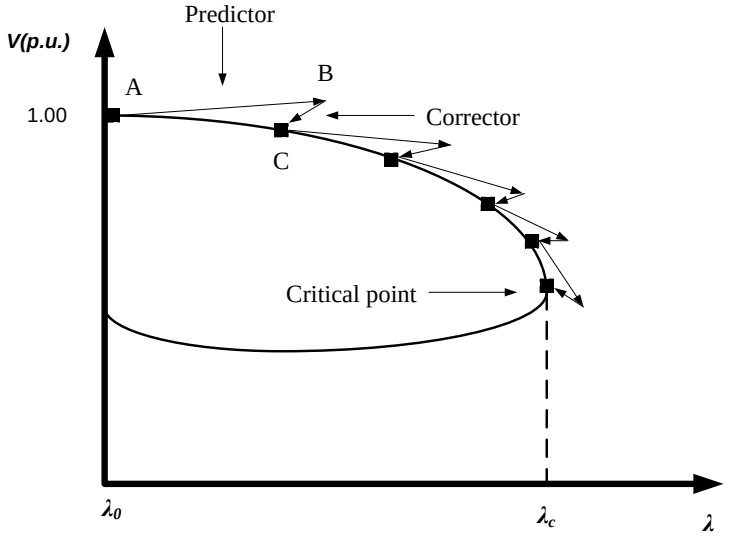

Figure 2.3: Predictor-corrector process in CPF.

Model-Based

Power systems are modeled with nonlinear differential algebraic equations (DAE) as follows:

$$\begin{bmatrix} \dot{x} \\ 0 \end{bmatrix} = \begin{bmatrix} f(x, y, \lambda, pc) \\ g(x, y, \lambda, pc) \end{bmatrix} \tag{2.1}$$

where $x \in \Re^{n_x}$ is a vector of state variables that stands for the dynamic states of generators, loads, and other system controllers; $y \in \Re^{n_y}$ represents algebraic variables that result from neglecting fast dynamics such as load voltage magnitudes and angles; $\lambda \in \Re^{n_\lambda}$ is a vector of "uncontrollable" parameters, typically representing a loading factor; and $pc \in \Re^{n_{pc}}$ stands for "controllable" parameters corresponding to control settings (e.g., Automatic Voltage Regulator (AVR) set points). The vector field of $f : \Re^{n_x} \times \Re^{n_y} \times \Re^{n_\lambda} \times \Re^{n_{pc}} \mapsto \Re^{n_x}$ is the system nonlinear differential equations directly associated with the state variables x. The function $g : \Re^{n_x} \times \Re^{n_y} \times \Re^{n_\lambda} \times \Re^{n_{pc}} \mapsto \Re^{n_y}$ represents the system nonlinear algebraic equations, such as load flow and generators stator algebraic equations.

If the Jacobean $D_y g(0)$ of the algebraic equations is non-singular (i.e., invertible) along the system time trajectories, the system can be transformed into the following Ordinary Differential Equation (ODE) model.

$$\dot{x} = f(x, y^{-1}(x, \lambda, pc), \lambda, pc) \tag{2.2}$$

where $y^{-1}(x, \lambda, pc)$ can be obtained from the Implicit Function Theorem applied to the algebraic constraints along the solution trajectories.

An equilibrium point (x_0, y_0) of (2.1) is defined as a solution of the nonlinear equations:

$$F(x_0, y_0, \lambda_0, pc_0) = \begin{bmatrix} f(x_0, y_0, \lambda_0, pc_0) \\ g(x_0, y_0, \lambda_0, pc_0) \end{bmatrix} = \begin{bmatrix} f|_0 \\ g|_0 \end{bmatrix} = 0 \tag{2.3}$$

where the $pc_0 \in \Re^{n_{pc}}$ represents a given set of controllable parameters at the operating point, which usually correspond to the "base" active power injections, voltage magnitudes at PV buses, and other controller settings, and $\lambda_0 \in \Re^{n_\lambda}$ defines the "base" active and reactive power injections at PQ buses and power injections at PV buses.

In small-perturbation stability analysis, (2.1) is linearized around an equilibrium point $(x_0, y_0, \lambda_0, pc_0)$ as follows:

$$\begin{bmatrix} \Delta\dot{x} \\ 0 \end{bmatrix} = \begin{bmatrix} J_1 & J_2 \\ J_3 & J_4 \end{bmatrix} = \begin{bmatrix} \Delta x \\ \Delta y \end{bmatrix} \tag{2.4}$$

where $J_1 = \frac{\partial f}{\partial x} \mid_0$, $J_2 = \frac{\partial f}{\partial y} \mid_0$, $J_3 = \frac{\partial g}{\partial x} \mid_0$, and $J_4 = \frac{\partial g}{\partial y} \mid_0$. Assuming that J_4 is non-singular, (2.4) can be reduced by eliminating the vector of the algebraic variable Δy as follows:

$$\Delta\dot{x} = (J_1 - J_2 J_4^{-1} J_3)\Delta x = A\,\Delta x \tag{2.5}$$

where A is a "reduced" system state matrix at an equilibrium point x_0 and given parameter values pc_0 and λ_0. The reduced system state matrix eigenvalues and eigenvectors are then defined by:

$$Aw_{ri} = \mu w_{ri} \tag{2.6}$$

$$A^T w_{le} = \mu w_{le} \tag{2.7}$$

where μ represents the eigenvalue, and w_{ri} and w_{le} are the right and left eigenvectors, respectively, associated with the reduced system state matrix.

The eigenvalues of A define the small-perturbation stability of the system near the equilibrium point x_0. Thus, if all eigenvalues of A are on the left-half of the complex plane, the system is locally stable around the equilibrium point x_0. The system is locally unstable if at least one eigenvalue is on the right-half of the complex plane. Finally, the equilibrium x_0 can be associated with a "bifurcation point" if one or more eigenvalues are on the imaginary axis of the complex plane.

System Identification

System identification consists of building mathematical models of complex systems by measured input-output data. It is a useful tool for a wide range of applications, such as obtaining simplified models of large systems and controller tuning.

Time-domain simulation software (e.g., PSCAD/EMTDC) or actual measurements provide data to analyze the dynamics of the system, which is then used in an appropriate modal estimation method. In this thesis, Prony and Steiglitz-McBride Iteration methods are used to estimate the system model from output signals. The System Identification Toolbox in MATLAB and ad-hoc coding are the basic tools used here to perform these studies.

Prony Method [86]

The Prony method has been widely used for modal estimation or obtaining equivalent linear models of power systems. This method is used to fit a deterministic damped exponential model to a set of sampled data. A generic output signal $\tilde{y}[\tilde{t}]$ can be mathematically represented as a sum of n damped complex sinusoids, as follows:

$$\tilde{y}[\tilde{t}] = \sum_{i=1}^{n} \bar{R}_i \tilde{Z}_i^{\tilde{t}} \tag{2.8}$$

where $\bar{R}_i$ is an output residue associated with the mode $\tilde{\mu}_i = \tilde{\alpha}_i + j\tilde{\beta}_i$; $\tilde{Z}_i = e^{\tilde{\mu}_i \tilde{T}_s}$; $\tilde{T}_s$ is the sampling time; and $\tilde{t}$ is integer time. Considering that $\tilde{y}[\tilde{t}]$ is the solution to a difference equation represented by an Auto-Regressive (AR) model:

$$\tilde{y}[\tilde{t}] = -b_1\tilde{y}[\tilde{t}-1] - b_2\tilde{y}[\tilde{t}-2] - ... - b_n\tilde{y}[\tilde{t}-n] \tag{2.9}$$

Equation (2.9) can be written in a matrix form, as follows:

$$Y = DB \tag{2.10}$$

where

$$Y = [\tilde{y}_{\tilde{t}+n}\ \tilde{y}_{\tilde{t}+n+1}\ \tilde{y}_{\tilde{t}+n+2}...\tilde{y}_{\tilde{t}+N}]^T_{N-n+1} \tag{2.11}$$

$$B = [-b_1 - b_2 ... - b_n]^T \tag{2.12}$$

$$D = \begin{bmatrix} \tilde{y}_{\tilde{t}+n-1}, \tilde{y}_{\tilde{t}+n-2}; ...; \tilde{y}_{\tilde{t}} \\ \tilde{y}_{\tilde{t}+n}; \tilde{y}_{\tilde{t}+n-1}, ..., \tilde{y}_{\tilde{t}+1} \\ ... \\ \tilde{y}_{\tilde{t}+N-1}; \tilde{y}_{\tilde{t}+N-2}; ...; \tilde{y}_{\tilde{t}+N-n} \end{bmatrix}_{(N-n+1)\times n} \tag{2.13}$$

where N is the number of samples. The vector B can be computed by the least square method. The eigenvalues of the system can be computed using vector B, which are the roots of the system's characteristic equation:

$$\tilde{Z}^n + b_1\tilde{Z}^{n-1} + b_2\tilde{Z}^{n-2} + ... + b_n = 0 \tag{2.14}$$

Although the Prony method estimates well the system signal for a large disturbance, it cannot follow the signal properly when the system becomes unstable. This is illustrated for a sample system in Section 4.3.3.

Steiglitz-McBride Iteration Method

This method is based on the calculation of the equivalent transfer function $\bar{N}(\bar{Z})/\bar{D}(\bar{Z})$ of a system, where $\bar{N}(\bar{Z})$ and $\bar{D}(\bar{Z})$ can be written as:

$$\bar{N}(\bar{Z}) = \bar{\alpha_0} + \bar{\alpha_1}\bar{Z}^{-1} + ... + \bar{\alpha_{n-1}}\bar{Z}^{-(n-1)} + \bar{\alpha_n}\bar{Z}^{-n} \tag{2.15}$$

$$\bar{D}(\bar{Z}) = \bar{\beta_0} + \bar{\beta_1}\bar{Z}^{-1} + ... + \bar{\beta_{n-1}}\bar{Z}^{-(n-1)} + \bar{\beta_n}\bar{Z}^{-n} \tag{2.16}$$

where $\bar{\alpha_i}\ \forall i \in \{0, ..n\}$ and $\bar{\beta_i}\ \forall i \in \{0, ..n\}$ are numerator and denominator coefficients, respectively. The coefficients $\bar{\alpha_i}\ \forall i \in \{0, ..n\}$ and $\bar{\beta_i}\ \forall i \in \{0, ..n\}$ are calculated iteratively, such that the response of the estimated signal approximates the response of the actual signal [87]. These coefficients can be calculated through a simple optimization method available in MATLAB [88]. Although this method usually converges rapidly, it may not converge if the order of the system is too high.

2.3.3 Transient Stability

Time-domain simulations are mainly used for transient stability analysis of power systems following a contingency. In some power system software, time-domain simulations are carried out by solving the complete set of DAEs by means of step-by-step trapezoidal or predictor-corrector integration. In this thesis, time-domain simulations of test cases were carried out by means of PSAT [89], which is a MATLAB-based toolbox for studies of power systems, and PSCAD/EMTDC [90], which is an ad-hoc software for time-domain simulations of detailed (e.g., unbalanced) power system models.

Various criteria can be used to evaluate the transient stability of a system. For example, CCT can serve as an index to evaluate system robustness [91]. The CCT represents the point in time beyond which the system is unable to recover its stability, after clearing the fault (contingency). When a fault occurs in the system, the difference between the actual clearing time for a stable system and the CCT may be used to define a transient stability margin for the system. The CCT is not usually used as a stand-alone index to study the transient stability of power systems, but it can be used for comparative system stability analyses.

Other transient stability index used in practice is oscillation durations [80]. The oscillation durations are defined as the time interval between fault occurrence and the instant when the rotor speed stays within a specific bandwidth, since when a fault is applied, the rotor speed deviates from its rated value. This index indicates that the longer the oscillation duration, the less stable the system.

2.4 DG Technologies

There is currently no common agreement on the definition of DGs. Definitions differ from one country to another, depending on voltage level, unit connection, types of prime movers (e.g., renewable or conventional cogeneration), maximum power rating, and so on. The International Council on Large Electricity Systems (CIGRE) working group defines DGs as the units that are smaller than 50-100 MW, not centrally planned, not centrally dispatched, and usually connected to the distribution network [92]. IEEE defines DGs as "the generation of electricity by facilities that are sufficiently smaller than central generating plants, so as to allow interconnection at nearly any point in a power system" [93].

Because of the many varieties of DG technologies and prime-mover energy sources, DGs can operate by means of rotating electricity machines or static (electronic) interfaces. In the case of rotating electricity machines, i.e., synchronous or induction machines, and if the generated power is at the system frequency or close to it, the generator can be connected directly to the grid. If the frequency of generated power is different from the system frequency, an electronic interface should be used. In cases where DG technologies produce dc power (e.g., FCs, photovoltaics), power electronic interfaces (dc/ac) are required. Thus, based on different DG technologies, the DG connection to the power grid can be classified into two categories:

- Direct grid-connected DG without converters.
- Indirect grid-connected DG through converters.

The general scheme of the DG models proposed here is illustrated in Figure 2.4.

Different energy sources are used to provide power through wind turbines, photovoltaic arrays, FCs, MTs, conventional diesel generators, and energy storage technologies. An overview of various types of DG units that are commonly found in MGs is briefly discussed next. Developed models of each DG studied in this thesis are provided in Chapter 3.

2.4.1 Micro Turbines (MTs)

MTs are basically small and simple gas turbines, with a typical output range between 25 to 300 kW. Certain advanced options can be incorporated in MTs, such as recuperation systems, low NOx technologies, and the potential use of advanced materials such as ceramics in hot section parts [94]. Because most MTs use natural gas, they are typically

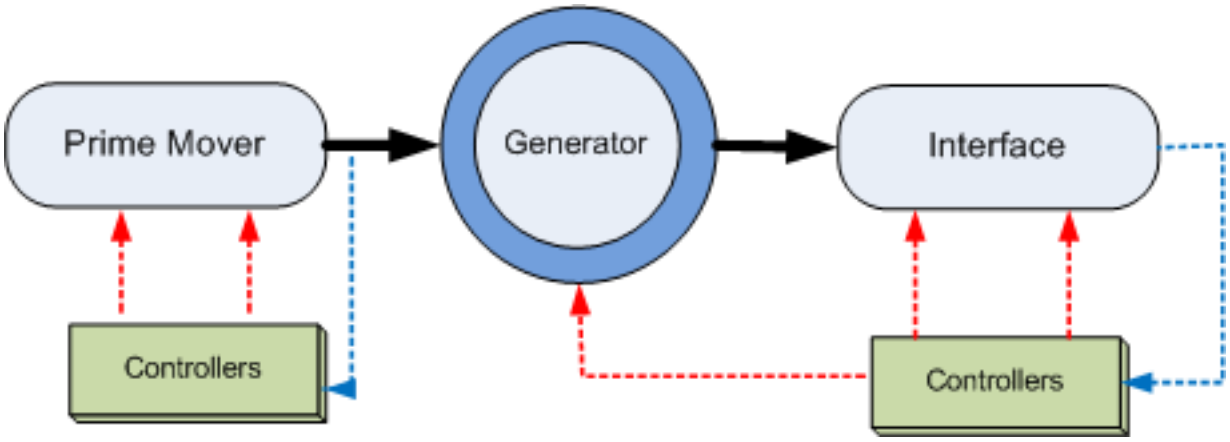

Figure 2.4: General scheme of DG models.

characterized by low emission levels and can operate on the same principles as conventional gas turbines. Small gas turbines were developed by Allison in the 1960s, where the first application was to supply a radar set and control station of a U.S. Army Patriot Missile system. Technical and manufacturing developments have encouraged the use of MTs as DG units.

MTs have three main components: compressor, combustor, and turbine. The high-pressure air from the compressor, when mixed with the injected fuel, forms a combustible mixture. This mixture is then ignited in the combustor to produce a hot gas flow that drives the turbine.

There are essentially two types of MTs: single and split shaft. Single-shaft MTs are high speed in nature (50,000 to 120,000 rpm), with a compressor and a turbine mounted on the same shaft. This kind of MT needs an interface, which consists of an ac/dc converter, a dc link with capacitance, and a dc/ac converter. A split-shaft MT design has its generator connected to the turbine shaft via a gearbox [94]. These kinds of MTs have a rated power level that can influence the dynamics of a distribution system.

In [94], a classical gas turbine and governor model is used to model a simple-cycle, split-shaft turbine. Although this model is widely used in the literature for analyzing the dynamic effects of MTs on distribution systems, fast dynamics are not considered. The MT model used in this thesis and presented in Chapter 3 is based on the gas turbine model presented in [95], which was successfully adopted for MT modeling by several authors [96, 97], and validated by tests [98].

2.4.2 Diesel Generators

Diesel-engine-powered SGs are another type of DG that consists of a diesel combustion engine, a drive-train, and an SG with simple frequency and voltage controllers. These units are popular in remote community MGs throughout Canada and are also widely used for back-up, emergency, and stand-by power.

In [99], a suitable model of an emergency diesel generator is presented. In this model, the transient processes of the drive-train are ignored, with the model being validated by field tests. This model is adopted in this thesis.

2.4.3 Wind Turbines

Wind energy is an attractive renewable energy resource. A wind turbine generates electricity by converting kinetic wind energy passing through its blades, with ratings from a few kW to a few MW. The electrical efficiency of wind turbines is about 20-40% and they range in size from 0.3 kW to 5 MW. In areas with significant wind energy, large-scale wind farms are being implemented. Due to the un-dispatchable nature of wind generation, the impact of wind generation on the system is significant.

Wind power generators available today can be categorized into the following four main turbine types:

- Type A: Fixed-speed wind-turbine with a direct-grid-connected induction generator.
- Type B: Variable-speed wind turbine with a variable rotor resistance induction generator directly connected to the grid.
- Type C: Variable-speed wind turbine with a direct-grid-connected doubly-fed induction generator and dc/ac rotor converter.
- Type D: Variable-speed wind turbine with synchronous machine and full scale ac/dc/ac converter.

A review of wind turbine market penetration shows that Types A, C and D currently dominate the market of installed wind power generation [100]. Therefore, Type B units are not considered for modeling purposes in this thesis.

Different dynamic models have been proposed to model wind power generators for stability studies. In [34], suitable models for stability analysis of different types of wind

power units are presented, assuming balanced conditions; the model for wind turbines Type A is used in this thesis for the "standard" stability analysis presented in Chapter 3. The model presented in [74] for wind turbines Type C under unbalanced conditions is used as a base for the model developed in Chapter 5 for detailed stability studies.

2.4.4 Fuel Cells (FCs)

Another type of DG resource for supplying electrical and thermal energy to residential and commercial loads is FC, which is an electrochemical device that converts chemical energy into electricity and heat. FCs are considered to be suitable for DG applications ranging from a few kW to a few MW, and are portable and modular, with low noise pollution and low to zero emissions. They also have high reliability and can use a variety of hydrogen-rich fuels (e.g., natural gas, gasoline, biogas or propane). These characteristics make them suitable as DGs, especially in remote areas. In the future, if electrical systems are combined with hydrogen and gas infrastructures, the use of FCs is expected to increase, since these provide clean energy and heat for several applications.

FCs typically are classified by electrolyte type, i.e., polymer electrolyte or proton exchange membrane fuel cell (PEMFC), alkaline fuel cell (AFC), phosphoric acid fuel cell (PAFC), molten carbonate fuel cell (MCFC), and solid oxide fuel cell (SOFC). PAFCs and PEMFCs have been successfully commercialized, and second-generation SOFCs and PEMFCs are likely to be used in power plants. Each of these types of FCs has a specific dynamic model, with various published works describing the associated detailed models. Some published static performance studies are based on the Nernest and Butler-Volmer equation.

Dynamic models have been developed for autonomous power plants for different types of FCs (e.g., [101, 102, 103]). However, the majority of these models do not consider interactions with the system or other types of DG units.

2.4.5 Photovoltaic Generators

A photovoltaic power generation system is another renewable energy source that generates power directly from sunlight. A photovoltaic cell includes semiconductor layers with specific properties, that when is exposed to sunlight, the electrons move in one direction and a direct current is generated. Cells can be connected together in the form of a module to form photovoltaic systems that provide a quiet, low maintenance, pollution-free, safe, reliable, and independent alternative to conventional generation sources. Current ratings

of photovoltaic units are from a few kW to few MW. The technical and manufacturing developments of photovoltaic units have encouraged the adoption of photovoltaics as another attractive energy resource for small- and large-scale usage.

Since the 1990s, a limited number of large-scale photovoltaic systems have been installed through photovoltaic farms similar to wind farms. However, because of cost issues and low electrical energy generation, these farms are not yet economically viable without some financial incentives. On the other hand, small-scale photovoltaic panels in the range of kW are being widely deployed.

In general, the impact of photovoltaic systems on voltage fluctuation and harmonic injection is not very significant and can be mitigated by reactive power control through inverter controllers. Several studies are available on the internal controls of photovoltaic systems for better power tracking and energy processing [104]. A few companies have developed models for photovoltaic cells, but because there is no agreement on the modeling approach, there are presently no industry standard models in existence.

Previous academic studies have concentrated on detailed photovoltaic models for power quality purposes. These models represent switching inverter characteristics of photovoltaics, but this level of detail is unnecessary for power system stability studies, since fast transient switchings are not relevant for conventional transient stability studies. In this thesis, the model presented in [105] for photovoltaic systems is used.

2.4.6 Energy Storage System (ESS)

A variety of storage technologies, which are capable of smoothing out fluctuating powers and voltages produced by non-dispatchable sources, enhance system performance. Some of these storage technologies are superconducting magnetic energy storage, supercapacitors, flywheels, compressed air energy storage, hydro-pumped storage, and BESS. The main issues with most of these technologies are their cost, operation, and maintenance requirements. ESS is always interfaced to the grid via a power electronic converter. It is important to mention that ESS is not really a DG, as it can operate both in charging (load) and discharging (generation) modes; however, in the context of the short-term stability studies discussed in this thesis, it is assumed to operate only as a DG in discharging mode. In this thesis, a suitable model of a BESS with its inverter for stability studies has been developed, and is discussed in Chapter 3.

2.5 Microgrid

MGs are viewed as subsystems of "small" generators and loads; a typical MG structure is shown in Figure 2.5. It consists of radial feeders (part of a distribution system), a set of DGs (e.g., wind turbine, FC, diesel generator, photovoltatic, and storage devices), and loads of various lines. The MG is interfaced to the main grid at the point of common coupling (PCC), and the static switch SD is utilized to island Feeders 1 and 2 from the grid. When there is a problem in the power grid, the SD is opened, isolating the MG from the main power grid.

Each component of an MG can be modeled based on its characteristics. The local DGs have local controllers with a communication function that exchanges information between other local controllers and a possible upstream central controller. For example, a central controller could act as a power-flow controller to monitor the power exchanged between the MG and the power system. The central controller may have the main responsibility of optimizing the MG operation, or it may regulate the actions of the controllable units in terms of market and management. In this case, the MG is presented to the host grid at the PCC as a single controllable entity.

The MG can operate in grid-connected mode or islanded mode, or it can transition between grid-connected and islanded modes. In grid-connected mode, the PCC voltage and frequency is dominated by the main grid, and the MG acts as a virtual power plant.

2.6 Summary

In this chapter, power system stability concepts were discussed, along with general models of the power system required for stability studies. The tools for stability studies that will be used in this work were also introduced. Finally, an overview of an MG was presented, including different DG technologies and their interfaces to the grid. The concepts presented in this chapter are used throughout the next chapters of this thesis.

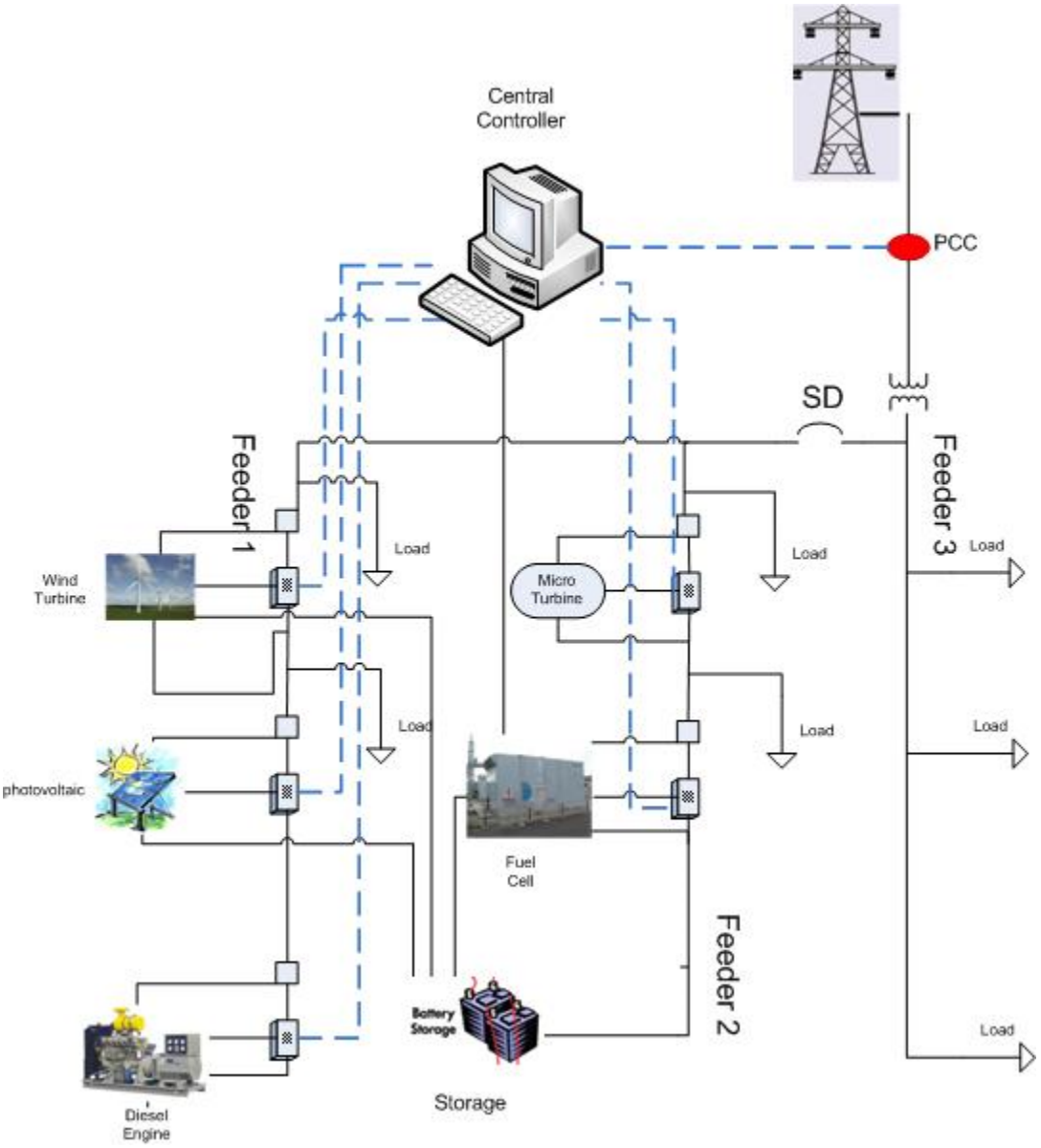

Figure 2.5: Typical MG structure.

Chapter 3

Modeling and Stability Studies Under Balanced Conditions

3.1 Introduction

In this chapter, the dynamic models of different DGs under balanced conditions are presented. Differential and algebraic equations of various DG models are formulated and discussed; these models are generally based on existing dynamic models of different DGs for stability studies. Two test distribution systems are used for testing, demonstration, and comparison of the various models and corresponding DG technologies, and for novel, comprehensive, and complete stability studies of these systems. For the latter, voltage stability studies are performed based on P-V curves; small-perturbation stability studies are carried out based on eigenvalue analyses of the linearized system models; and transient stability studies are performed using time-domain simulations of various contingencies. These studies are performed in PSAT [89], by implementing the models presented here in this software tool.

3.2 Dynamic Models

3.2.1 Micro Turbine Generator

The MT model presented in this thesis is based on the gas turbine model in [95], which has been successfully adopted for MT modeling by several authors [96], [97], and validated by

tests [98]. The MT model contains three main components: the compressor, the combustor, and the turbine, in addition to the electrical generator. The dynamic model of the MTs is based on the dynamics of these components.

In the case of diesel generator and MT, these units can be modeled using "standard" ac generator machines; thus, the SG is modeled using a sixth-order model [89]. In addition, the excitation system is modeled based on an AVR IEEE Type II model [89].

The compressor turbine is at the heart of the MT. When the input to the compressor changes, the output cannot change instantaneously; thus, the compressor is a dynamic device with a time constant τ_{cd} associated with the compressor discharge volume. There is also a small time constant τ_{ecr} associated with the combustion reaction. The fuel system consists of the fuel valve positioner and fuel system actuator; the fuel flow dynamics are dominated by the inertia of the fuel system actuator and the valve positioner. The valve positioner and fuel system actuator are modeled using first-order transfer functions.

Based on these models, Figure 3.1 depicts the complete block diagram of the MT model proposed here. The parameters τ_s, τ_f, and τ_{ecr} are associated with the time constants of the valve positioner, the fuel system, the combustor, and the compressor discharge value, respectively. Here, W_{min} represents the minimum fuel flow, and K_f and K_a are fuel system feedback and valve positioner gain, respectively. The function of f_{mt} yields the shaft torque, and is defined by:

$$f_{mt} = 1.3(W_F - 0.23) + 0.5(1 - \omega_e) \tag{3.1}$$

where ω_e is the electrical rotor speed [106].

The speed control is incorporated into the MT model as illustrated in Figure 3.2. This controller can operate in droop mode or isochronous mode; the constant K_z in the speed controller represents the governor mode (droop mode for $K_z = 1$, or isochronous mode for $K_z = 0$). In the droop mode, the output of the governor is proportional to the speed error which is associated with a straight proportional speed controller. In the isochronous mode, the rate of change of the output is proportional to the speed error associated with a Proportional-Integral (PI) controller. The speed of the generator remains constant regardless of the change in load. The parameters τ_x and τ_y represent governor lead and lag time constants, respectively; and the speed governor gain is given by K_w.

The algebraic and deferential equations and associated Jacobians for the MT model in Figure 3.1 were implemented in PSAT to study the static and dynamic behavior of the MT model. These equations are:

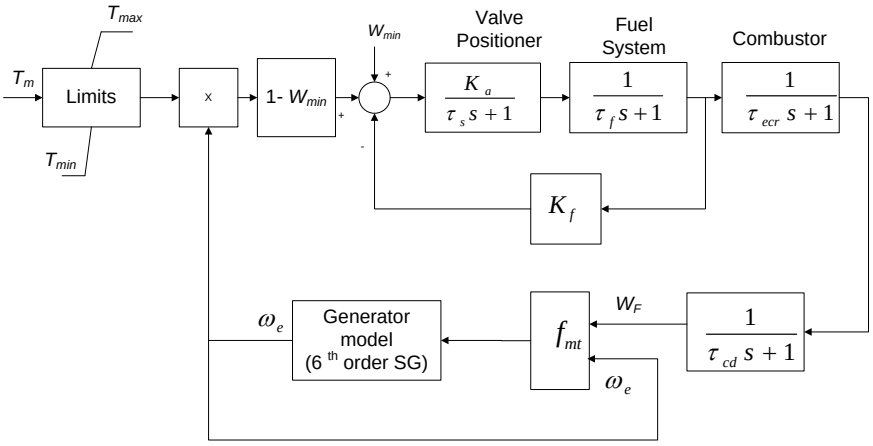

Figure 3.1: Block diagram of the MT model.

$$\dot{x_1} = \frac{K_a temp - x_1}{\tau_s} \tag{3.2}$$

$$temp = T_m\,\omega_e(1 - W_{min}) + W_{min} - K_f\,x_2 \tag{3.3}$$

$$\dot{x_2} = \frac{x_1 - x_2}{\tau_f} \tag{3.4}$$

$$\dot{x_3} = \frac{x_2 - x_3}{\tau_{ecr}} \tag{3.5}$$

$$\dot{x_4} = \frac{x_3 - x_4}{\tau_{cd}} \tag{3.6}$$

$$\text{if} \quad T_m \geq T_{max} \Rightarrow T_m = T_{max} \tag{3.7}$$

$$\text{if} \quad T_m < T_{min} \Rightarrow T_m = T_{min} \tag{3.8}$$

where $x_i \forall i \in \{1, ..4\}$ are the state variables of the MT DG; T_m, T_{min}, and T_{max} represent the mechanical torque and the lower and the upper torque limit, respectively. Similarly, the equations and Jacobians for the governor model shown in Figure 3.2 were also implemented in PSAT. The equations and Jacobians for the generator and corresponding AVR were already available in PSAT.

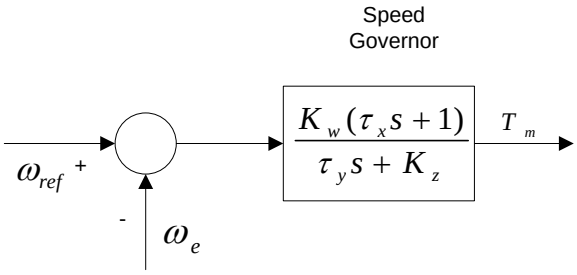

Figure 3.2: Speed controller of the MT.

3.2.2 Diesel Generator

A diesel generator can be modeled using a "standard" ac generator machine. Therefore, the generator of the diesel unit is modeled using a sixth-order SG, and the excitation system is modeled based on an AVR IEEE Type II model [89]; these models were already available in PSAT.

The governor of diesel units consists of three main parts: electric control box, actuator, and engine [99]; Figure 3.3 depicts a typical block diagram of the diesel generator model. The corresponding differential equations of the governor model can be represented as follows:

$$\dot{x_1} = -\frac{1}{\tau_{d2}}x_1 - \frac{1}{\tau_{d1}\tau_{d2}}x_2 + (\omega_e - \omega_{ref}) \tag{3.9}$$

$$\dot{x_2} = x_1 \tag{3.10}$$

$$\dot{x_3} = \frac{1}{\tau_{sd}}\left[K_{ds}\left(1 - \frac{\tau_{d4}}{\tau_{d5}}\right)\left(-\frac{\tau_{d3}}{\tau_{d1}\tau_{d2}}x_1 - \frac{1}{\tau_{d1}\tau_{d2}}x_2\right) - x_3\right] \tag{3.11}$$

$$\dot{x_4} = x_3 + K_{ds}\frac{\tau_{d4}}{\tau_{d5}}\left(-\frac{\tau_{d3}}{\tau_{d1}\tau_{d2}}x_1 - \frac{1}{\tau_{d1}\tau_{d2}}x_2\right) \tag{3.12}$$

$$\dot{x_5} = \frac{x_4 - x_5}{\tau_{d6}} \tag{3.13}$$

$$\dot{x_6} = \frac{x_5 - x_6}{\tau_{Dd}} \tag{3.14}$$

$$\text{if} \quad x_5 \geq T_{max} \Rightarrow x_5 = T_{max} \tag{3.15}$$

$$\text{if} \quad x_5 < T_{min} \Rightarrow x_5 = T_{min} \tag{3.16}$$

where $x_i \forall i \in \{1, ..5\}$ are the state variables of the diesel unit; $\tau_{dj} \forall j \in \{1, ..6\}$ are the time

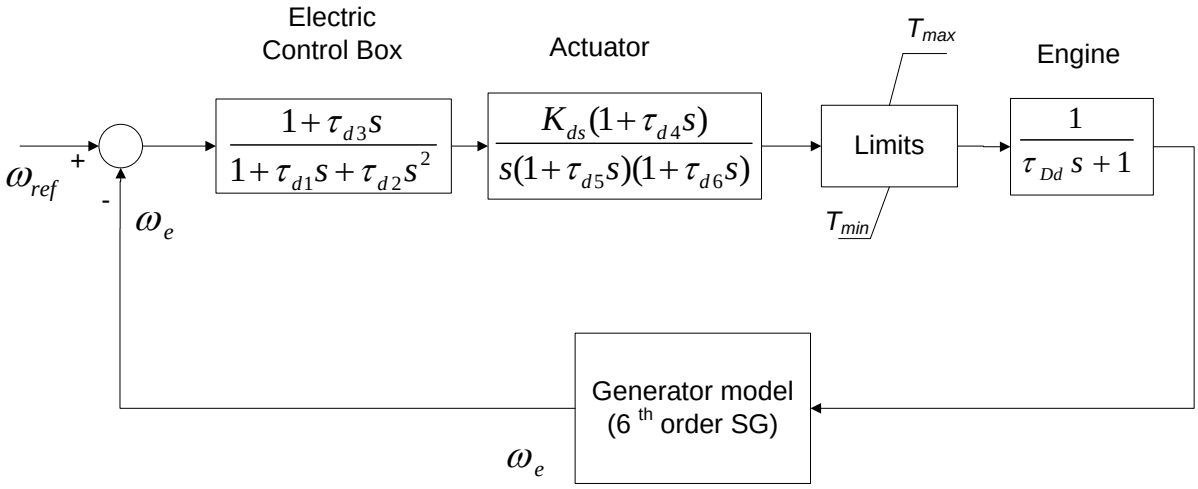

Figure 3.3: Block diagram of the diesel DG model.

constants of the control box and actuator models; τ_{Dd} is associated with the time constant of the engine of the diesel unit; K_{ds} is the gain of the actuator; ω_e is the electrical rotor speed; and T_{min} and T_{max} represent the lower and the upper torque limit, respectively. These equations and corresponding Jacobians were implemented in PSAT.

3.2.3 Wind Turbine Generator

As previously mentioned, Types A, C and D (i.e., fixed-speed wind-turbine with induction generator, variable speed wind turbine with DFIG, and variable speed wind turbine with synchronous machine and full converter) dominate today's market of installed wind power generation. Since Type A is cheaper than other types, this type is commonly used in distribution systems as a DG. Therefore, fixed-speed wind-turbines with induction generators are used as the wind DGs under balanced condition in this thesis.

The dynamic model of wind turbines for stability studies used in this work is presented in [34]. One of the most common fixed-speed wind-turbine is a squirrel cage induction generator; this type of wind turbines use an induction machine with short-circuited rotor. The general equations of an induction generator in terms of the dq axes can be written as:

- The output active and reactive power are:

$$P_{out} = V_d I_d + V_q I_q \tag{3.17}$$
$$Q_{out} = V_q I_d - V_d I_q \tag{3.18}$$

where the d and q stator machine voltages are defined by:

$$V_d = -V sin\theta \tag{3.19}$$
$$V_q = V cos\theta \tag{3.20}$$

and I_d and I_q are the d and q axes stator currents, respectively.

- The differential equations of the internal d and q voltages are:

$$\dot{E_d}' = 2\pi f(1-\omega_m)E'_q - \frac{E'_d - (X_0 - X')I_q}{T'_0} \tag{3.21}$$
$$\dot{E_q}' = -2\pi f(1-\omega_m)E'_d - \frac{E'_q + (X_0 - X')I_d}{T'_0} \tag{3.22}$$

where E'_d and E'_q are defined by:

$$E'_d = V_d + R_s I_d - X' I_q \tag{3.23}$$
$$E'_q = V_q + R_s I_q + X' I_d \tag{3.24}$$

ω_m is the rotor angular speed; f is the frequency; and X_0, X', and T'_0 are obtained from the generator parameters as follows:

$$X_0 = X_s + X_m \tag{3.25}$$
$$X' = X_s + \frac{X_r X_m}{X_r + X_m} \tag{3.26}$$
$$T'_0 = \frac{X_r + X_m}{2\pi f R_r} \tag{3.27}$$

where X_s, X_r, X_m, and R_r are stator reactance, rotor reactance, magnetizing reactance, and rotor resistance, respectively.

- For the mechanical system, a two-mass representation of the wind turbine is used. Thus, the mechanical differential equations of the shaft can be described as:

$$\dot{\omega_t} = \frac{T_t - K_s\gamma}{2H_t} \tag{3.28}$$
$$\dot{\omega_m} = \frac{K_s\gamma - T_e}{2H_m} \tag{3.29}$$
$$\dot{\gamma} = 2\pi f(\omega_t - \omega_m) \tag{3.30}$$

where H_t and H_m are the turbine and the rotor inertias; K_s is the shaft stiffness; and ω_t is the wind turbine angular speed. Mechanical and electrical torques (i.e., T_t and T_e) are defined by:

$$T_t = \frac{P_m}{\omega_t} \tag{3.31}$$

$$T_e = \frac{E'_d I_d + E'_q I_q}{\omega_e} \tag{3.32}$$

where P_m is the mechanical power extracted from the wind source.

3.2.4 Photovoltaic Generator

This model is based on a VSC with dq current control, as proposed in [105]. Two models are used for the photovoltaic source for stability studies based on PQ and PV control models. Among various possibilities for the inverter model, first-order transfer functions with steady-state gain and closed-loop control transfer functions are the most appropriate; since both models yield similar results, the first-order transfer function is adopted here.

Figure 3.4 and Figure 3.5 present the block diagram of the photovoltaic PQ and PV models, respectively. In these models, the current set points can be obtained based on the desired active and reactive powers and current measurements in the dq reference-frame. The corresponding equations and associated Jacobians were implemented in PSAT.

3.2.5 Fuel Cell

Typically, FC consists of three main parts: reformer, stack, and power conditioner. The complexity and very nonlinear behavior of electrical, chemical, and thermodynamic processes result in complex models [2]. The parameters of such models are difficult to estimate. However, for FCs using fully controlled inverters with large capacitors or some energy storage capabilities, the voltage or the reactive power is assumed to be controlled through full controlled inverters. Hence, a third-order nonlinear model of FC based on [2] is used for stability studies in this thesis; the first-order delay action represents the reformer and the stack. A nonlinear resistance is used to represent the voltage drop of the system; this resistance is based on the characteristics of FC at steady-state [2]. Base on this, the equations

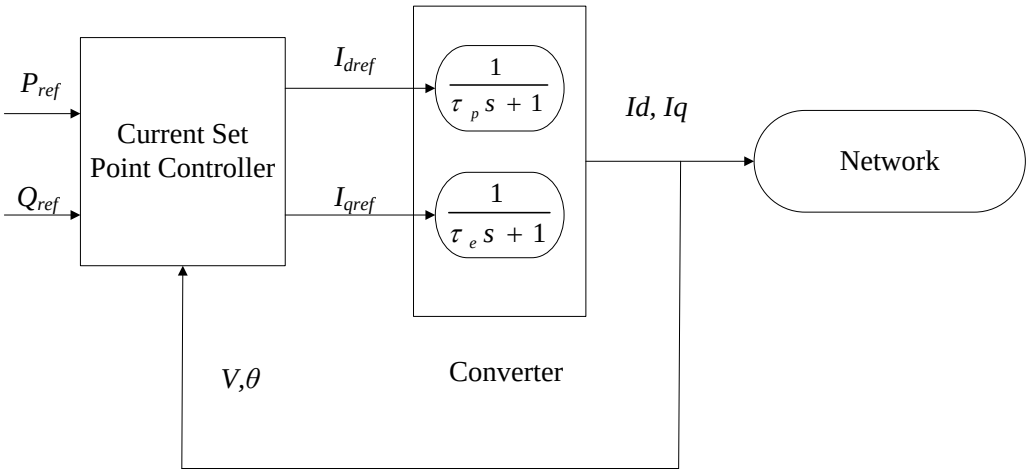

Figure 3.4: Model of photovoltaic DG with PQ control.

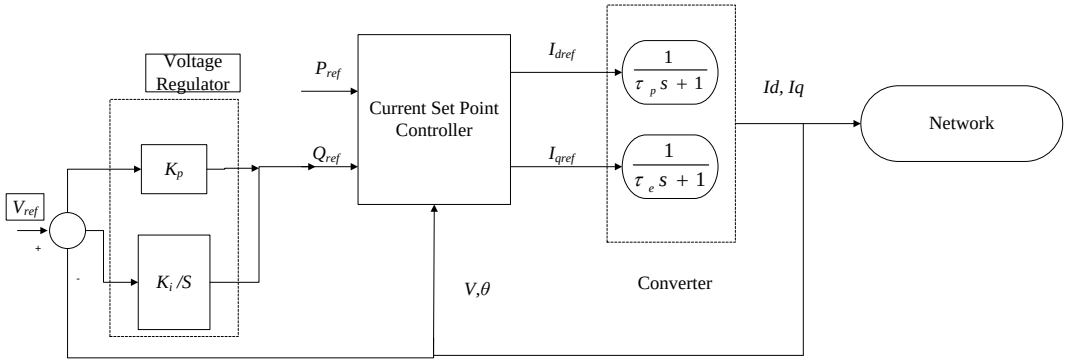

Figure 3.5: Model of photovoltaic DG with PV control.

implemented in PSAT for the FC model used here are:

$$\dot{x_1} = \frac{q_f - x_1}{\tau_{ref}} \tag{3.33}$$

$$\dot{x_2} = \frac{x_1 - x_2}{\tau_{st}} \tag{3.34}$$

$$\dot{x_3} = \frac{I_{ref} - x_3}{\tau_d} \tag{3.35}$$

$$V_{fc} = x_2 - R_{in}x_3 - B_{fc}\ln(C_{fc}x_3) \tag{3.36}$$

where $x_i \forall i \in \{1, ..3\}$ are the state variables of the FC; the parameters τ_{ref}, τ_{st}, and τ_d are associated with the time constants of the reformer, the stack, and the electrical response of the FC; R_{in} is the internal resistance; V_{fc} is the FC dc voltage; q_f is associated with input fuel rate; and B_{fc} and C_{fc} are the constant parameters used to represent the nonlinear losses. Figure 3.6 illustrates the block diagram of the FC.

The dc power of the FC is considered to be the active power injected in the network. The FC is connected to the system through a transformer via a VSC, which is assumed to include relevant filters. Thus, the active and reactive link between the ac and dc networks implemented in PSAT is given by:

$$P = \frac{V_t V}{X_t} sin(\delta_t - \delta) = P_{dc} = V_{fc}x_3 \tag{3.37}$$

$$Q = \frac{V_t V}{X_t} cos(\delta_t - \delta) - \frac{V^2}{X_t} \tag{3.38}$$

$$V_t = \sqrt{3/8} m V_{fc} \tag{3.39}$$

where X_t is the reactance of the transformer; m is modulating signal amplitude; and $V_t \angle \delta_t$ and $V \angle \delta$ represent the voltage phasors of the two sides of the transformer.

The ac voltage control of the FC implemented in PSAT is also illustrated in Figure 3.6. Here, K_m and τ_m represent the gain and the time constant of the voltage control loop, and m_{max} and m_{min} are the maximum and the minimum modulating signal amplitudes.

3.2.6 Battery Energy Storage System

One of the most common ESS is the battery, which is connected to the grid via an inverter interface. As this work concentrates on short-term stability studies, the BESS is assumed

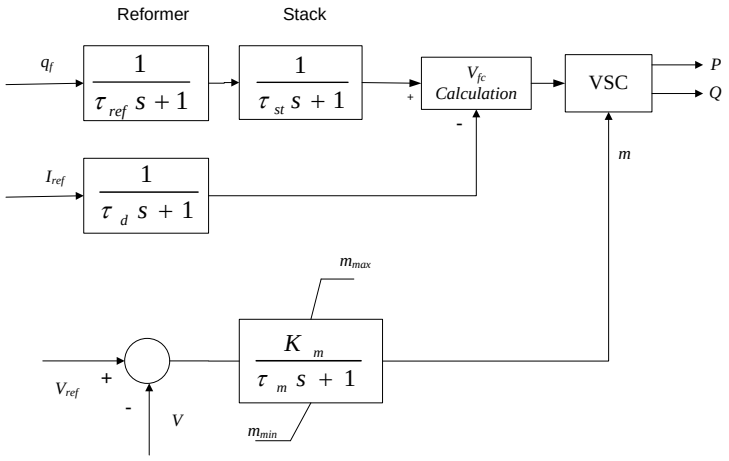

Figure 3.6: Block diagram of the FC model.

here to operate only in discharging (generation) mode with constant active power. The inverter model used here is the same as the one for a FC DG.

There are a few dynamic battery models that have been proposed for power system studies. The third-order battery model developed in [107] and [108] is used as a base for the model proposed in this thesis, due to its accurate representation of battery charge/discharge characteristics, and its direct representation of the State-Of-Charge (SOC) and Depth-Of-Charge (DOC) of the battery. A modified second-order battery model is considered here in which the dynamics of the temperature variable is ignored. Figure 3.7 depicts the electrical diagram of the battery model used here and implemented in PSAT. This model contains three parts:

- The main branch containing the elements E_m, R_1, C_1, and R_2 approximates the battery charge-discharge dynamics.
- The parasitic branch models the self-discharge.
- R_0 approximates the overcharge resistance.

The parameters R_0, R_1, R_2, and R_p are nonlinear resistances; C_1 is a nonlinear capacitance; and E_m is the internal voltage of the battery. Most of these resistive elements are determined empirically. The general equations of battery model can then be stated as follows:

- The battery capacity $C(I_{batt}, \Theta)$ is a function of the discharge current I_{batt} and electrolyte temperature Θ as follows:

$$C(I_{batt}, \theta) = \frac{K_c C_{0*} \left(1 + \frac{\Theta}{-\Theta_f}\right)^{\epsilon}}{1 + (K_c - 1)\left(\frac{I_{batt}}{I^*_{batt}}\right)^{\beta}} \tag{3.40}$$

where K_c, C_{0*}, Θ_f, ϵ, β, and I^*_{batt} are constant parameters. Note that because of the time frame of most stability studies, it is assumed here that the battery operates at constant temperature.

- The SOC and DOC are modeled as follows:

$$SOC = 1 - \frac{x_1}{C(0, \Theta)} \tag{3.41}$$

$$DOC = 1 - \frac{x_1}{C(I_{avg}, \Theta)} \tag{3.42}$$

where I_{avg} is the average discharge current; and x_1 is a state variable for the battery.

- The internal voltage of battery is represented as:

$$E_m = E_{m0} - K_e(273 + \Theta)(1 - SOC) \tag{3.43}$$

where E_{m0} and K_e are constant parameters provided in [107].

- The nonlinear parameters are modeled as follows:

$$R_0 = R_{00}[1 + A_0(1 - SOC)] \tag{3.44}$$

$$R_1 = -R_{10} \ln(DOC) \tag{3.45}$$

$$R_2 = \frac{R_{20} \exp[A_{12}(1 - SOC)]}{1 + \exp\left(\frac{A_{22} I_m}{I^*_{batt}}\right)} \tag{3.46}$$

$$C_1 = \frac{\tau_{batt}}{R_1} \tag{3.47}$$

$$I_p = V_{PN} G_{p0} \exp\left(\frac{V_{PN}}{v_{p0} + A_p\left(\frac{1-\Theta}{\Theta_f}\right)}\right) \tag{3.48}$$

where τ_{batt} is the time constant of the battery, and I_m and I_p are the currents of the main and the parasitic branches. The parameters R_1 and C_1 are associated with the

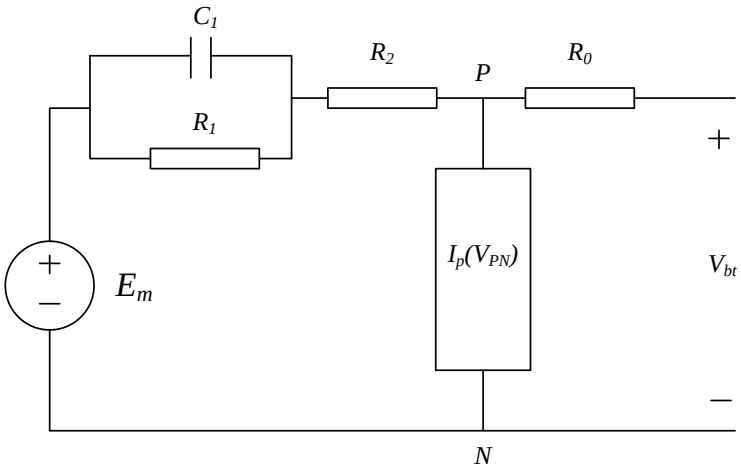

Figure 3.7: Modified BESS model.

battery discharging, and I_p and R_2 are associated with the battery charging. The parameters E_{m0} , K_e, R_{00}, A_0, R_{10}, R_{20}, A_{12} , A_{22}, G_{p0}, V_{p0}, A_p, and Θ_f are constants extracted from [107].

- The dynamic equations of the model are:

$$\dot{x_1} = -I_m \tag{3.49}$$

$$\dot{x_2} = \frac{1}{\tau_{batt}}(I_m - I_p) \tag{3.50}$$

where $x_i \forall i \in \{1, 2\}$ are the state variables of the battery.

3.3 Voltage Stability Model

For static studies, there are three different models of DG units that may be used in stability studies:

- Constant active power P and constant reactive power Q control (PQ model) to represent constant power factor control.
- Constant active power P and constant voltage V control (PV model) to represent voltage control.

- Constant active power P and constant impedance Z (PZ model) to represent lack of output control.

A DG unit can work in one or two of the aforementioned static control models. For example, MTs and diesel generators are modeled here using a PV model, and FCs, BESSs, and photovoltaic DGs are modeled using both PQ and PV models. The behavior of an induction generator in steady-state and at a given speed can be modeled using a constant impedance, and hence the induction generator can be modeled using a PZ model; however, one needs to consider that the speed of the induction generator affects the value of Z.

3.4 Results

All numerical studies presented in this chapter are carried out using PSAT [89]. This software package includes power flow, CPF, optimal power flow, small-perturbation stability analysis, and time-domain simulation tools.

3.4.1 Japanese Test System

The first system used to test and compare the various models is illustrated in Figure 3.8 and is based on a distribution system in the Kumamoto area in Japan [109]. The original system has been modified to connect a 3.125 MW DG unit at Bus 16, since the load at the neighboring Bus 11 is the largest in the system (about 5 to 10 times larger than the rest of the loads). Thus, the test system consists of a DG unit (including prime mover, generator, interface, and associated controllers) with transformer, feeders, and loads, all connected to an infinite bus representing the "main" grid. The heavy load at Bus 11 is tripped in order to study a contingency in the system, which constitutes a significant disturbance for this system. All loads are modeled as constant active and reactive power loads. The network data for this system and the DG parameters are provided in the Appendix.

Voltage Stability Analysis

The CPF yields P-V curves for static voltage stability assessment by increasing the system loading level up to the maximum loadability point at which the system experiences voltage collapse. For the PV model of the DG, Figure 3.9 shows the voltage magnitude at Bus 4 (the bus with the lowest voltage magnitude in the system) for the test system in "normal"

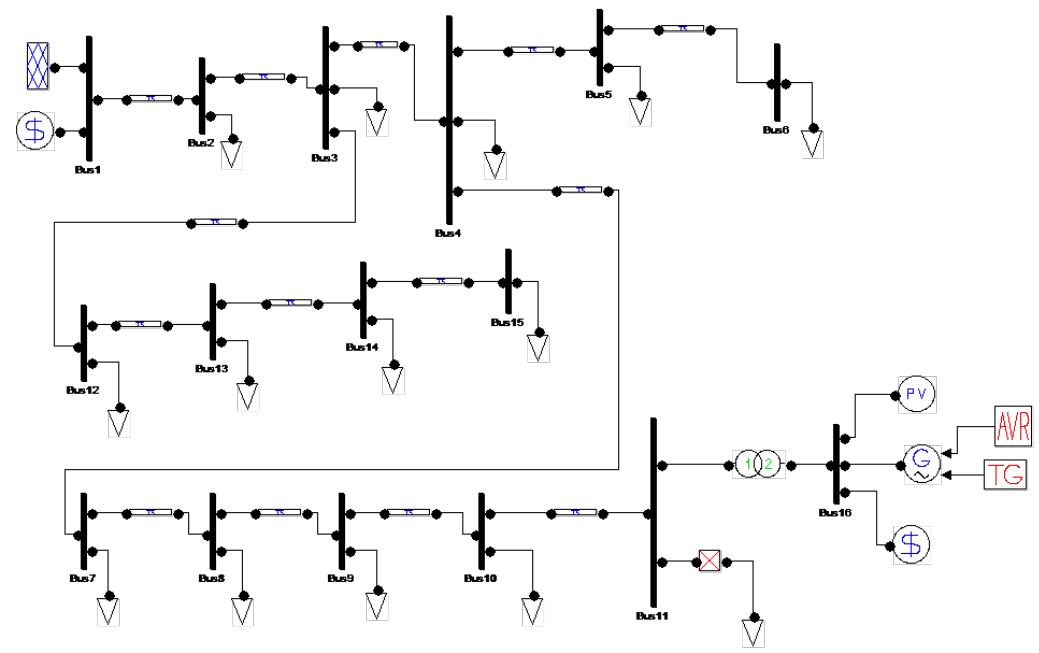

Figure 3.8: Kumamoto, Japan distribution test system from [3].

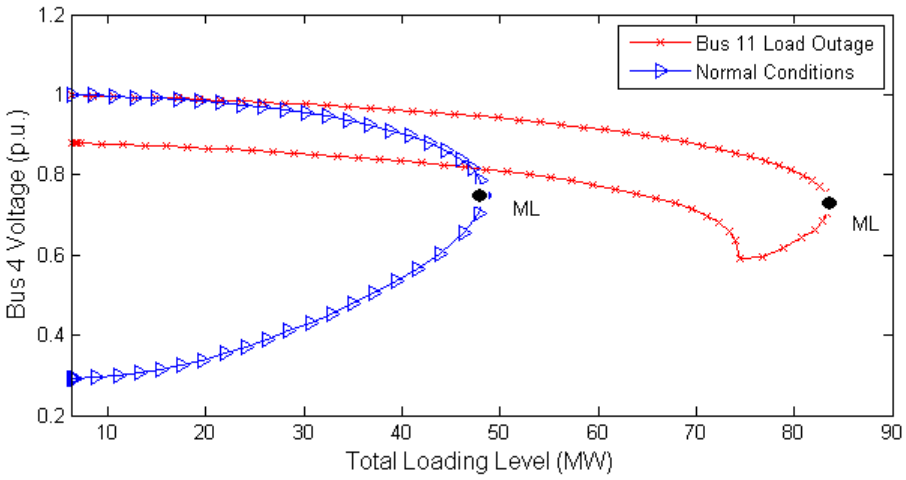

Figure 3.9: P-V curve for the first test system with DG PV model.

and contingency conditions. Observe that the static load margin or maximum load (ML) in the case of normal operating condition is 48.23 MW, while for a Bus 11 load outage this ML is increased to 83.58 MW; this is due to the fact that the system is less stressed when the loads or feeders are tripped, which is a typical contingency in distribution system.

Figure 3.10 shows the comparison of the P-V curves at Bus 4 for PZ, PQ, and PV models of the DG at normal operating conditions. The PV model yields a larger ML than the PQ and PZ models, as expected. With the PQ model, the DG unit injects constant active and reactive power to the system, and there is no direct voltage control. Note that the worst case from the point of view of ML is the PZ model with a capacitor bank at its terminals required for reactive power compensation; in this case, the injected reactive power is proportional to the square of the voltage, and thus the PZ model yields the least ML of all static models.

Small-perturbation Stability Analysis

An eigenvalue analysis is carried out for small-perturbation stability studies. Figures 3.11 and 3.12 show the eigenvalues of the test system with MT and diesel DGs; the most relevant modes of the SG, the excitation system, the MT, and the diesel DG are shown. Note that the governor modes are relatively far away from the imaginary axis, and thus the most critical modes are associated with the SG and AVR. In the case of a load outage at Bus 11, some of the critical eigenvalues of the system move to the left and a few slightly to the

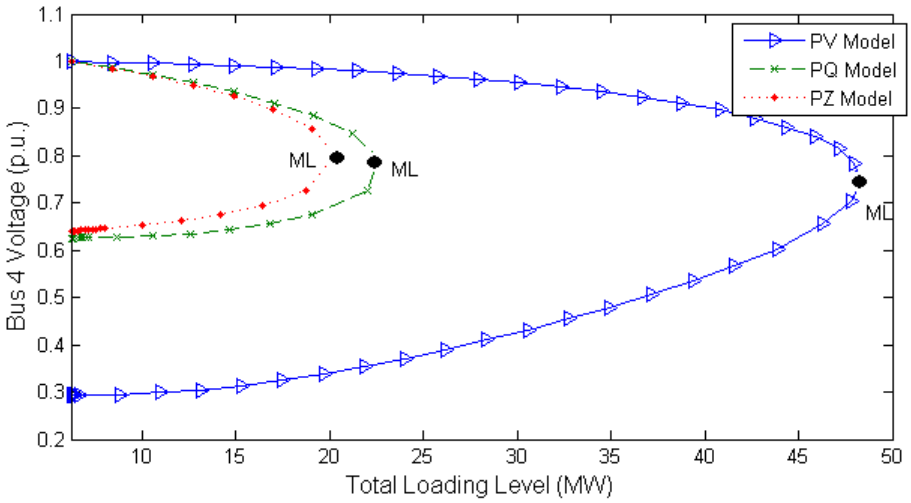

Figure 3.10: P-V curves for different static models for the first test system.

right; thus, in general, the system small-perturbation stability does not change significantly in this case.

Figure 3.13 shows the eigenvalues of the test system with a fixed-speed wind-turbine DG. Note that some eigenvalues of the induction generator are close to the imaginary axis. The load outage does not change significantly the critical eigenvalues of system; this is due to lack of feedback controls in this case.

Figures 3.14, 3.15, and 3.16 show the eigenvalues of the test system with FC, photovoltaic, and BESS DGs in voltage control mode, respectively. Note that because of the instantaneous voltage control through the VSC, the load outage has less effect on the system modes when compared with the rotating electric machines. Note that the eigenvalues of the converter and voltage controller are far away from the imaginary axis, which results in a more stable system.

Transient Stability Analysis

Transient stability studies are performed using time-domain simulations of a given contingency. Figure 3.17 shows a comparison of the voltage magnitude at Bus 11 for a load outage at this bus with a diesel, MT, fixed-speed wind-turbine, FC, BESS, and photovoltaic DGs. In the case of the diesel and the MT DGs, observe that after the trip, the voltage of Bus 11 reaches steady-state after 8 s; since the DG voltage controller tries to keep the

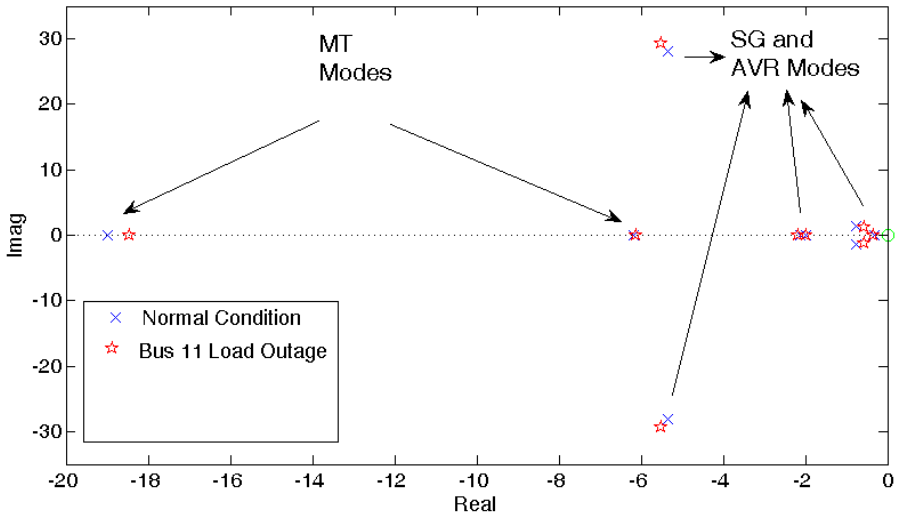

Figure 3.11: Most critical eigenvalues of the first test system with an MT DG.

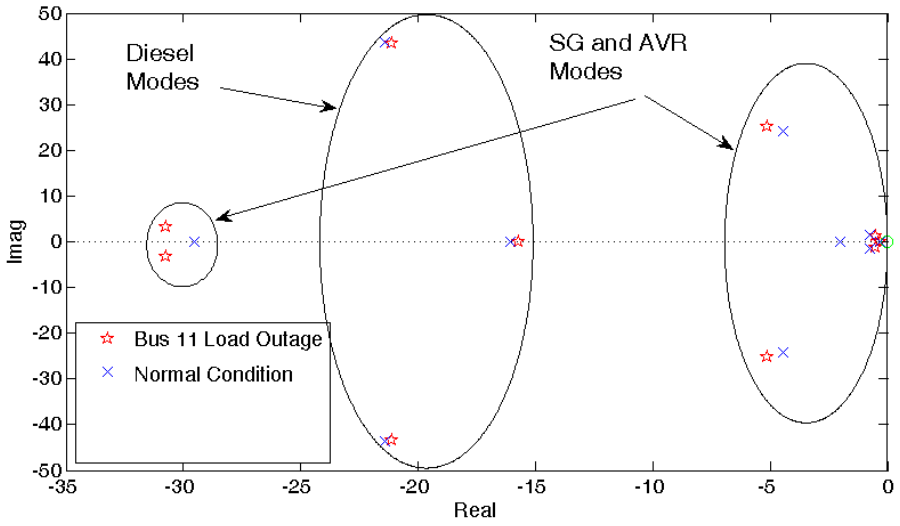

Figure 3.12: Most critical eigenvalues of the first test system with a diesel DG.

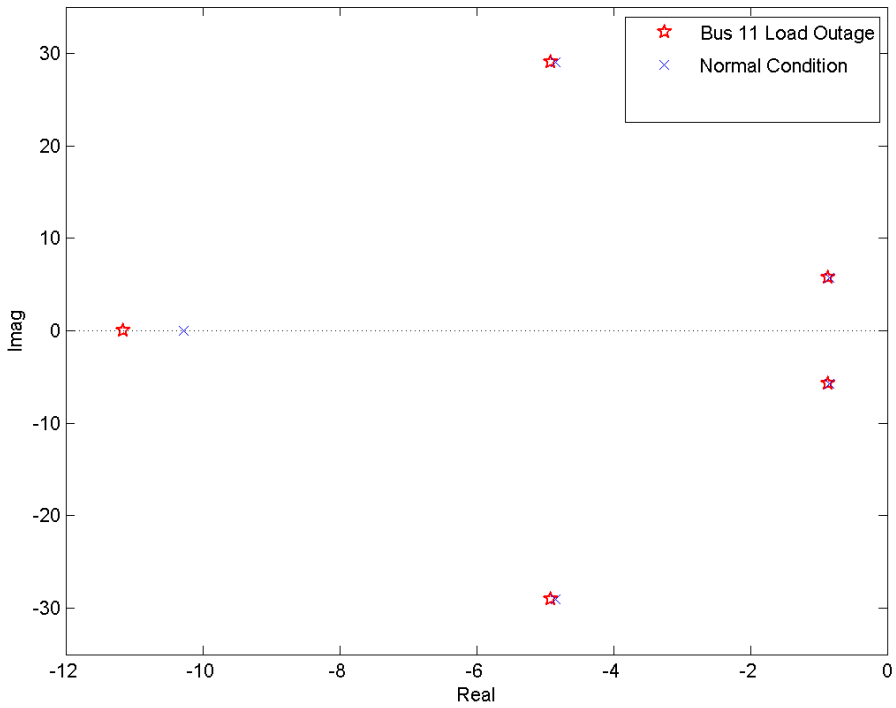

Figure 3.13: Eigenvalues of the first test system with a fixed-speed wind-turbine DG (induction machine modes).

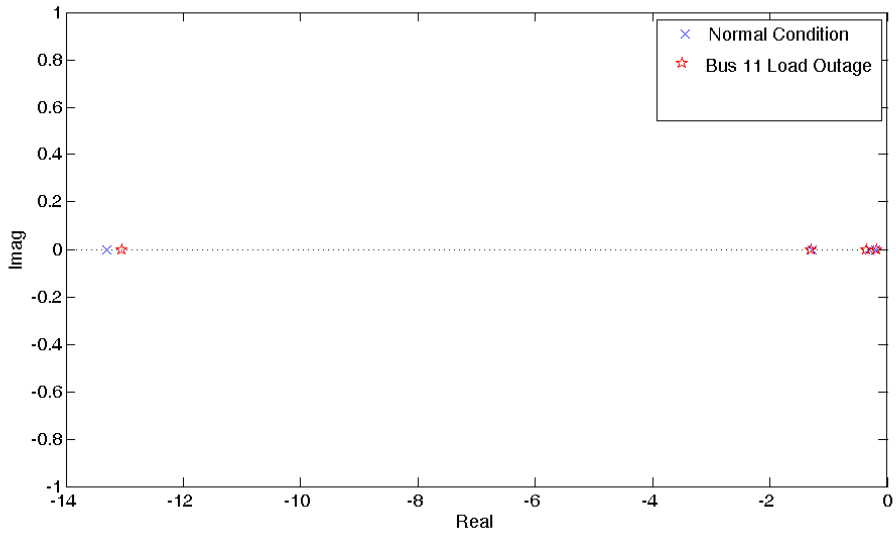

Figure 3.14: Eigenvalues of the first test system with an FC.

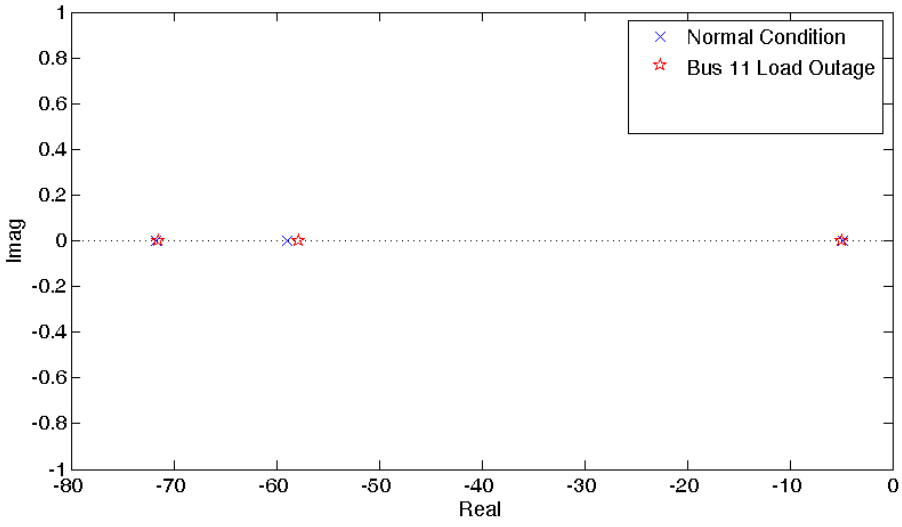

Figure 3.15: Eigenvalues of the first test system with a photovoltaic DG.

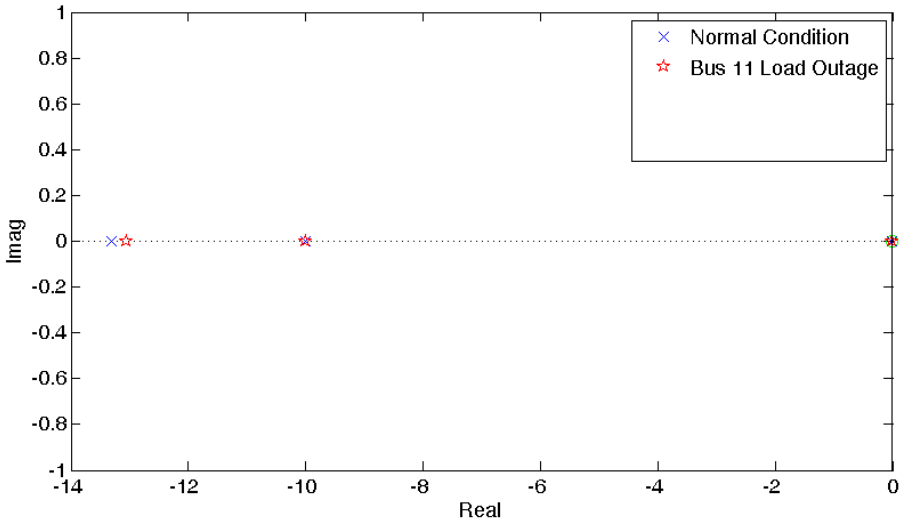

Figure 3.16: Eigenvalues of the first test system with a BESS.

voltage at Bus 16 close to the set point (considering the AVR droop), the injected reactive power decreases. Note the quick response of the FC and photovoltaic DGs in voltage control mode after the contingency, due to the fast PI voltage controllers. Furthermore, as previously shown in the P-V curves, these time-domain simulations demonstrate that the voltage deviations at Bus 11 are less for DGs with PQ control than for the fixed-speed wind-turbine, and are more than the DGs with voltage control, as expected.

Figures 3.18 and 3.19 depict the mechanical P_m and electrical power P_e of the diesel and the MT DGs for a load outage at Bus 11, respectively. Observe that the mechanical power is damped after the load outage. The mechanical damping in the diesel DG is less than in the case of the MT DG .

3.4.2 CIGRE Test System

The developed DG models were also tested on a modified version of CIGRE medium voltage network presented in [110]. A single-line diagram of the 15-bus 10 kV test system is shown in Figure 3.20. The system has a total installed capacity of 3363 kW, and the ratings of DGs are shown in Table 3.1, with typical values being assumed for the DG parameters. In this test system, switch S1 is normally open and switch S2 and S3 are normally closed. The voltage of the MT, diesel, and BESS DGs are set at 1, 0.98, and 0.98 p.u., respectively;

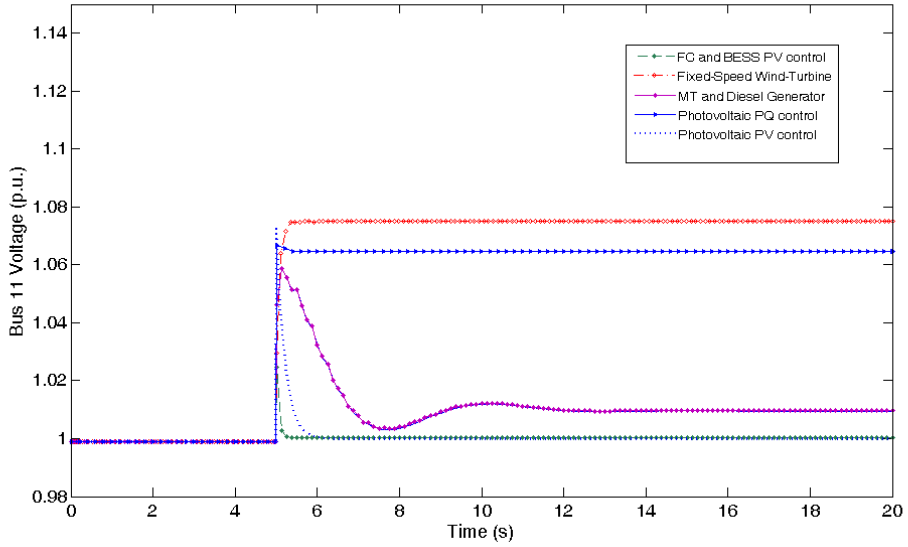

Figure 3.17: Comparison of the time-domain simulations for a load outage at Bus 11 in the first test system with different DGs.

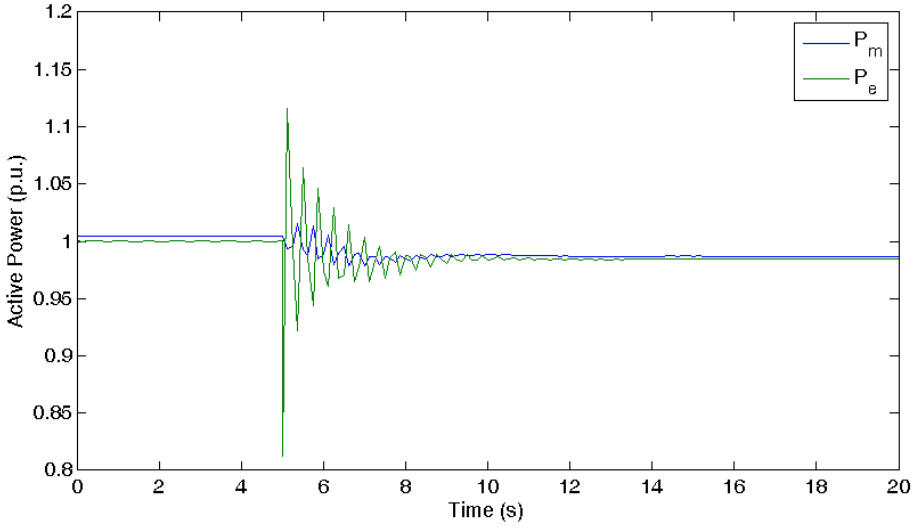

Figure 3.18: Mechanical and electrical power of diesel DG for a load outage at Bus 11 in the first test system.

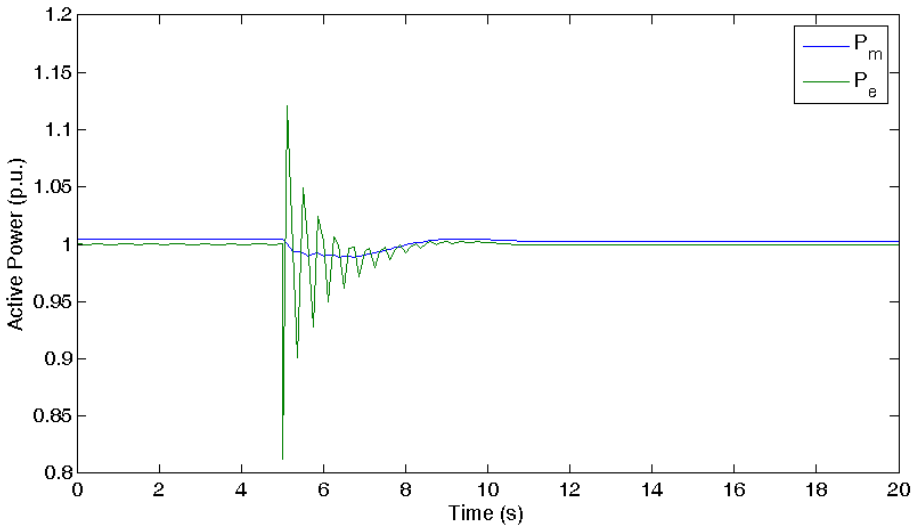

Figure 3.19: Mechanical and electrical power of MT DG for a load outage at Bus 11 in the first test system.

the maximum and minimum reactive power limits for the DGs are set at 0.8 and -0.2 p.u., respectively. The test system and DG parameters are provided in the Appendix.

In order to compare the effects of different DG technologies on the system loadability, the following cases are studied:

- $C1$: This case contains only loads, without any DGs in the system.
- $C2$: In this case, 8 photovoltaic DGs are added to the system as per Table 3.1.
- $C3$: Two FCs are added to $C2$ as per Table 3.1.
- $C4$: A fixed-speed wind-turbine is added to $C3$ as per Table 3.1.
- $C5$: An MT is added to $C4$ as per Table 3.1.
- $C6$: A diesel unit is added to $C5$ as per Table 3.1.
- $C7$: Two BESSs are added to $C6$ as per Table 3.1.

Figure 3.21 shows the P-V curves at Bus 8 for the different test cases. Observe that, as the DG penetration level increases, the maximum loadability of the system increases, as

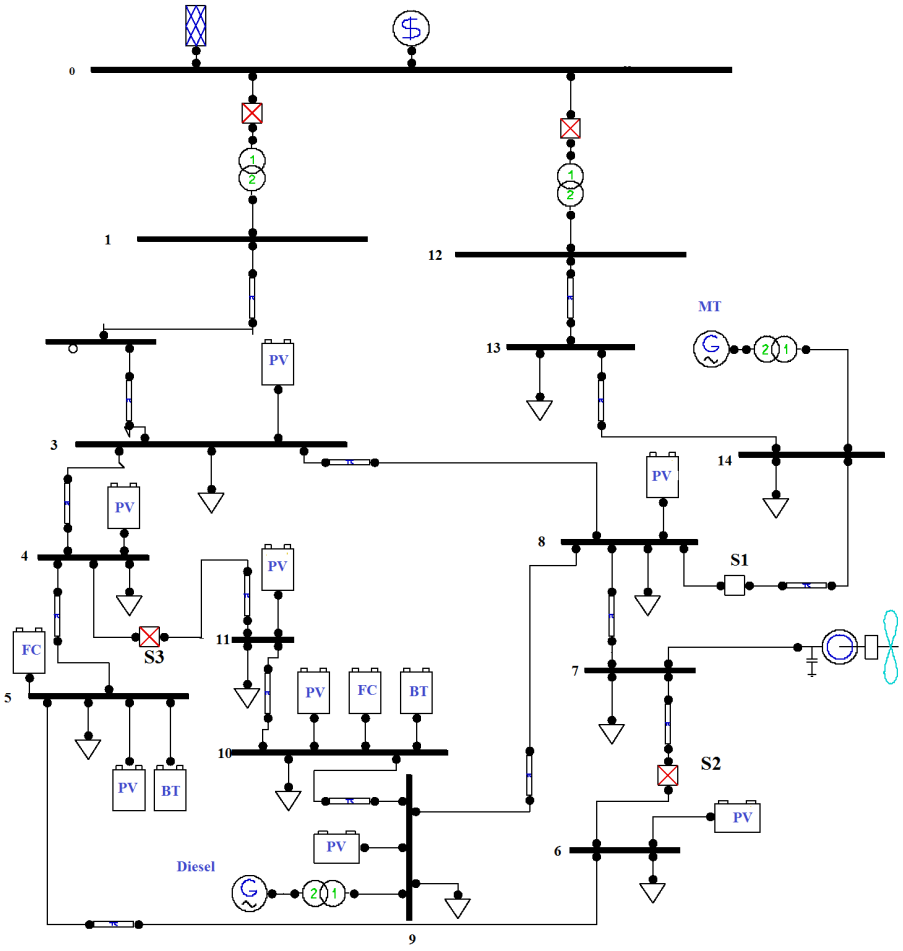

Figure 3.20: Modified CIGRE microgrid benchmark.

Table 3.1: CIGRE microgrid test system DGs ratings

Node	DG type	P_{max} [kW]
3	Photovoltaic	20
4	Photovoltaic	20
5	Photovoltaic	30
5	BESS	600
5	FC	33
6	Photovoltaic	30
7	Wind turbine	1500
8	Photovoltaic	30
9	Photovoltaic	30
9	Diesel generator	500
10	Photovoltaic	40
10	BESS	200
10	FC	14
11	Photovoltaic	10
14	CHP MT	310

expected. It is worth noticing that the maximum loadability of the system will be limited in practice by voltage limits. Table 3.2 shows the maximum power loadabilities associated with LIBs and voltage limits of the DGs for the different test cases. Figure 3.22 illustrates the P-V curves at Buses 3, 6, 8 and 10; observe that the voltage magnitude at Bus 3 is relatively higher than those of Buses 6, 8, and 10, due to being closer to the main grid.

Figure 3.23 shows the eigenvalues of the test system for $C7$ for the base case. Observe that all eigenvalues of the system are on the left-half of the complex plane and thus the system is stable. Note that as the load increases, the DGs may reach reactive power and voltage limits, which affect the eigenvalues of the system. Figures 3.24 depicts the system eigenvalues for $C7$ for a loading level of 1.68 p.u. associated with voltage limits. Observe that some of the critical eigenvalues of the system move to the right and a few slightly to the left; in this case, some DGs also reach reactive power limits and hence operate in PQ control, resulting in a less stable system, in general.

Figure 3.25 illustrates the critical eigenvalues of the system for $C7$ for a loading level of 2.98 p.u., where the critical eigenvalues cross the imaginary axis and thus the system experiences a Hopf bifurcation.

A three-phase-to-ground fault of short-duration at Bus 8 is considered as a contingency for the test system. The simulation time is 20 s, and the fault occurs at $t = 10$ s. Figures

Table 3.2: Maximum active power loadability of the CIGRE microgrid test system for different test cases.

Case	Maximum active power loadability associated with LIBs (p.u.)	Maximum active power loadability associated with voltage limits (p.u.)
$C1$	3.523	1.3448
$C2$	3.536	1.3449
$C3$	3.542	1.3450
$C4$	3.700	1.5161
$C5$	3.701	1.5845
$C6$	3.771	1.5846
$C7$	3.868	1.6779

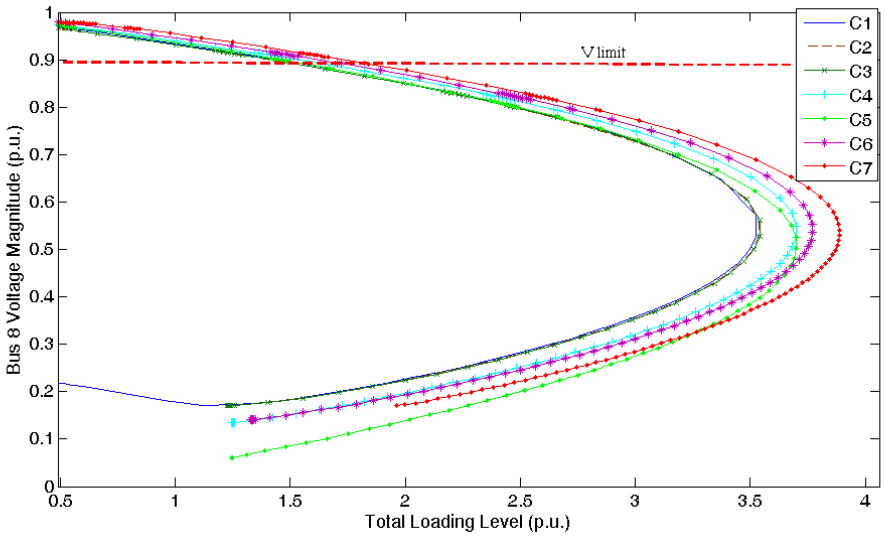

Figure 3.21: P-V curves at Bus 8 of the CIGRE microgrid test system for different test cases.

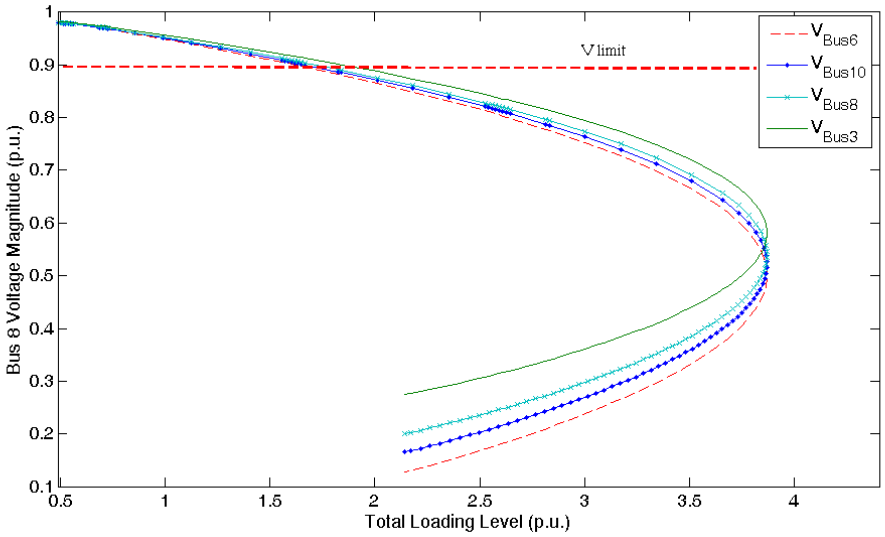

Figure 3.22: P-V curves at Buses 3, 6, 8 and 10 of the CIGRE microgrid test system for $C7$.

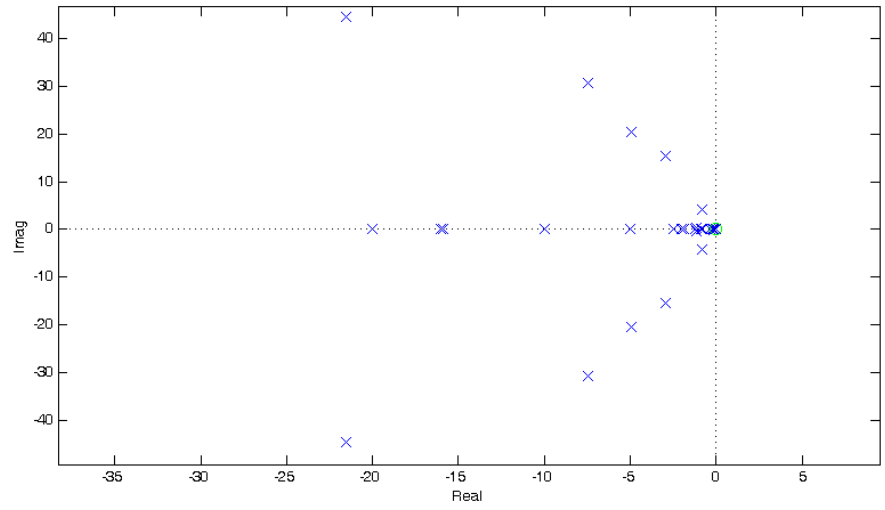

Figure 3.23: Eigenvalues of the CIGRE microgrid test system for $C7$ at the base case.

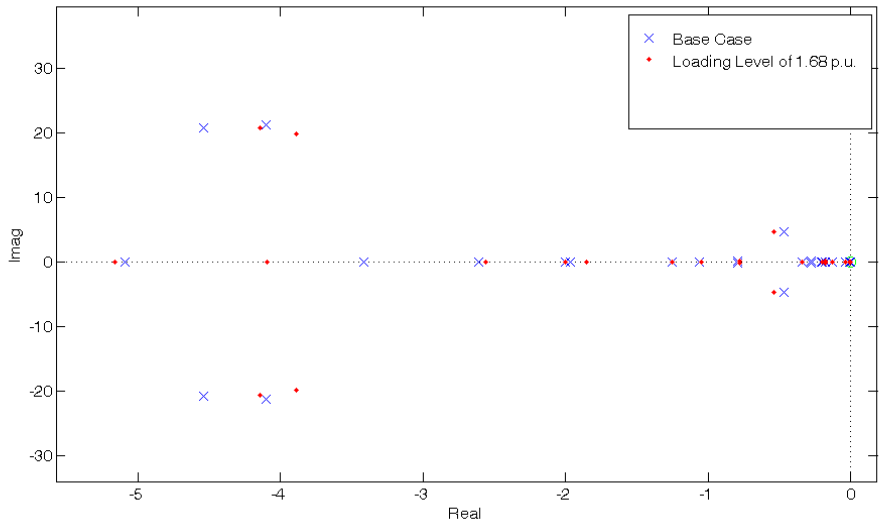

Figure 3.24: Eigenvalues of the CIGRE microgrid test system for $C7$ at a loading level of 1.68 p.u.

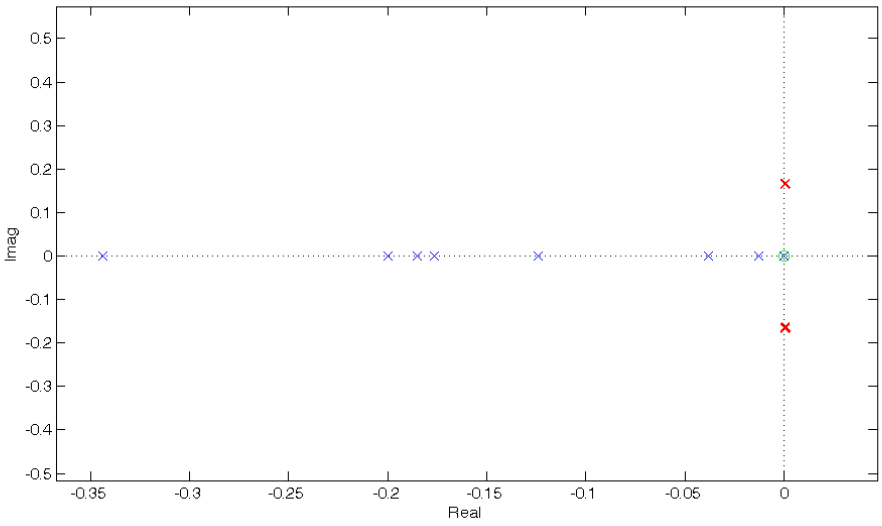

Figure 3.25: Eigenvalues of the CIGRE microgrid test system for $C7$ at a loading level of 2.98 p.u.

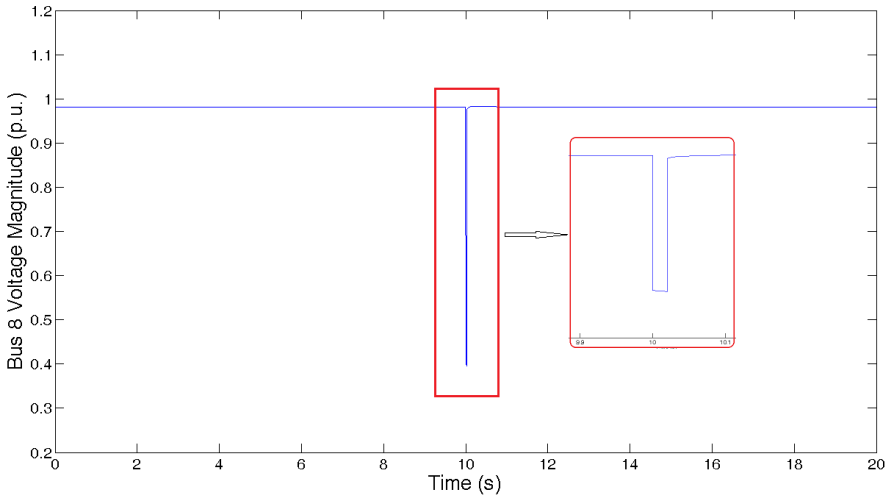

Figure 3.26: Transient behavior of the voltage magnitude at Bus 8 for the CIGRE microgrid test system.

3.26, 3.27, 3.28, and 3.29 illustrate the transient behavior of various DGs for $C7$. Observe that the voltage magnitude quickly recovers due to the fast voltage regulators of the inverter-based DGs. Furthermore, the speed of MT is damped after 2 s, while that of the induction generator is damped after 4 s; this is due to lack of a controller for the induction generator.

3.5 Summary

In this chapter, the static and the dynamic models of different DGs for stability studies of balanced distribution systems were presented. These models include the dynamic models of the primary governor, generators, and their interfaces. The proposed diesel, MT, FC, fixed-speed wind-turbine, BESS, and photovoltaic models were implemented and tested in PSAT.

The DG models were tested and compared using two realistic distribution systems with multiple DGs to study their static and dynamic behaviors. The comparison of P-V curves for different static DG models showed , in general, that PV control yields more loading margin than PQ and no controls. Thus, fixed-speed wind-turbine DGs are the worst from the point of view of voltage stability. Furthermore, it was observed that the best DG

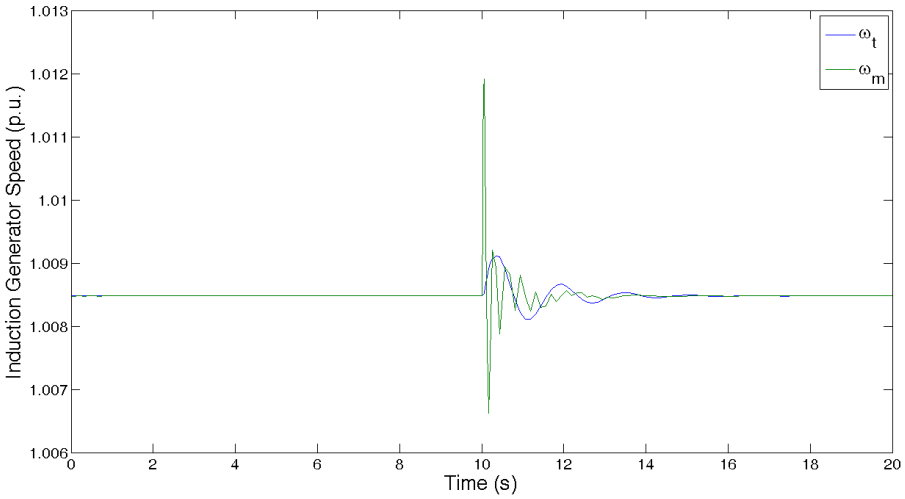

Figure 3.27: Wind turbine and mechanical induction generator speed for the CIGRE microgrid test system.

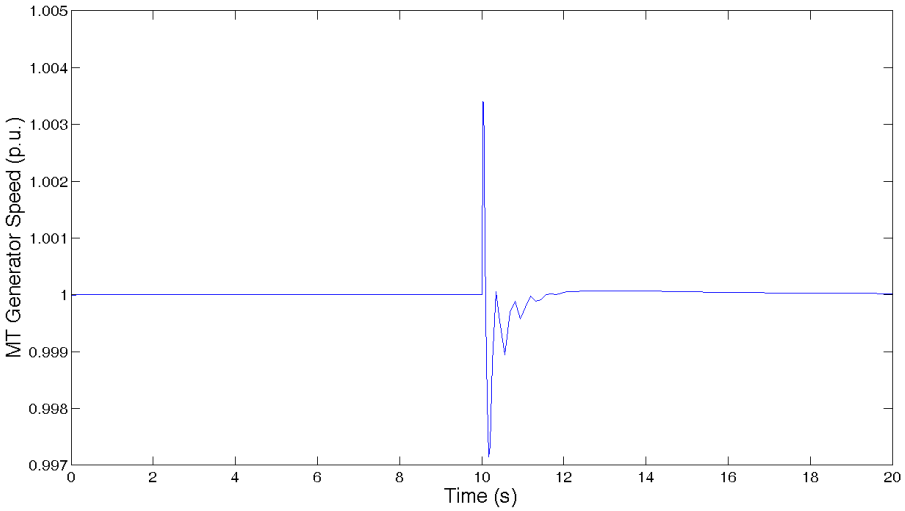

Figure 3.28: MT generator speed for the CIGRE microgrid test system.

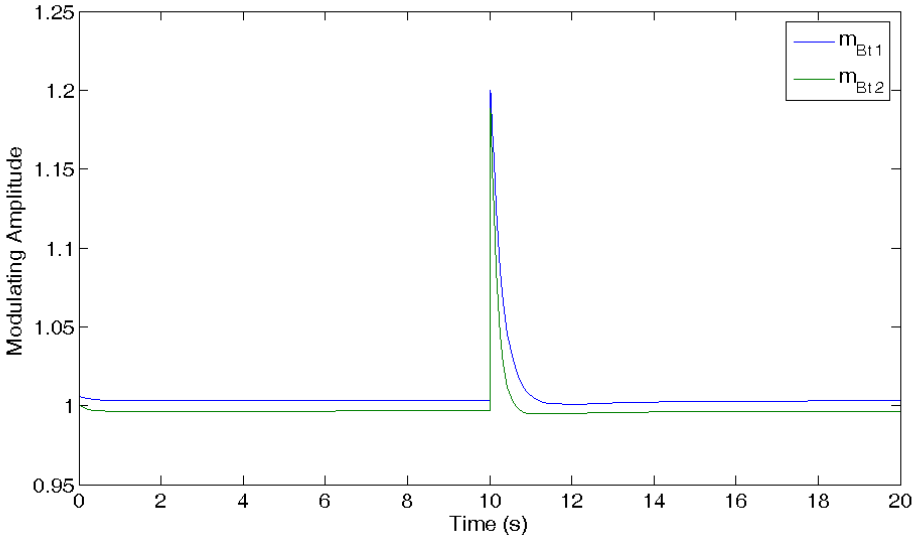

Figure 3.29: Modulating signal amplitude of the BESS inverters for the CIGRE microgrid test system.

response in the case of a typical load/feeder contingencies is that of inverter-based DGs, which can be considered a general conclusion of this work.

Chapter 4

Unbalanced Diesel Generator Stability and Control

4.1 Introduction

This chapter presents comprehensive studies on voltage, small-perturbation, and transient stability of unbalanced distribution systems with SG-based DGs. Both dynamic and static voltage stability analyses are carried out using three-phase P-V curves and maximum system loadability. Transient stability studies are performed using time-domain simulations of contingencies under various unbalanced conditions, based on three-phase detailed models. Small-perturbation stability studies are carried out using a model identification approach to compute eigenvalues and thus study the impact of load unbalancing in heavily loaded systems. Finally, control strategies based on a novel UVS are proposed to improve the stability of unbalanced distribution systems with SGs, using time-domain simulations and eigenvalue analysis to demonstrate their effectiveness. A simple grid, feeder, and load test system is used to better understand and explain stability issues associated with unbalanced SGs.

4.2 Three-phase Models

A detailed representation of the SG model is used here for simulations and studies [90]; hence, three-phase stator and rotor windings in the *dqo* reference frame are used [80]. Since small SG-based DGs are very likely to have simple PI voltage regulators, AVRs Type II

(AC4A [90]) are used here. Moreover, considering that the type of voltage feedback in the excitation system affects the dynamic behavior of the SG [111], a typical voltage feedback represented by the average value of the voltage magnitude for each phase is used in this thesis [90].

Lines are modeled as constant coupled impedance branches, and loads are treated as constant impedances, since the loads are not connected to the medium-voltage grid through voltage-regulated transformers, and most loads are assumed in practice not to be drive-controlled motors. Therefore, the following loading factor l is defined to model load impedance Z_l increases in each phase, which increase the active and reactive power demand:

$$Z_l = \frac{Z_\phi}{l} \tag{4.1}$$

where Z_ϕ is the base-load impedance for each phase. A load unbalance factor is defined to analyze different unbalanced scenarios as the load varies [62]. Thus, as the impedance of the load in one phase is increased, the load impedance in another phase is decreased, so that total impedance of the three-phase load remains constant in all cases, as follows:

$$Z_{al} = (1 + k)Z_l \tag{4.2}$$

$$Z_{bl} = Z_l \tag{4.3}$$

$$Z_{cl} = (1 - k)Z_l \tag{4.4}$$

where k is the load unbalance factor, and Z_{al}, Z_{bl}, and Z_{cl} are the phase impedances of the load.

All time-domain simulations in this chapter are carried out in PSCAD/EMTDC [90] with detailed representation of generators, controllers, loads, and lines.

4.3 Analysis Methodology

4.3.1 Voltage Stability Studies

As discussed in Chapter 2, it is common practice to carry out loadability studies using P-V curves [84]. The continuation power flow yields these curves for voltage stability assessment by increasing the system loading level up to a maximum loadability point at which the system becomes unstable. Hence, in this chapter, both dynamic and static analyses are carried out using the P-V curves and maximum loadability computations. However, static voltage stability studies are based on *three-phase* power flows; hence, the static maximum

loadability is associated with a loading level at which there is no three-phase power flow solution.

Dynamic voltage stability studies are carried out using time-domain simulations in PSCAD/EMTDC, based on the detailed dynamic models of SGs and their voltage regulators. Since the generator is assumed to operate as a voltage source for the initial point of time-domain simulations, if the difference between the steady-state condition and the initial point is too large, it may lead to numerical instability. Thus, the initial variables of the generator (e.g., terminal voltage phase) are calculated using a static three-phase power flow, which are then used in PSCAD/EMTDC as the initial point for simulations.

Since the results of time-domain simulations under steady-state conditions are needed for loadability studies, voltage and active and reactive powers should be in steady-state conditions. Hence, the results of time-domain simulations after a long settling time (20 s in this chapter) are used to obtain dynamic P-V curve points, which may be different from the static P-V curves, since the static models are just approximations of the dynamic ones.

Three-phase power flow calculations are based on node voltages and branch currents. For each series element (e.g., transmission line, transformer, etc.) connecting two nodes, the node voltages and branch currents at each end can be represented by the following equation [112]:

$$\begin{bmatrix} V_a \\ V_b \\ V_c \\ I_a \\ I_b \\ I_c \end{bmatrix}_s = \begin{bmatrix} [A] & [B] \\ [C] & [D] \end{bmatrix}_l \begin{bmatrix} V_a \\ V_b \\ V_c \\ I_a \\ I_b \\ I_c \end{bmatrix}_r = [ABCD]_l \begin{bmatrix} V_a \\ V_b \\ V_c \\ I_a \\ I_b \\ I_c \end{bmatrix}_r \tag{4.5}$$

where $[ABCD]_l$ is the three-phase equivalent ABCD-parameter matrix of the series element; V_a, V_b, V_c are line-to-ground voltage phasors; and I_a, I_b, I_c are line current phasors. Based on the π-model of feeders depicted in Figure 4.1, the three-phase ABCD-parameter matrices of the feeders can be calculated as follows:

$$[A] = I_3 + \frac{1}{2}[Z_{abc}][Y_{abc}] \tag{4.6}$$

$$[B] = [Z_{abc}] \tag{4.7}$$

$$[C] = [Y_{abc}] + \frac{1}{4}[Y_{abc}][Z_{abc}][Y_{abc}] \tag{4.8}$$

$$[D] = I_3 + \frac{1}{2}[Z_{abc}][Y_{abc}] \tag{4.9}$$

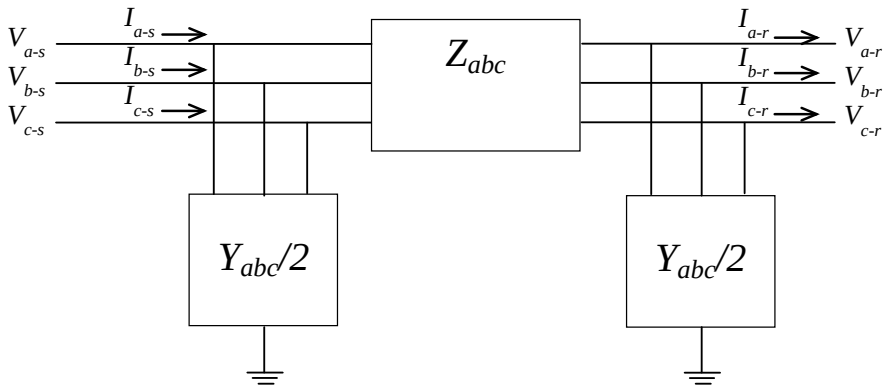

Figure 4.1: Series element π-model.

where I_3 is the 3×3 identity matrix. Matrices $[Z_{abc}]$ and $[Y_{abc}]$ in (4.6)-(4.9) can be approximated from the sequence-reference-frame diagonal impedance matrices $[Z_{seq}]$ and $[Y_{seq}]$, respectively, as follows:

$$[Z_{abc}] = [A]\,[Z_{seq}]\,[A]^{-1} \tag{4.10}$$

$$[Y_{abc}] = [A]\,[Y_{seq}]\,[A]^{-1} \tag{4.11}$$

where

$$[A] = \begin{bmatrix} 1 & 1 & 1 \\ 1 & a^2 & a \\ 1 & a & a^2 \end{bmatrix}; a = 1\angle 120^\circ \tag{4.12}$$

SGs can be modeled as a special case of series elements connecting the internal bus voltages to terminal voltages through a series impedance [51]. The series impedance of a generator in the *abc* reference-frame can be calculated from the sequence-reference-frame impedances as shown previously, where sequence impedances are obtained from machine parameters [113]. Internal bus voltages are assumed to be balanced, which is modeled using the following equations:

$$|E_a| = |E_b| = |E_c| \tag{4.13}$$

$$E_a + E_b + E_c = 0 \tag{4.14}$$

It is important to note that the (4.13) and (4.14) also hold for a negative-sequence voltage, and a reasonable starting point for variables E_a, E_b, and E_c ensures convergence

to a positive-sequence internal voltage. For modeling PV-buses, the power injected by a particular generator is assumed fixed, as follows:

$$Re\left\{ \begin{bmatrix} V_a & V_b & V_c \end{bmatrix}_G \begin{bmatrix} I_a \\ I_b \\ I_c \end{bmatrix}_G \right\} = P_G \tag{4.15}$$

Additional relations imposed by impedance loads are:

$$\begin{bmatrix} V_a \\ V_b \\ V_c \end{bmatrix}_{Load} = [Z_{Load}] \begin{bmatrix} I_a \\ I_b \\ I_c \end{bmatrix}_{Load} \tag{4.16}$$

where Z_{Load} is a diagonal matrix, with the phase-to-ground load impedances in the diagonal.

The power flow equations are completed by applying KCL at each node of the system. For small systems, this set of nonlinear equations can be readily implemented in Matlab [114], and solved within reasonable computational times using the `fsolve` function with different robust numerical algorithms (e.g., Trust-region and Levenberg-Marquardt).

4.3.2 Transient Stability Studies

In this chapter, as explained in Chapter 2, transient stability studies are based on CCT. This index can be used for comparative system stability analyses, as different contingencies yield different CCTs and the larger this value is, the more stable the system is. In this chapter, three-phase-to-ground faults are considered as the contingencies.

4.3.3 Small-Perturbation Stability Studies

As explained in Chapter 2, eigenvalue analysis of the system state matrix is one of the common tools for small-perturbation stability studies. In the context of power systems, several simplifications such as system modeling under balanced conditions are applied. Thus, the system is usually modeled with single-phase equivalents, so that small-perturbation stability analysis of a balanced power system can be normally carried out by the linearization of the power system model around an equilibrium point. Many commercial programs use phasor models for small-perturbation stability studies, and assume a specific equilibrium point under steady-state conditions. In the case of unbalanced condition, equilibrium points are

non-stationary with respect to the angular velocity of the SGs, since the generator velocity is sinusoidal under steady-state conditions; hence, standard phasor-based linearization techniques are not applicable in this case [62].

There are two approaches for small-perturbation stability studies under unbalanced conditions: a model based approach, and a modal estimation approach [62, 115]. In this chapter, small-perturbation stability analyses are performed using modal estimations, in particular, the Prony method and the Steiglitz-McBride iteration method explained in Chapter 2, based on time-domain simulations.

As mentioned in Chapter 2, PSCAD/EMTDC provides data to analyze the dynamics of the system, which is then used here in an appropriate modal estimation method, i.e., Steiglitz-McBride iteration and Prony, to estimate the system eigenvalues. The conventional Prony method available in Matlab is used in this thesis [114]. In the studies presented in this chapter, the generator speed from time-domain simulations is used as a signal for the modal estimation method. The Prony method is suitable for transient stability studies with high signal to noise ratio (SNR). Figure 4.2 shows a comparison of the measured data and the estimated signal by Prony and Steiglitz-McBride iteration methods with a large disturbance for the test system discussed in Section 4.5.1. However, when the system becomes unstable, the Prony method cannot follow the signal properly; in this case, the Steiglitz-McBride iteration method has better performance. Figure 4.3 presents a comparison of the measured data and the estimated signal by Prony and Steiglitz-McBride iteration methods when the system is unstable; note that the Steiglitz-McBride iteration method fits the signal well, while the Prony method is unable to extract the true poles of the signal when the system is unstable.

Since the length of the output data of the time-domain simulation is too long (e.g., 20000 points in a 10 s simulation), it is assumed that the signal is divided in sets of 0.5 s window data, with each set of data being then used in the identification methods to estimate the signal, yielding a number of poles and zeros. Based on the nature of the signal and using mean-square-errors, the number of poles was set to 8 here.

4.4 Unbalanced Voltage Stabilizer

When a system is more heavily loaded, it can become unstable as unbalancing increases and the critical poles cross the imaginary axes, as discussed in Section 4.5.4. Since this results in oscillatory modes, a novel and simple UVS is proposed here to mitigate these oscillations, integrating it with the generator voltage regulator to provide an auxiliary stabilizing signal.

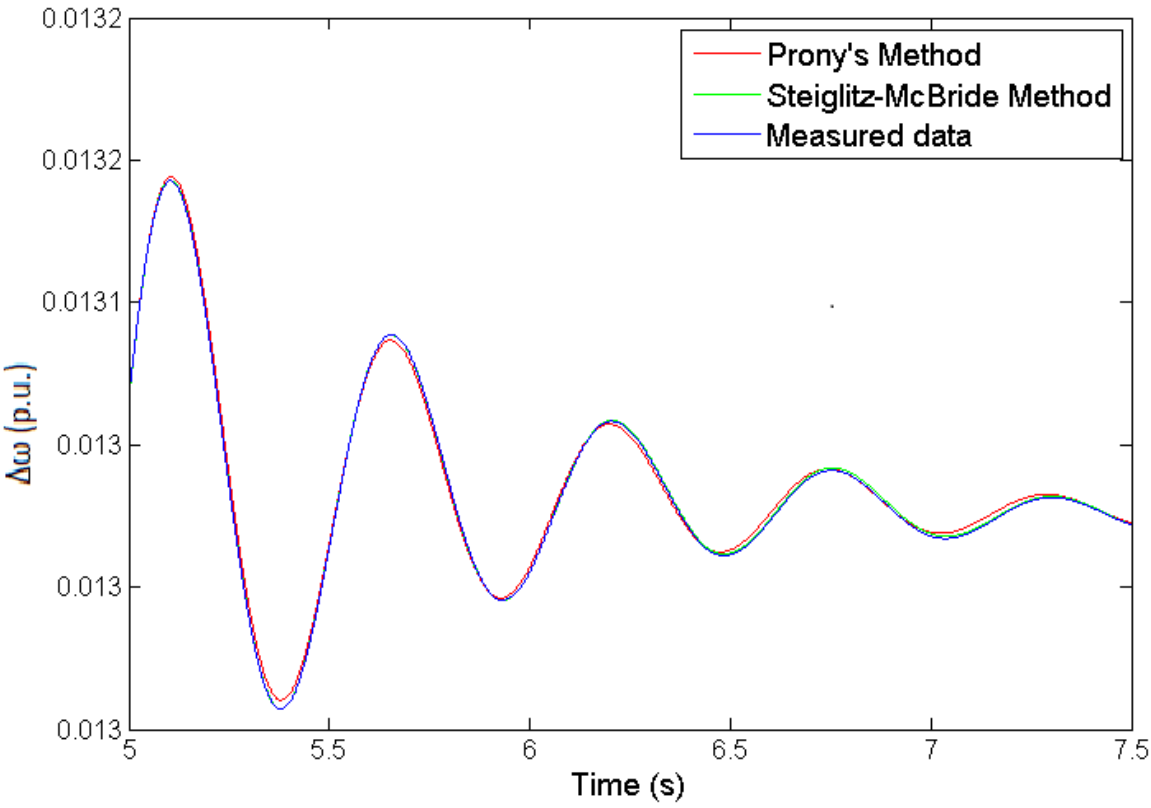

Figure 4.2: Measured data and estimated signal with a large disturbance for the test system discussed in Section 4.5.1.

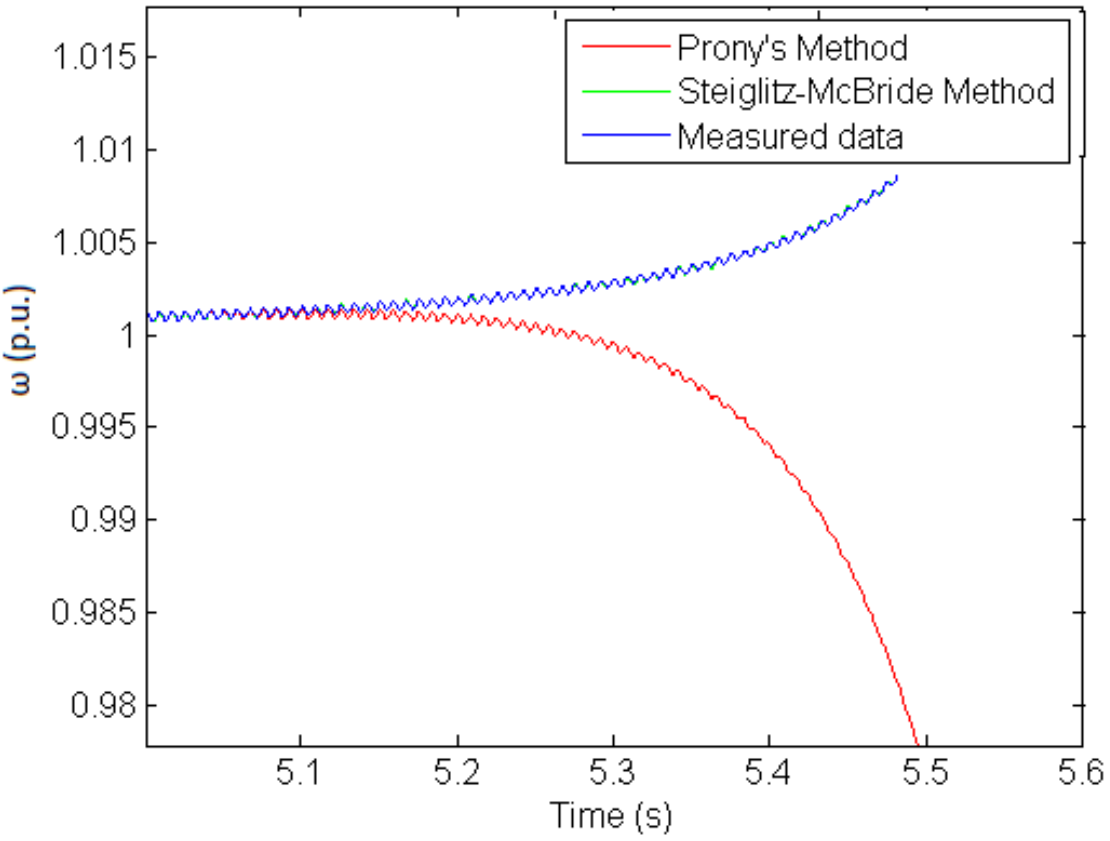

Figure 4.3: Measured data and estimated signal when the test system of Section 4.5.1 is unstable.

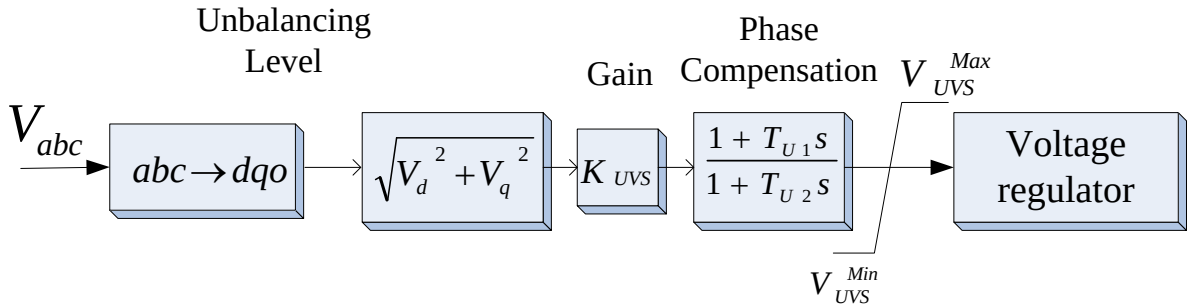

Figure 4.4: Block diagram of the proposed UVS for SG-based DG units.

Figure 4.4 shows the proposed UVS for SG-based DGs. This UVS provides a damping torque component when the system is unbalanced. Hence, the input signals used here are the voltage magnitudes in all phases; these are then converted to the *dqo* reference-frame based on:

$$\begin{bmatrix} V_d \\ V_q \\ V_o \end{bmatrix} = \begin{bmatrix} \cos(\theta) & \cos(\theta - 120) & \cos(\theta - 240) \\ \sin(\theta) & \sin(\theta - 120) & \sin(\theta - 240) \\ \frac{1}{2} & \frac{1}{2} & \frac{1}{2} \end{bmatrix} \begin{bmatrix} v_a \\ v_b \\ v_c \end{bmatrix} \tag{4.17}$$

For $\theta = 0$, the transformation $\sqrt{V_d^2 + V_q^2}$ can be used to reflect the degree of unbalance, since as the unbalance increases, the output signal increases as well. The gain K_{UVS} determines the damping factor provided by the UVS, and the first-order phase compensation block provides appropriate phase lead to compensate for the phase lag between the voltage regulator input and the generator electrical torque. The limits V_{UVS}^{max} and V_{UVS}^{min} constrain the output signal, which is an auxiliary negative-feedback signal for the voltage regulator, based on the fact that by decreasing the generator terminal voltages, the load demand decreases, thus reducing the system stress as demand and unbalance increase. Therefore, stability can be improved as the load increases with the proposed UVS.

The tuning of the UVS parameters would be similar to that of the power system stabilizer in power systems. Thus, the gain K_{UVS} should be set to guarantee system stability, since if this gain is tuned improperly, the system may be unstable, and the time constants should be selected to compensate for the phase lags of the system. The UVS parameter values used here are provided in the Appendix.

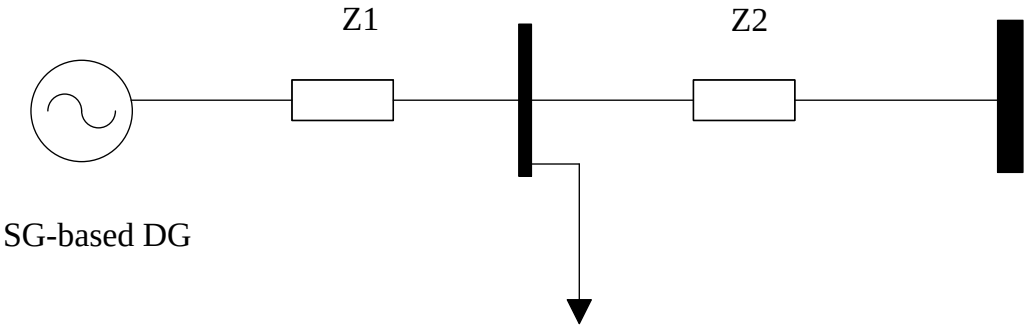

Figure 4.5: A simple grid, feeder, load and DG test system.

4.5 Results

4.5.1 Test System

The distribution system in the Kumamoto area in Japan from [109] described in Chapter 3, is used to develop the simplified test system depicted in Figure 4.5. This simple test system can be used to represent distribution systems in Canada and Brazil where there is a single SG-based DG, as is the case of the sugarcane facilities in Brazil [116] and remote feeders in Ontario [117]. This system is also useful to better understand and explain stability issues associated with unbalanced DGs. Thus, the system comprises an SG unit, feeders and load, all connected to an infinite bus representing the main grid. In order to study a contingency in the system, short-duration three-phase faults close to the load, with some impedance to ground, are simulated.

The load is modeled as constant impedance, based on rated voltage and active and reactive powers; in the base case, the active and reactive powers are $P_{Load} = 3$ MW, and $Q_{Load} = 1$ Mvar, respectively. Because of the low voltage at the load bus at high loading levels, a balanced capacitor bank is connected at the load bus; the reactive power of the bank for the base case is $Q_{cap} = 0.7$ Mvar, and increases linearly with the loading factor l. All test system parameters are given in the Appendix.

4.5.2 Voltage Stability Analysis

The SG and slack bus (main grid) are assumed to share the injected power inversely proportional to the line impedances Z_1 and Z_2 as the load is increased, considering limits on

SG active power. Table 4.1 shows the comparison of the maximum active power loadability, and loading factor for different unbalanced conditions obtained with three-phase power flows and time-domain simulations for the SG-based DGs. Table 4.2 shows the maximum loadability and the voltage magnitude in phases a, b, and c for different realistic unbalanced conditions for the SG. Observe from Table 4.1 and 4.2 that when the system unbalancing increases, the maximum loadability of the system decreases. Also, the difference between the maximum loading factors obtained from the static and dynamic studies arise because of the effects of detailed modeling of generator and voltage regulator on time-domain simulations. The system becomes unstable due to eigenvalues crossing the imaginary axes, as discussed in detail in Section 4.5.4, which cannot be observed in power flow studies.

Figure 4.6 illustrates the voltage magnitude at the load under balanced and unbalanced conditions, and Figure 4.7 depicts the P-V curve under balanced and unbalanced condition for $k = 20\%$ for the SG. Observe that the voltage magnitude in phase b is close to the voltage magnitude for the balanced condition, and the voltage magnitudes of phases c and a are greater and less than that of phase b, respectively, as expected. The voltage magnitude in phase c is relatively high, which is due to the capacitor bank. Note that since the loads are modeled based on constant impedances, the maximum power for the system does not necessarily correspond to the maximum loading factor, due to the active and reactive powers being proportional to the square of the voltage and the loading factor. It is worth noticing that the maximum loadability of the system will be limited in practice by voltage limits.

Table 4.3 shows the voltage magnitude difference in phases a, b, and c for various values of k with respect to the voltage magnitude in balanced conditions for the base loading factor (i.e., $l = 1$ p.u.). Observe that the voltage difference increases as the system unbalance increases. Also, the difference in phase a is greater than that in phases c and b, due to the impedance model of the load.

4.5.3 Transient Stability Analysis

Three-phase-to-ground faults of short-duration and close to the load are considered as contingencies for the SG. The simulation time is 20 s, and the fault occurs at $t = 3$ s. Figure 4.8 illustrates the CCT of the test system with the SG for different values of k for the base loading factor (i.e., $l = 1$ p.u.). Observe that the CCT decreases as the unbalance increases, decreasing by 30% for the SG as k increases from 0% to 25%. It should be noted that, as the load increased, it was observed that the CCT remained unchanged, due to the fact that the DG is at its maximum power output at base load.

Table 4.1: Maximum active powers and loading factors for different unbalanced conditions for static three-phase power flow and time-domain simulations with SG.

$k(\%)$	Maximum loading factor (p.u.)		Maximum active power loadability (p.u.)	
	Time-domain simulations	Three-phase power flow	Time-domain simulations	Three-phase power flow
0	2.2	2.24	0.692	0.6925
5	2.2	2.24	0.692	0.6925
10	2.2	2.22	0.691	0.6923
15	2.2	2.22	0.691	0.6917
20	2.15	2.20	0.689	0.6912
25	2.1	2.18	0.687	0.6903

Table 4.2: Maximum active power and voltage magnitude in all phases for different unbalanced conditions with SG.

$k(\%)$	Maximum active power loadability (p.u.)	V_a(p.u.)	V_b(p.u.)	V_c(p.u.)
0	0.692	1.0089	1.0089	1.0089
5	0.692	0.9836	1.0076	1.0337
10	0.691	0.9554	1.0058	1.0558
15	0.691	0.9199	0.9985	1.0709
20	0.689	0.9050	1.0172	1.1097
25	0.687	0.8826	1.0292	1.1310

Table 4.3: Difference in voltage magnitude in all phases for different unbalanced conditions with SG.

$k(\%)$	ΔV_a(p.u.)	ΔV_b(p.u.)	ΔV_c(p.u.)
5	-0.0168	0.0049	0.011
10	-0.034	0.010	0.023
15	-0.0522	0.0175	0.0348
20	-0.0711	0.0252	0.0462
25	-0.0912	0.0341	0.0578

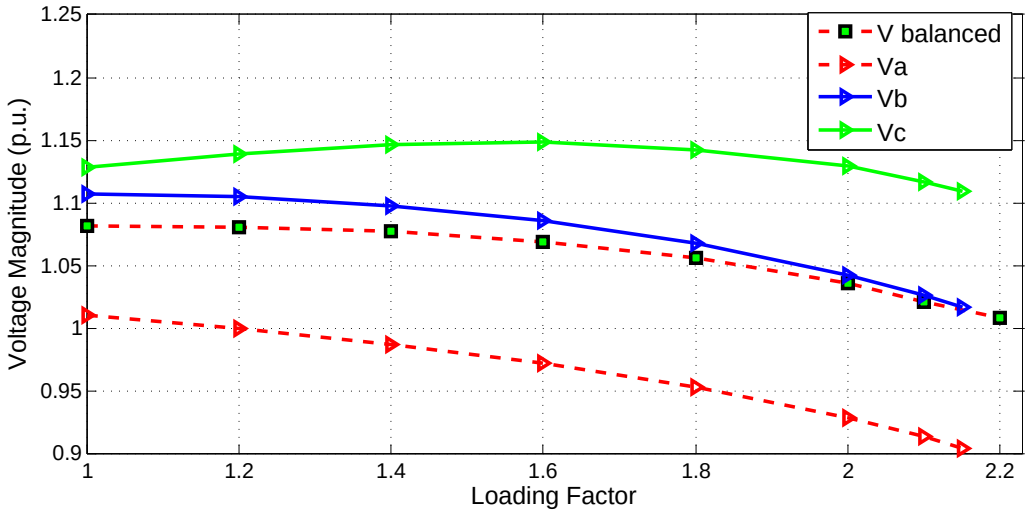

Figure 4.6: Load voltage magnitude versus loading factor with SG for $k = 20\%$.

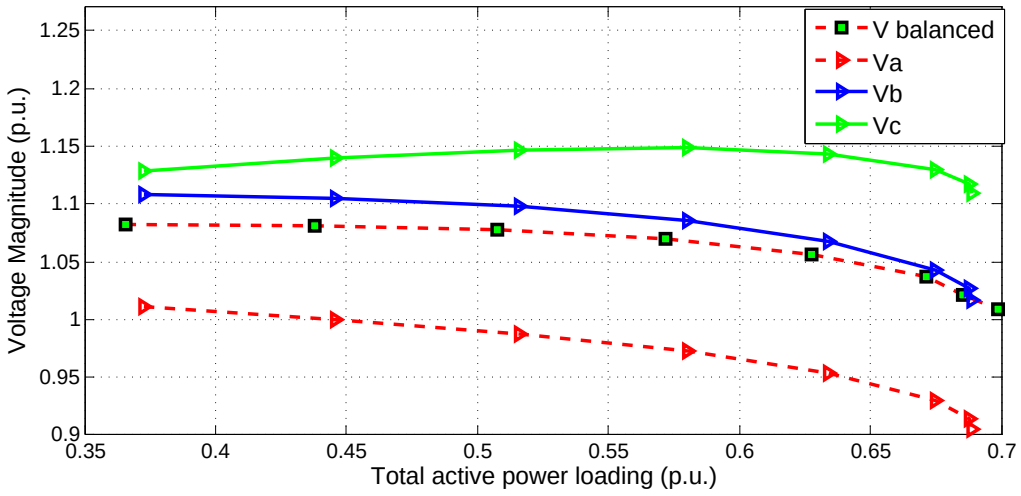

Figure 4.7: PV curves with SG for $k = 20\%$.

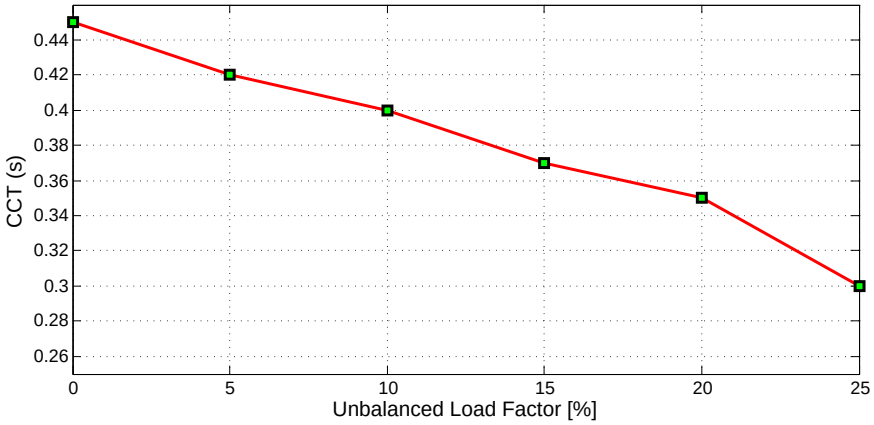

Figure 4.8: CCT of the test system at base load ($l = 1$ p.u.) for a three-phase-to-ground fault.

Figures 4.9 and 4.10 depict the transient behavior of the SG at a loading factor $l = 1.5$ p.u. and $k = 25\%$ for the studied fault before and after the CCT. Observe that the system is stable for a clearing time 0.12 s, and unstable for clearing times greater than 0.12 s.

4.5.4 Small-Perturbation Stability Analysis

Two scenarios are considered to analyze the effects of unbalanced conditions on small-perturbation stability for the SG, as follows:

Effect of Unbalanced Conditions at Base Load

In the first scenario, the load is at the base case (i.e, $l = 1$ p.u.), and the system is perturbed with a short-duration three-phase fault at $t = 1$ s, so that the critical system modes can be obtained using the identification approach. This is used to study the system stability under various unbalanced conditions at low loading levels, demonstrating the impact of unbalancing on the stable system. The critical poles of the generator speed associated with the oscillatory mode at the base load are shown in Figure 4.11. Table 4.4 illustrates the damping factors and frequency of the critical poles at the base load for different unbalanced conditions. Note that as k increases, the frequency decreases, while the damping factor increases; similar observations were reported in [62] and [115].

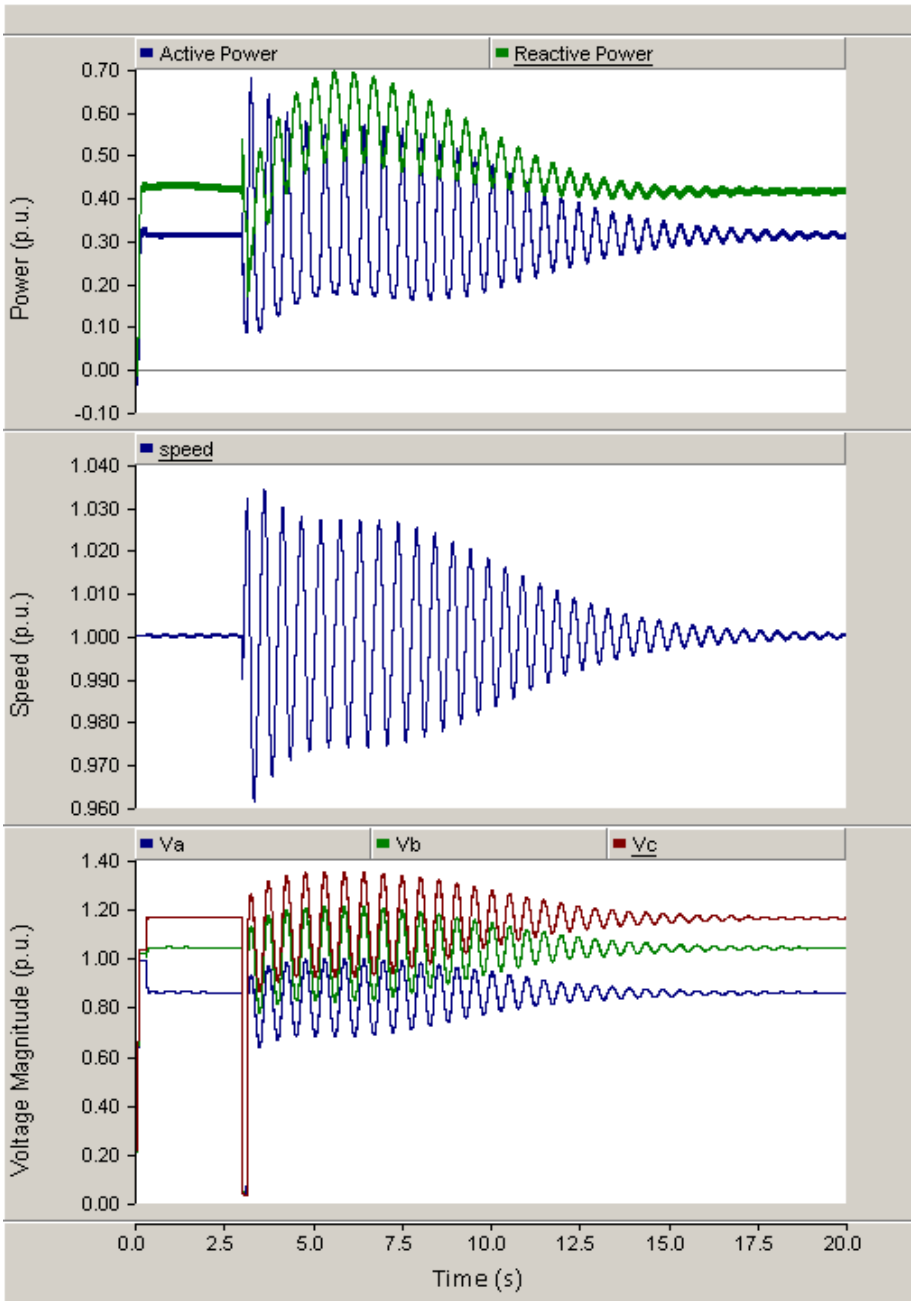

Figure 4.9: Transient behavior of SG at $k = 25\%$ before CCT.

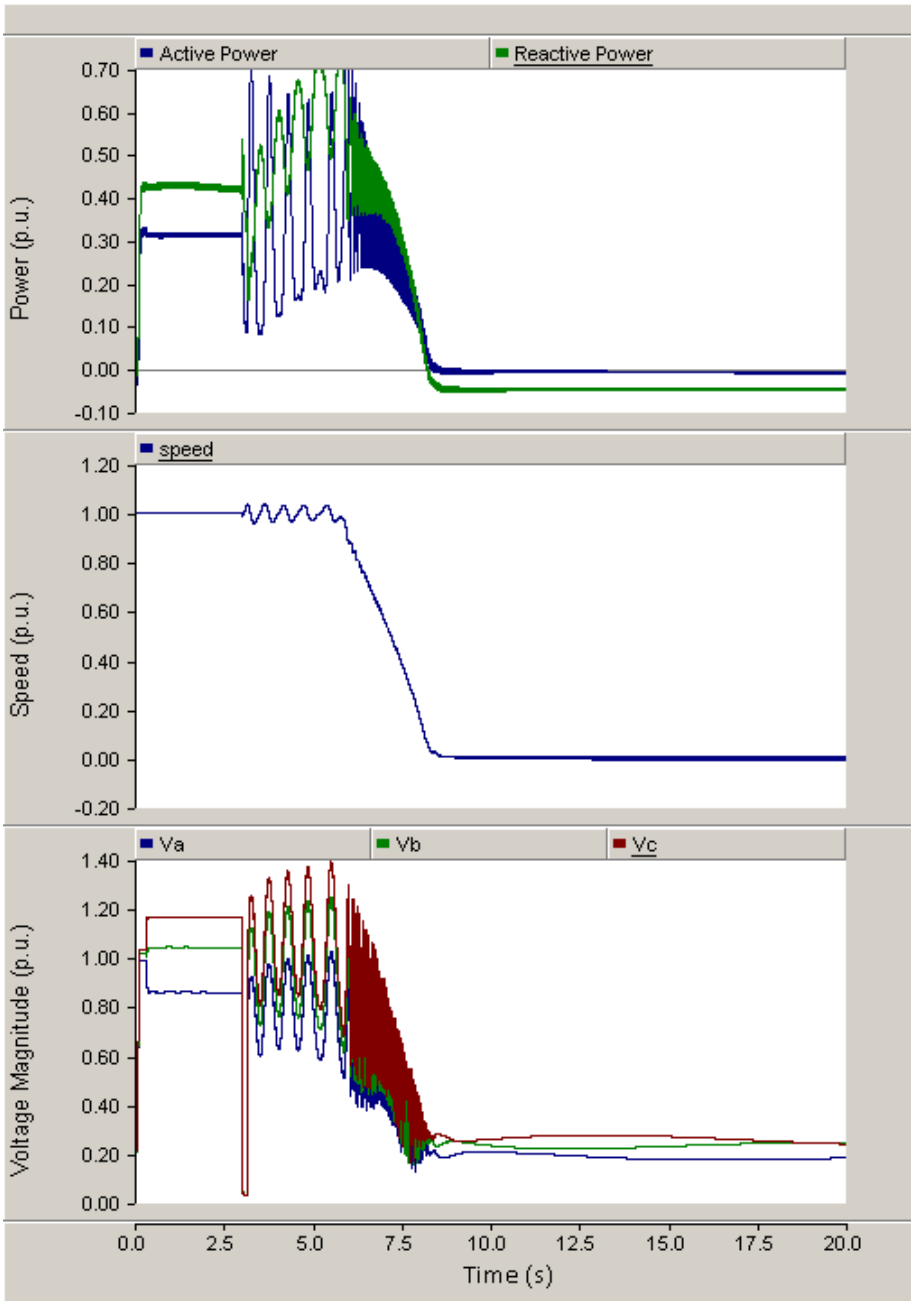

Figure 4.10: Transient behavior of SG at $k = 25\%$ after CCT.

Table 4.4: Damping factors and frequency of oscillations for different unbalanced conditions.

	Pole	Damping factor (%)	Frequency (rad/s)
$k = 0\%$	-1.09 + j12.7	8.53	12.7
$k = 5\%$	-1.11 + j12.6	8.82	12.6
$k = 10\%$	-1.12 + j12.5	8.89	12.6
$k = 15\%$	-1.13 + j12.4	9.03	12.5
$k = 20\%$	-1.14 + j12.3	9.25	12.3
$k = 25\%$	-1.16 + j12.0	9.65	12.1

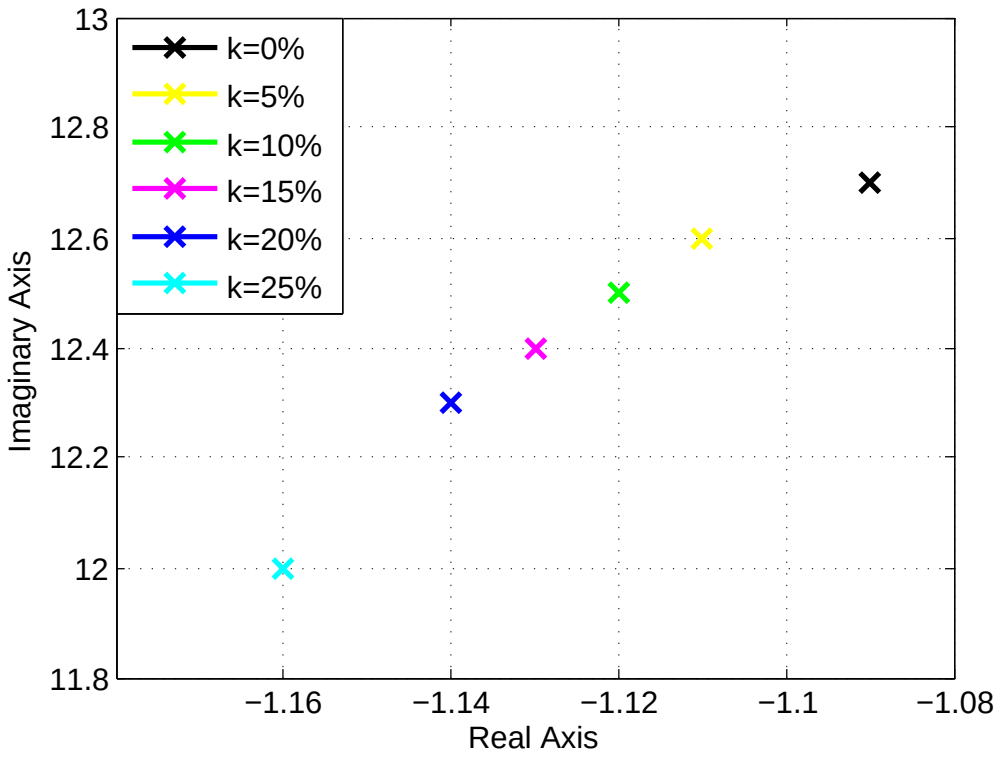

Figure 4.11: Critical poles of the generator speed associated with the oscillatory mode for a short-duration three-phase-to-ground fault.

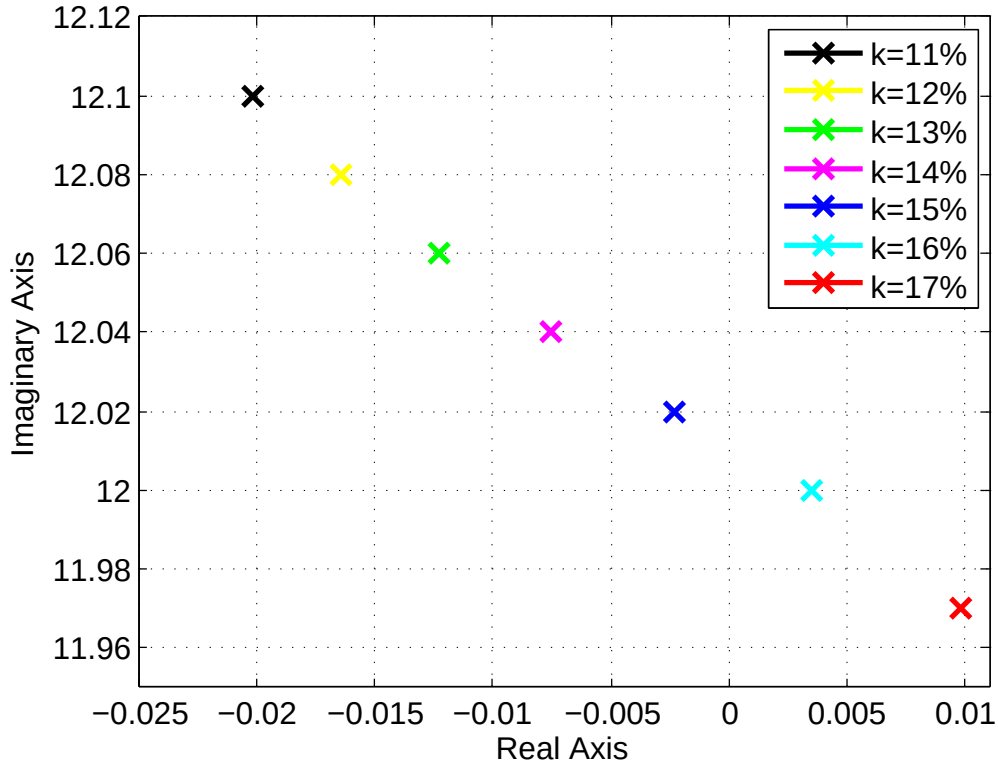

Figure 4.12: Zero-pole map of SG speed around critical unbalanced conditions.

Effect of Unbalanced Conditions on High Loading Levels

In the second scenario, the system load is increased close to its maximum value ($l = 2.2$ p.u.), and the machine is then connected at $t = 0.5$ s. This is used to study the stability of the system for various unbalance conditions at high loading levels, demonstrating how unbalancing leads the system to instability. Figure 4.12 illustrates the critical poles of the SG speed for various levels of unbalanced conditions. Observe that, beyond $k = 15\%$, the critical pole crosses the imaginary axis and thus the system experiences a Hopf bifurcation with 1.91 Hz frequency.

For a loading level of 2.2 p.u. and unbalancing of $k = 25\%$, the system is unstable as the critical poles of the SG speed move to the right side of the imaginary axis. This can be corrected by introducing the proposed UVS. Thus, Figure 4.13 shows the effects of UVS on the critical poles for different K_{UVS} values. Note that as the gain of UVS increases, the critical poles move to the left side of the imaginary axis and the system becomes more

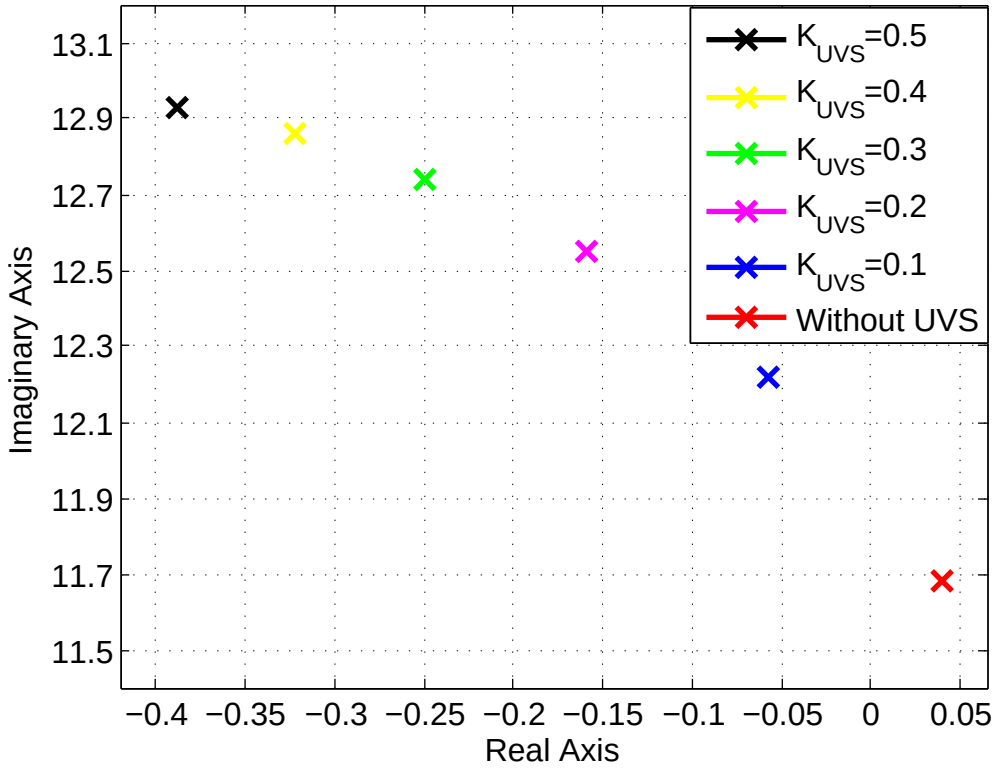

Figure 4.13: Critical poles of SG speed associated with the oscillatory mode with and without UVS.

stable. Figure 4.14 illustrates the generator speed with and without UVS at $l = 2.2$ p.u., $k = 25\%$, and $K_{UVS} = 0.2$, when the machine is connected, showing that the generator speed is sufficiently damped and the system becomes stable with the UVS.

4.6 Summary

This chapter concentrated on the stability analyses of SG-based DGs under unbalanced conditions. Voltage stability analyses were performed based on P-V curves obtained from both power flow and dynamic studies; transient stability studies were carried out based on detailed time-domain simulations of contingencies; and small-perturbation stability studies were performed based on identification techniques. The P-V curves showed, in general, that the loadability of the system decreased as unbalancing increased, and from the point of view

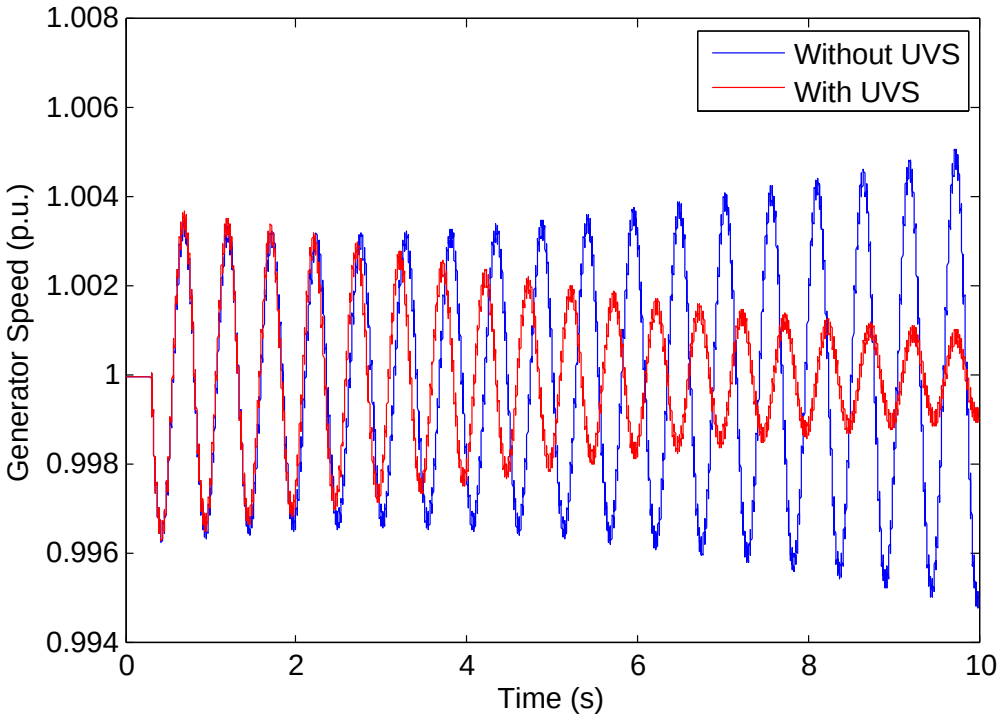

Figure 4.14: Transient behavior of SG speed with and without UVS.

of transient stability, the time-domain simulations demonstrated that the system was less stable as unbalancing increased. Another interesting result was that, as the system load increased, the critical poles crossed the imaginary axes and the system became unstable as unbalancing increased. A UVS was proposed to improve the stability of the system, demonstrating the effectiveness of the stabilizer by eigenvalue analyses and time-domain simulations.

Chapter 5

Unbalanced DFIG Wind Generator Stability and Control

5.1 Introduction

In this chapter, unbalanced DFIG model and controls are presented. A control method based on the injection of negative sequence components, considering rotor-side converter, to mitigate electrical torque and active power oscillations is presented. Voltage stability analyses are carried out using three-phase P-V curves and maximum system loadability, and transient stability studies are performed using time-domain simulations of contingencies. Finally, a UVS is proposed to improve the stability of a distribution system with DFIG.

5.2 Dynamic Model of DFIG

The DFIG is modeled here using a classical and detailed asynchronous machine model with a wound rotor [80], and a detailed model of the back-to-back ac/dc/ac converter controlling the rotor [118]. Figure 5.1 depicts the general structure of a DFIG.

The DFIG model and controls used here are based on the analysis of voltage, flux, and current vector components in the $\alpha\beta$ and dq reference-frames, as shown in Figure 5.2, where the variable F represents voltage, current or stator flux on different reference frames. The Clarke's transformation maps the three-phase instantaneous flux, voltages, and currents in the abc reference-frame into the instantaneous flux, voltages, and currents in the $\alpha\beta$ reference-frame. This transformation can be written as follows:

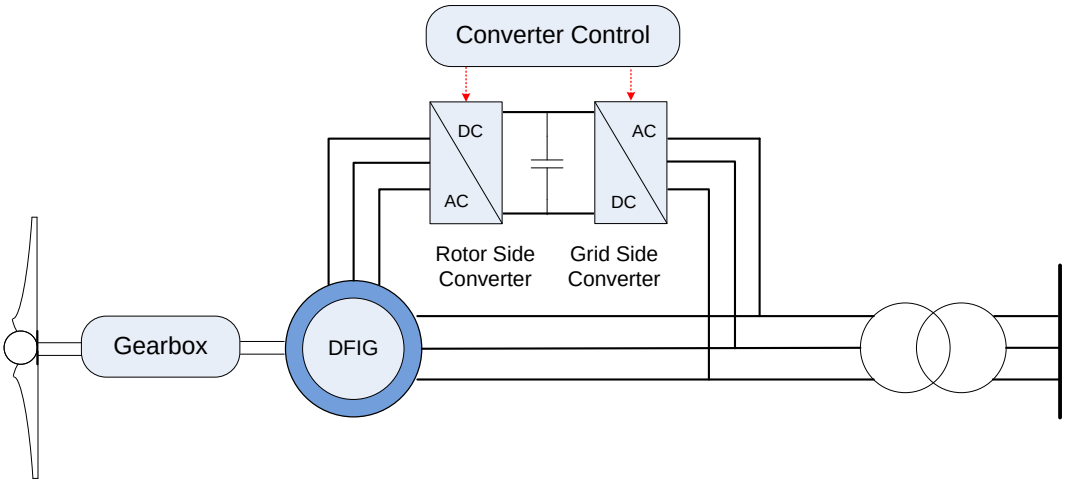

Figure 5.1: General structure of a DFIG.

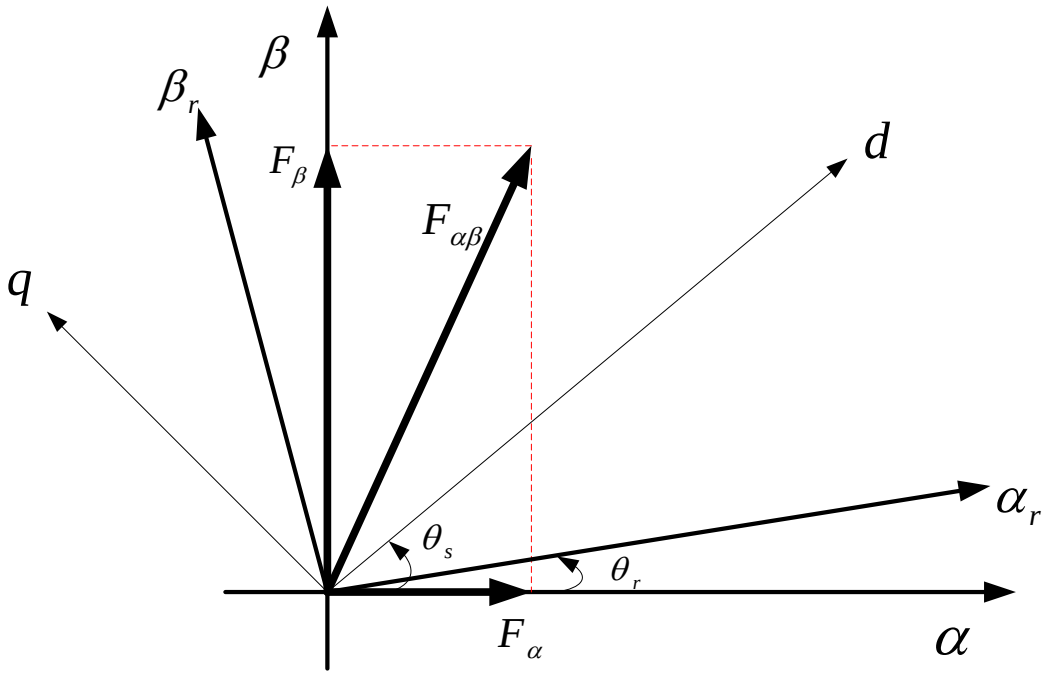

Figure 5.2: Phasor diagram of a DFIG.

$$\begin{bmatrix} F_\alpha \\ F_\beta \end{bmatrix} = 2/3 \begin{bmatrix} 1 & -1/2 & -1/2 \\ 0 & \sqrt{3}/2 & -\sqrt{3}/2 \end{bmatrix} \begin{bmatrix} F_a \\ F_b \\ F_c \end{bmatrix} \tag{5.1}$$

And the transformations from the $\alpha\beta$ reference-frame to the dq and $\alpha_r\beta_r$ reference-frames are given by:

$$F_{dq} = F_{\alpha\beta} e^{-j\theta_s} = F_d + jF_q \tag{5.2}$$
$$F_{\alpha_r\beta_r} = F_{\alpha\beta} e^{-j\theta_r} = F_{\alpha_r} + jF_{\beta_r} \tag{5.3}$$

where θ_s and θ_r are the stator and rotor angle, respectively.

The equivalent circuit of the DFIG model can be presented in various reference-frames [74, 119, 120]. Figure 5.3 shows the equivalent circuit of the DFIG model in the synchronous reference-frame rotating at the speed ω_e [74]; thus, the stator and rotor flux phasors Ψ_s and Ψ_r, and the stator and rotor voltage phasors V_{sdq} and V_{rdq}, respectively, in the synchronous reference-frame can be written as:

$$\Psi_{rdq} = L_r I_{rdq} + L_m I_{sdq} \tag{5.4}$$
$$\Psi_{sdq} = L_s I_{sdq} + L_m I_{rdq} \tag{5.5}$$
$$V_{rdq} = R_r I_{rdq} + j(\omega_e - \omega_r)\Psi_{rdq} + \frac{d\Psi_{rdq}}{dt} \tag{5.6}$$
$$V_{sdq} = R_s I_{dqs} + j\omega_e \Psi_{rdq} + \frac{d\Psi_{sdq}}{dt} \tag{5.7}$$

where s stands for the stator; r stands for the rotor; L_s is the stator inductance; L_r is the rotor inductance; L_m is the mutual inductance; and ω_r is the rotor angular frequency. From (5.4)-(5.7) and assuming that the voltage drop and $d\Psi_s/dt$ are negligible, the output stator active and reactive powers can be expressed approximately as follows:

$$\begin{aligned} P_s + jQ_s &= -\frac{3}{2} V_{sdq}\, I^C_{sdq} \approx -\frac{3}{2} j\omega_e \Psi_{sdq} \frac{1}{L_s} (\Psi^C_{sdq} - L_m I^C_{rdq}) \\ &= -\frac{3}{2} j\omega_e \Psi_{sdq} \frac{1}{L_s} \left[\Psi^C_{sdq} - (L_m I_{rd} - jL_m I_{rq})\right] \\ &= \frac{3}{2} \frac{\omega_e \Psi_{sdq}}{L_s} \left[L_m I_{rq} - j(\Psi^C_{sdq} - L_m I_{rd})\right] \end{aligned} \tag{5.8}$$

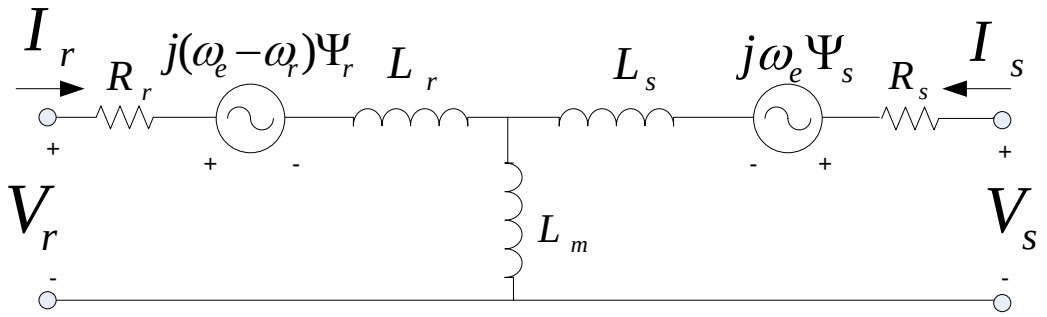

Figure 5.3: Equivalent circuit of DFIG model in the synchronous reference-frame rotating at the speed ω_e.

where C is the complex conjugate. Unbalance loading in DFIGs introduce negative sequence components in the voltage, current, and flux, which can result in significant oscillations in torque, active and reactive power with a double frequency; hence, a DFIG model that considers the positive and negative sequence components is needed to study this phenomenon. This is accomplished using a three-phase signal in the stationary $\alpha\beta$ reference-frame expressed by the positive and negative sequence components as follows:

$$\begin{aligned} \begin{bmatrix} F_\alpha(t) \\ F_\beta(t) \end{bmatrix} &= \begin{bmatrix} F_\alpha^+(t) + F_\alpha^-(t) \\ F_\beta^+(t) + F_\beta^-(t) \end{bmatrix} \\ &= F_{\alpha\beta}^+ e^{j(\omega_e t)} + F_{\alpha\beta}^- e^{-j(\omega_e t)} \end{aligned} \tag{5.9}$$

There are two approaches for the positive and negative sequence components separation under unbalanced conditions: separation by low pass filter (LPF), and separation by a signal delay cancellation [75]. In this thesis, the positive and negative sequence components separation is based on a LPF approach, in which, as the negative sequence components appear with the frequency $2\omega_e$ in the positive dq reference-frame, and the positive sequence appears with the frequency $2\omega_e$ in the negative dq reference-frame, a LPF can be used to extract dc components for both sequences. Figures 5.4 and 5.5 depict the separation of the positive and negative sequence components in the stator and rotor sides, respectively. Thus, the stator components (i.e., current, voltage, and flux) in the positive and negative sequence $\alpha\beta$ reference-frame yield:

$$\begin{aligned} F_{\alpha\beta}^+ &= F_{dq}^+ + F_{dq}^- e^{-j2\omega_e t} \\ F_{\alpha\beta}^- &= F_{dq}^- + F_{dq}^+ e^{-j2\omega_e t} \end{aligned} \tag{5.10}$$

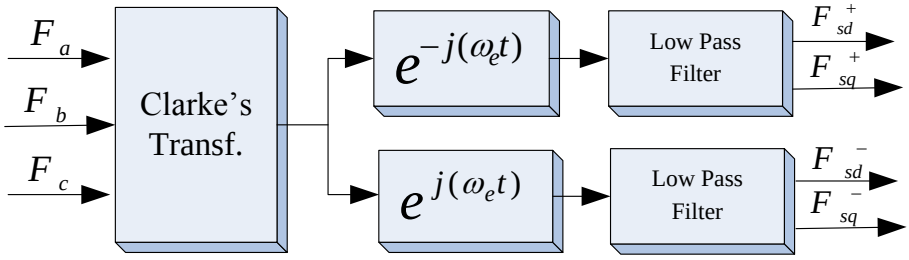

Figure 5.4: Separation of the positive and negative sequence components in the stator side.

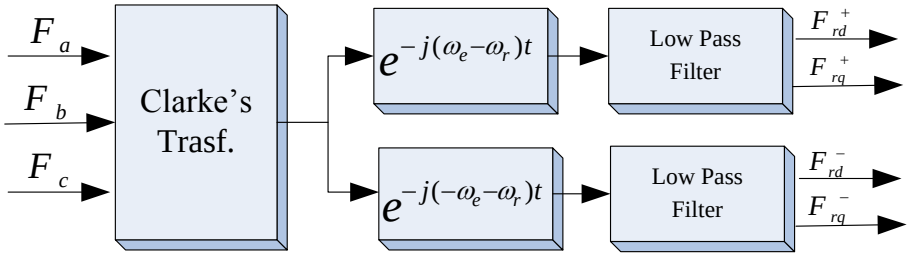

Figure 5.5: Separation of the positive and negative sequence components in the rotor side.

The d-axis for the positive sequence in the dq reference-frame is fixed to the positive sequence of stator flux rotating at the speed ω_e, while the d-axis for the negative sequence rotates at $-\omega_e$. Based on two reference-frames rotating at ω_e and $-\omega_e$, the voltage equations for the positive and negative sequences at the rotor and the stator sides are:

$$\begin{bmatrix} V_s^+ \\ V_r^+ \end{bmatrix} = \begin{bmatrix} L_s & L_m \\ L_m & L_r \end{bmatrix} \frac{d}{dt} \begin{bmatrix} I_s^+ \\ I_r^+ \end{bmatrix} + \begin{bmatrix} R_s + jL_s\omega_e & jL_m\omega_e \\ jL_m(\omega_e - \omega_r) & R_r + jL_r(\omega_e - \omega_r) \end{bmatrix} \begin{bmatrix} I_s^+ \\ I_r^+ \end{bmatrix} \tag{5.11}$$

$$\begin{bmatrix} V_s^- \\ V_r^- \end{bmatrix} = \begin{bmatrix} L_s & L_m \\ L_m & L_r \end{bmatrix} \frac{d}{dt} \begin{bmatrix} I_s^- \\ I_r^- \end{bmatrix} + \begin{bmatrix} R_s - jL_s\omega_e & -jL_m\omega_e \\ jL_m(-\omega_e - \omega_r) & R_r + jL_r(-\omega_e - \omega_r) \end{bmatrix} \begin{bmatrix} I_s^- \\ I_r^- \end{bmatrix} \tag{5.12}$$

Based on (5.11) and (5.12), the stator output active and reactive power under unbalance

conditions can be written as:

$$P_s = \frac{3}{2}\left[P_{so} + P_{ssin}\sin 2(\omega_e t) + P_{scos}\cos 2(\omega_e t)\right] \tag{5.13}$$

$$Q_s = \frac{3}{2}\left[Q_{so} + Q_{ssin}\sin 2(\omega_e t) + Q_{scos}\cos 2(\omega_e t)\right] \tag{5.14}$$

where P_s is the stator active power; Q_s is the stator reactive power; and:

$$\begin{bmatrix} P_{so} \\ Q_{so} \\ P_{ssin} \\ P_{scos} \\ Q_{ssin} \\ Q_{scos} \end{bmatrix} = \begin{bmatrix} V_{sd}^{+} & V_{sq}^{+} & V_{sd}^{-} & V_{sq}^{-} \\ V_{sq}^{+} & -V_{sd}^{+} & V_{sq}^{-} & -V_{sd}^{-} \\ V_{sq}^{-} & -V_{sd}^{-} & -V_{sq}^{+} & V_{sd}^{+} \\ V_{sd}^{-} & V_{sq}^{-} & V_{sd}^{+} & V_{sq}^{+} \\ -V_{sd}^{-} & -V_{sq}^{-} & V_{sd}^{+} & V_{sq}^{+} \\ V_{sq}^{-} & -V_{sd}^{-} & V_{sq}^{+} & -V_{sd}^{+} \end{bmatrix} \begin{bmatrix} I_{sd}^{+} \\ I_{sq}^{+} \\ I_{sd}^{-} \\ I_{sq}^{-} \end{bmatrix} \tag{5.15}$$

Since the electrical power is the sum of the power from the equivalent voltage source $j\omega_e\Psi_s$ and $j(\omega_e - \omega_r)\Psi_r$, the electrical torque of the DFIG can be written as:

$$T_e = P_e/\omega_r = \frac{3}{2}\frac{L_m}{L_s}\left[T_{eo} + T_{esin}\sin 2(\omega_e t) + T_{ecos}\cos 2(\omega_e t)\right] \tag{5.16}$$

where T_e is the electrical torque; P_e is the electrical power; and:

$$\begin{bmatrix} T_{eo} \\ T_{esin} \\ T_{ecos} \end{bmatrix} = \begin{bmatrix} -\Psi_{sq}^{+} & \Psi_{sd}^{+} & -\Psi_{sq}^{-} & \Psi_{sd}^{-} \\ -\Psi_{sq}^{-} & \Psi_{sd}^{-} & -\Psi_{sq}^{+} & \Psi_{sd}^{+} \\ \Psi_{sd}^{-} & \Psi_{sq}^{-} & -\Psi_{sd}^{+} & -\Psi_{sq}^{+} \end{bmatrix} \begin{bmatrix} I_{rd}^{+} \\ I_{rq}^{+} \\ I_{rd}^{-} \\ I_{rq}^{-} \end{bmatrix} \tag{5.17}$$

Note that, since the negative sequence of stator and rotor components are zero under balanced conditions, the *sin* and *cos* oscillating terms for the stator active and reactive powers, and the electrical toque disappear in this particular case.

The DFIG rotor control is based on the stator flux-oriented synchronous frame in the *dq*-axes. Thus, the stator flux linkage can be calculated as follows:

$$\frac{d\psi_{sabc}}{dt} = v_{sabc} - R_s i_{sabc}. \tag{5.18}$$

The stator flux in the polar form after Clarke's transformation can be written as:

$$|\Psi_s| = \sqrt{|\psi_{s\alpha}|^2 + |\psi_{s\beta}|^2} \tag{5.19}$$

$$\theta_s = \tan^{-1}\left(\frac{\psi_{s\beta}}{\psi_{s\alpha}}\right)$$

where the angle θ_s is the stator flux angle. Note that the transformation of dq reference-frame to $\alpha\beta$ reference-frame in the rotor-side is based on $\omega_{slip} = \omega_e - \omega_r$.

The stator active and reactive powers can be independently controlled by I_{rd} and I_{rq}, respectively; thus, two PI controllers are used to control the active and reactive powers. From the point of view of the reactive power, the DFIG may be in constant power factor (PF) mode, or voltage control mode. As the DFIG can control the reactive power or the output voltage, a PI controller is used to control the output voltage by controlling I_{rd}. The reference current I_{rd} and I_{rq} are converted to the $\alpha\beta$ and then to the abc reference-frames based on ω_{slip}. On the grid-side, two PI feedback controllers are used to decouple the current control. Figure 5.6 illustrates the DFIG control scheme, where E_c is the converter dc bus voltage.

Under unbalanced conditions, there are four degrees of freedom for rotor current components, i.e., the positive and negative sequence rotor current components; thus, different control objectives can be chosen. It is worth noticing that it is not possible to eliminate all oscillations in the electrical torque, the active and reactive powers, and the stator current at the same time. In this thesis, the main objective is to keep the electrical torque oscillations at a minimum for given active power and voltage values. Since I_{rd}^{+*} and I_{rq}^{+*} are obtained to control voltage magnitude and active power, respectively, as shown in Figure 5.6, and substituting $T_{esin}^{*} = T_{ecos}^{*} = 0$ in (5.17), the negative sequence rotor current references are given by:

$$\begin{bmatrix} I_{rd}^{-*} \\ I_{rq}^{-*} \end{bmatrix} = \begin{bmatrix} -\Psi_{sq}^{+} & \Psi_{sd}^{+} \\ -\Psi_{sd}^{+} & -\Psi_{sq}^{+} \end{bmatrix}^{-1} \begin{bmatrix} \Psi_{sq}^{-} I_{rd}^{+*} - \Psi_{sd}^{-} I_{rq}^{+*} \\ -\Psi_{sd}^{-} I_{rd}^{+*} - \Psi_{sq}^{-} I_{rq}^{+*} \end{bmatrix} \tag{5.20}$$

If the control target is to eliminate the stator active power oscillations, according to (5.15), the stator current references are:

$$\begin{bmatrix} I_{sd}^{+*} \\ I_{sq}^{+*} \\ I_{sd}^{-*} \\ I_{sq}^{-*} \end{bmatrix} = \begin{bmatrix} V_{sd}^{+} & V_{sq}^{+} & V_{sd}^{-} & V_{sq}^{-} \\ V_{sq}^{+} & -V_{sd}^{+} & V_{sq}^{-} & -V_{sd}^{-} \\ V_{sq}^{-} & -V_{sd}^{-} & -V_{sq}^{+} & V_{sd}^{+} \\ V_{sd}^{-} & V_{sq}^{-} & V_{sd}^{+} & V_{sq}^{+} \end{bmatrix}^{-1} \begin{bmatrix} P_{so}^{*} \\ Q_{so}^{*} \\ P_{ssin}^{*} \\ P_{scos}^{*} \end{bmatrix} \tag{5.21}$$

A grid-side converter provides the dc power to the rotor-side converter. A capacitor is used in the back-to-back converter in order to mitigate the oscillations. The grid-side pulse width modulation (PWM) converter operates based on reference quantities to keep a constant dc voltage.

If a voltage source converter with the constant dc voltage is connected to an ac grid through a transformer, the grid-side voltage equations in the synchronous reference-frame can be expressed as:

$$\begin{bmatrix} V_{gd} \\ V_{gq} \end{bmatrix} - \begin{bmatrix} V_{cd} \\ V_{cq} \end{bmatrix} = \begin{bmatrix} R_g & -L_g\omega_e \\ L_g\omega_e & R_g \end{bmatrix} \begin{bmatrix} I_{cd} \\ I_{cq} \end{bmatrix} + L_g \frac{d}{dt} \begin{bmatrix} I_{cd} \\ I_{cq} \end{bmatrix} \tag{5.22}$$

where g stands for the grid side; c stands for the converter side; R_g is grid resistance; and L_g is grid inductance. Active and reactive powers provided by the grid-side can be written as:

$$P_g = 3/2(V_{gd}I_{gd} + V_{gq}I_{gq}) \tag{5.23}$$
$$Q_g = 3/2(V_{gq}I_{gd} - V_{gd}I_{gq}) \tag{5.24}$$

The grid-side converter controls the reactive power and dc bus voltage. The dc bus voltage is controlled by I_d component using a PI controller. A linear controller based on decoupled dq components is used to control I_d and I_q, as shown in Figure 5.6 [121]. The decoupling can be written as:

$$\begin{bmatrix} {V_{cd}}' \\ {V_{cq}}' \end{bmatrix} = \begin{bmatrix} V_{gd} - V_{cd} \\ V_{gq} - V_{cq} \end{bmatrix} + L_g\omega_e \begin{bmatrix} I_{cq} \\ -I_{cd} \end{bmatrix} \tag{5.25}$$

$$\begin{aligned} \frac{d}{dt} \begin{bmatrix} I_{cd} \\ I_{cq} \end{bmatrix} &= \begin{bmatrix} -\frac{R_g}{L_g} & \omega_e \\ -\omega_e & -\frac{R_g}{L_g} \end{bmatrix} \begin{bmatrix} I_{cd} \\ I_{cq} \end{bmatrix} + \frac{1}{L_g} \begin{bmatrix} V_{gd} - V_{cd} \\ V_{gq} - V_{cq} \end{bmatrix} \\ &= -\frac{R_g}{L_g} \begin{bmatrix} I_{cd} \\ I_{cq} \end{bmatrix} + \frac{1}{L_g} \begin{bmatrix} {V_{cd}}' \\ {V_{cq}}' \end{bmatrix} \end{aligned} \tag{5.26}$$

5.3 Unbalanced Voltage Stabilizer

When a system is more heavily loaded, it can become unstable as system unbalancing increases; thus, a UVS for the DFIG is proposed here to improve the stability of the system in the voltage control mode, integrating it with the rotor-side controller to provide a negative auxiliary stabilizing signal. The proposed UVS for the DFIG is based on similar principles as the SG UVS in Chapter 4.

Figure 5.7 shows the proposed UVS for the DFIG. Since the negative-sequence components of terminal voltages are available for DFIG control, these signals are used here

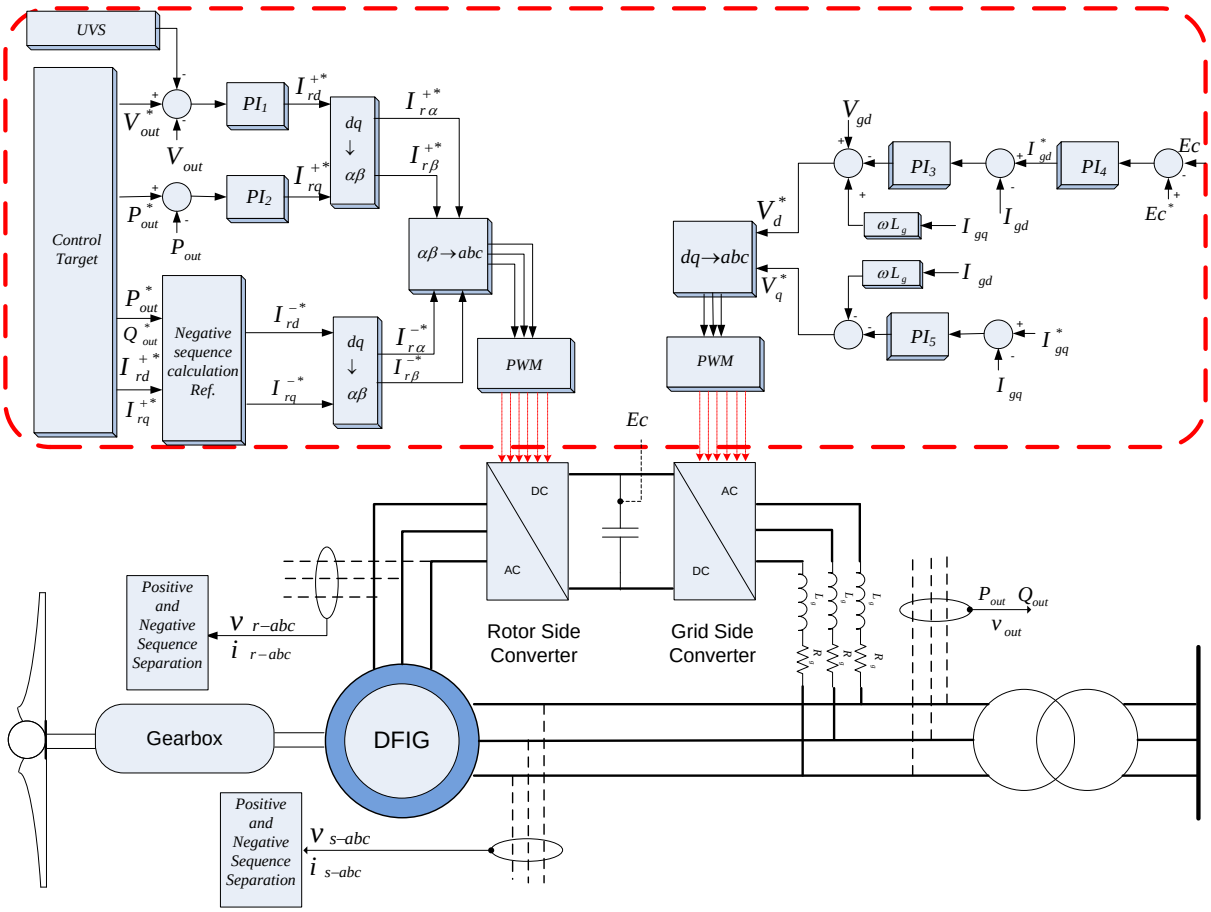

Figure 5.6: Control scheme of the DFIG under unbalanced conditions.

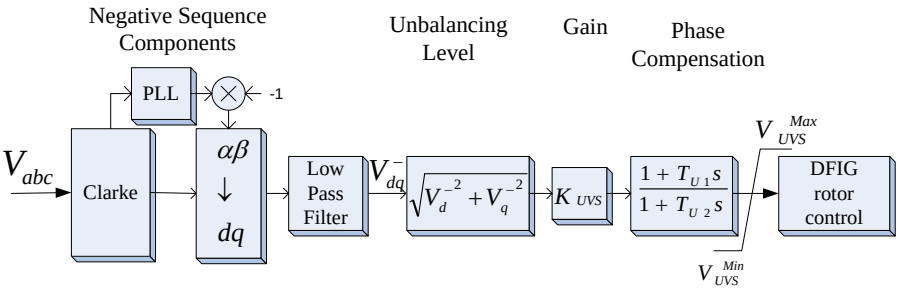

Figure 5.7: Block diagram of the proposed UVS for a DFIG-based DG unit.

and then converted to the dq^{-} reference-frame. The transformation $\sqrt{V_d^{-2}+V_q^{-2}}$ can be used to reflect the degree of unbalance, since as the unbalance increases, the output signal increases as well. The gain K_{UVS} determines the damping factor provided by the UVS, and the first-order phase compensation block provides appropriate phase lead to compensate for the phase lag between the rotor-side controller input and the generator electrical torque. The limits V_{UVS}^{max} and V_{UVS}^{min} constrain the output signal, which is an auxiliary signal for the voltage reference in the rotor-side controller. The data for the UVS for the DFIG used here is provided in the Appendix.

The output signal of the UVS is a negative feedback to the rotor-side controller similar as UVS for the SG, due to the fact that by decreasing the generator terminal voltages, the load demand decreases, thus reducing the system stress as demand and system unbalance increase. Therefore, the stability is improved at high loading levels with the proposed UVS.

5.4 Results

The grid, feeder, and load test system described in Chapter 4 is used here to study stability analysis for unbalanced distribution system with a DFIG. The load is modeled as constant impedance, based on rated voltage, active, and reactive power. In the base case, active and reactive powers are $P_{Load} = 3$ MW, and $Q_{Load} = 1$ Mvar, respectively. Because of the low voltage at the load bus at high loading levels, a balanced capacitor bank is connected at the load bus; the reactive power of the bank is set at $Q_{cap} = 2.17$ Mvar.

The main objective of the grid-side converter is to control the dc link voltage by controlling I_{gd}. The DFIG is assumed to be in speed control at 1.2 p.u, i.e., the rotor speed is set externally, as the large inertia of the wind turbine results in slow changes of the rotor

Table 5.1: Maximum active power and voltage magnitude in all phases for different unbalanced conditions with DFIG.

$k(\%)$	Maximum loading factor (p.u.)	Maximum active power loadability (p.u.)	V_a(p.u.)	V_b(p.u.)	V_c(p.u.)
0	1.24	0.389	0.996	0.996	0.996
5	1.22	0.384	0.978	0.998	1.015
10	1.20	0.379	0.962	0.998	1.035
15	1.12	0.359	0.950	1.007	1.056
20	1.08	0.350	0.935	1.011	1.073
25	1.02	0.335	0.921	1.016	1.090

speed. To start the simulations, the rotor-side converter is first set in PF control mode and at $t = 1$ s the controller is switched to voltage control; otherwise, the system is unstable.

All time-domain simulations in this chapter, are carried out in PSCAD/EMTDC with detailed representation of generators, ac/dc/ac converters, controllers, loads, and lines. All test system parameters are provided in the Appendix.

5.4.1 Voltage Stability Analysis

Table 5.1 shows the maximum active power loadability, loading factor, and the voltage magnitudes in phases a, b, and c for different realistic unbalanced conditions of the distribution system with DFIG. Observe that when the system unbalancing increases, the maximum loadability of the system decreases, and the voltage magnitude differences in phases a, b, and c with respect to the voltage magnitudes in balanced conditions increase.

Figure 5.8 shows the voltage magnitude at the load under balanced and unbalanced conditions for $k = 15\%$ with DFIG, and Figure 5.9 depicts the P-V curve under balanced and unbalanced conditions. Observe that the voltage magnitude in phase b is close to the voltage magnitude for the balanced condition, and the voltage magnitudes of phases c and a are greater and less than that of phase b, respectively, as expected.

5.4.2 UVS Impact on DFIG

In order to compare existing control strategies and the proposed UVS for the DFIG, the following scenarios are studied for $k = 15\%$ and $l = 1.15$ p.u.:

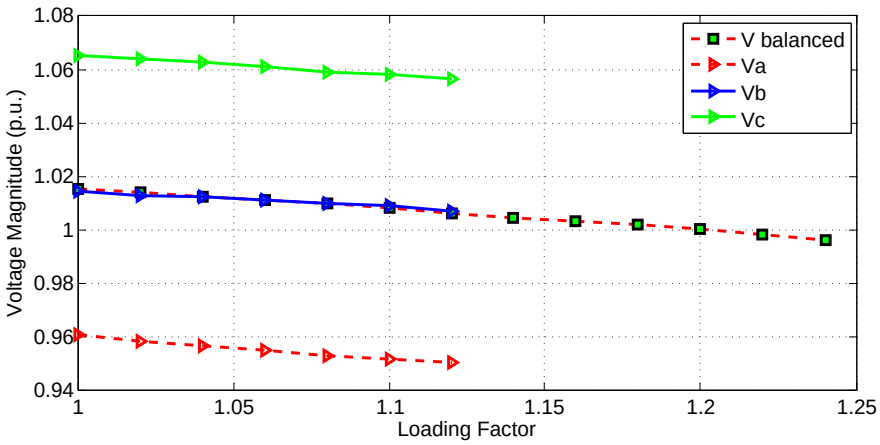

Figure 5.8: Load voltage magnitude versus loading factor for k=15%.

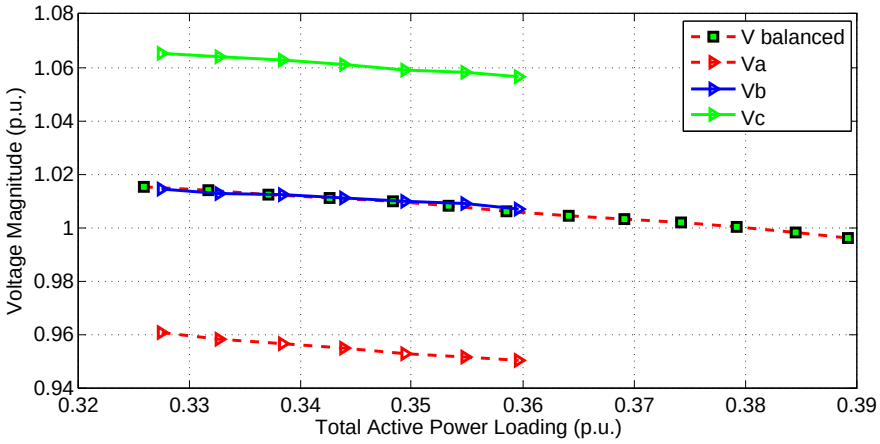

Figure 5.9: PV curves for k=15%.

- $S1$: This is the classical control balanced approach, which does not take into account the possibility of unbalanced voltages. In this case, the synchronous reference frame is aligned with the stator flux and has no negative sequence injections.
- $S2$: This case is based on limiting the electrical torque oscillations in (5.20); thus, the negative sequence components are adjusted to limit the electrical torque.
- $S3$: This case is based on limiting the stator active power in (5.21); thus, the negative sequence rotor currents are adjusted to limit the stator active power oscillations.
- $S4$: This is the same as $S1$ with the UVS added.
- $S5$: This is the same as $S2$ with the UVS added.
- $S6$: This is the same as $S3$ with the UVS added.

The output active and reactive powers are set at $P_{out} = 1$ MW, and $Q_{out} = 0$ Mvar, respectively. Based on different control targets, Figure 5.10 depicts the simulated results with the various control strategies for PF control mode. The control was initially set to $S1$ and changed to $S2$ at $t = 2$ s, and then to $S3$ at $t = 3$ s, respectively. During the simulation, the grid-side converter was enabled, then the DFIG stator was energized, and finally the machine was connected at $t = 0.5$ s; thus, the DFIG is in steady-state after 1 s. Since the transient behavior of the starting process is not the focus of this thesis, this process is not shown in any of the plots. Observe that when the controller is set to $S1$, the negative sequence components of rotor current references are zero; hence, the active and reactive powers, electrical torque, stator voltage and current all contain significant oscillations at 120 Hz, which may damage the DFIG. In the rotor side, the currents contain both the fundamental component of the rotor mechanical frequency minus the stator frequencies $(f_r - f_s)$ and the harmonic component of $(f_s + f_r)$. At $t = 2$ s, the control in $S2$ is activated, resulting in the torque oscillations being reduced over 90% compared to $S1$; however, the power oscillations increase. On the other hand, when the control in $S3$ is activated, the opposite takes place, i.e., the torque oscillations increase but the power oscillations decrease.

Figure 5.11 illustrates the results of the DFIG with voltage control, but without UVS. In this case, the reference voltage is set at 1.03 p.u. to operate the system within the voltage limits. Observe that the system becomes unstable for $S2$ and $S3$, whereas it was stable under balanced conditions; hence, the voltage unbalance leads to instability.

Figure 5.12 depicts the results of the DFIG in voltage control mode with UVS. Thus, $S5$ takes place at $t = 2$ s, and $S6$ occurs at $t = 3$ s. Note that the system is now stable

and the electrical torque oscillations are reduced, with the best overall system performance being observed for $S5$. This demonstrates the clear advantage of introducing the proposed UVS for unbalanced system operation.

5.4.3 Transient Stability Analysis

Three-phase-to-ground faults of short-duration and close to the load are considered as contingencies for the DFIG. The simulation time is 10 s, and the fault occurs at $t = 3$ s. Figure 5.13 illustrates the CCT of the test system with the DFIG for different values of k for the base loading factor (i.e., $l = 1$ p.u.). Observe that the CCT decreases as the unbalance increases from 0% to 25%. It should be mentioned that the CCT in this case is defined based on the voltage overshoot at the DFIG, when it exceeds 20% for 0.16 s, the DG should be disconnected [93].

Figures 5.14 and 5.15 depict the transient behavior of the DFIG with and without UVS at a loading factor $l = 1$ p.u. and $k = 15\%$ for the studied fault after CCT. Observe that the system is unstable since cannot control the voltage and power of the DFIG within voltage limits without UVS for a clearing time after the CCT; however, the system becomes stable for the DFIG with UVS, demonstrating the advantage of the proposed UVS to improve transient stability under unbalanced conditions.

5.5 Summary

This chapter concentrated on the stability analyses of DFIG based DGs under unbalanced conditions. A detailed model and controls of a DFIG under unbalanced conditions were presented and formulated. Voltage stability analyses were performed based on P-V curves obtained from dynamic studies; transient stability studies were carried out based on detailed time-domain simulations of contingencies. The P-V curves showed, in general, that the loadability of the system decreased as unbalancing increased; the time-domain simulations demonstrated that the system was less stable as unbalancing increased. Existing control techniques to compensate the negative impact of unbalanced operation of DFIGs were demonstrated to be ineffective at heavily loading conditions. Hence, a UVS was proposed to improve the stability of the system, demonstrating the effectiveness of the stabilizer with time-domain simulations.

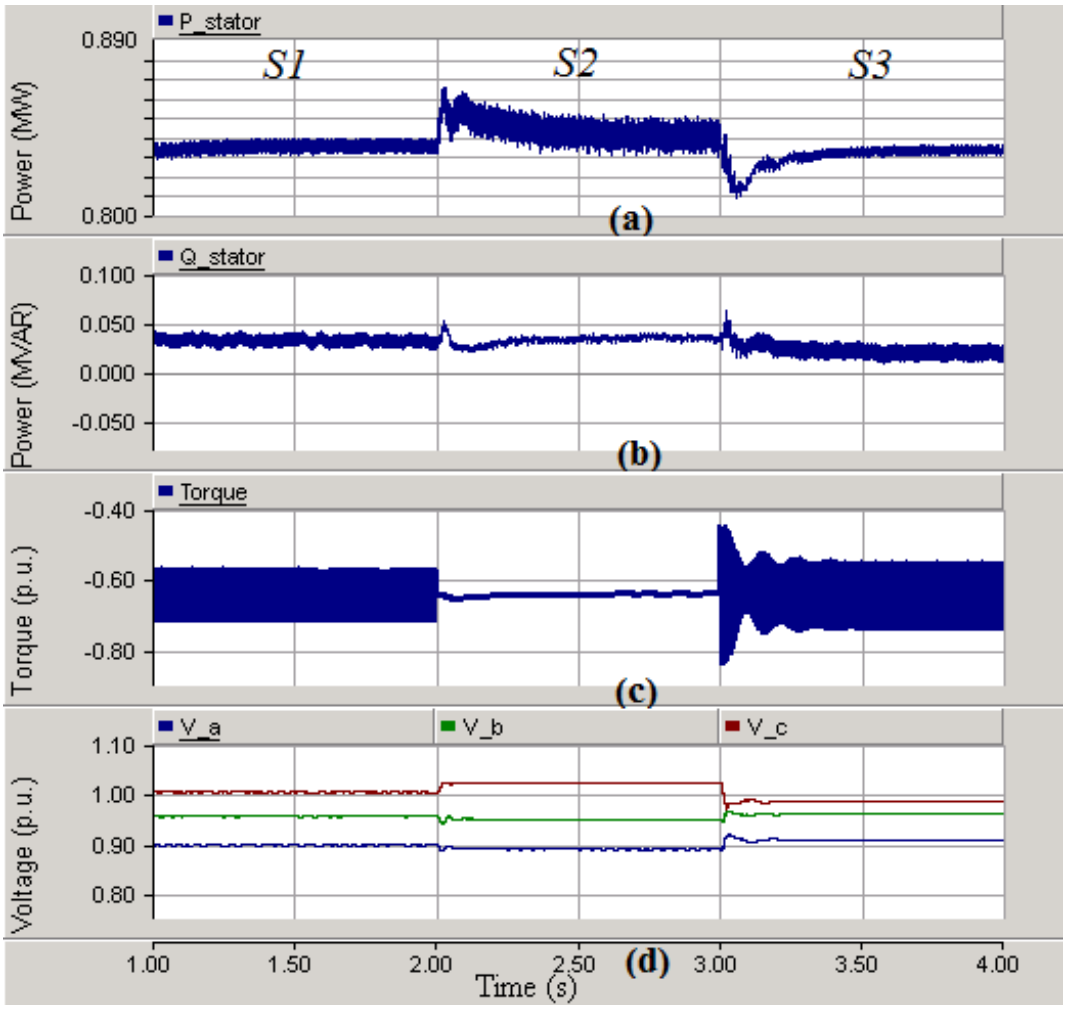

Figure 5.10: Transient behavior of DFIG with various control strategies for PF control mode: (a) stator active power; (b) stator reactive power; (c) electrical torque; and (d) voltage magnitude of the load.

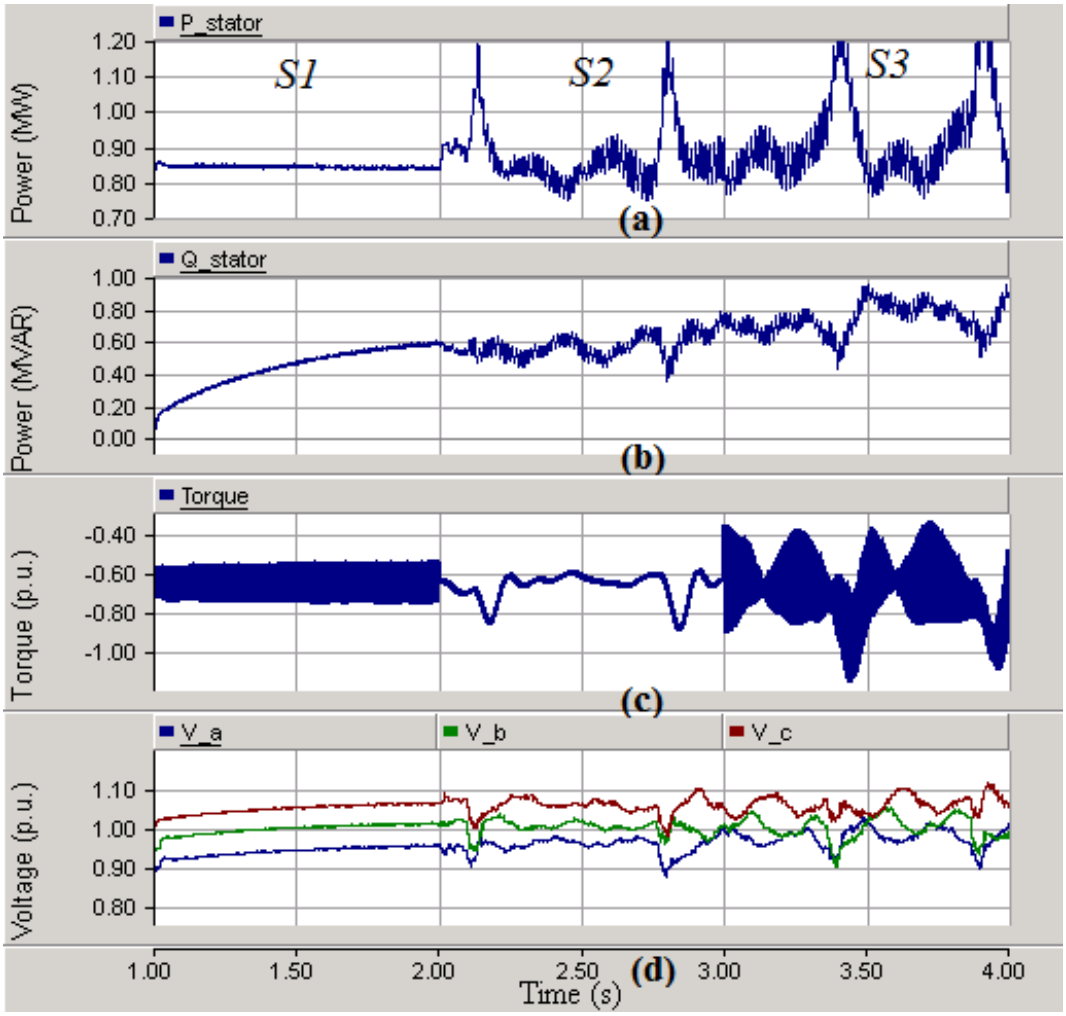

Figure 5.11: Transient behavior of DFIG with various control strategies for voltage control mode without UVS: (a) stator active power; (b) stator reactive power; (c) electrical torque; and (d) voltage magnitude of the load.

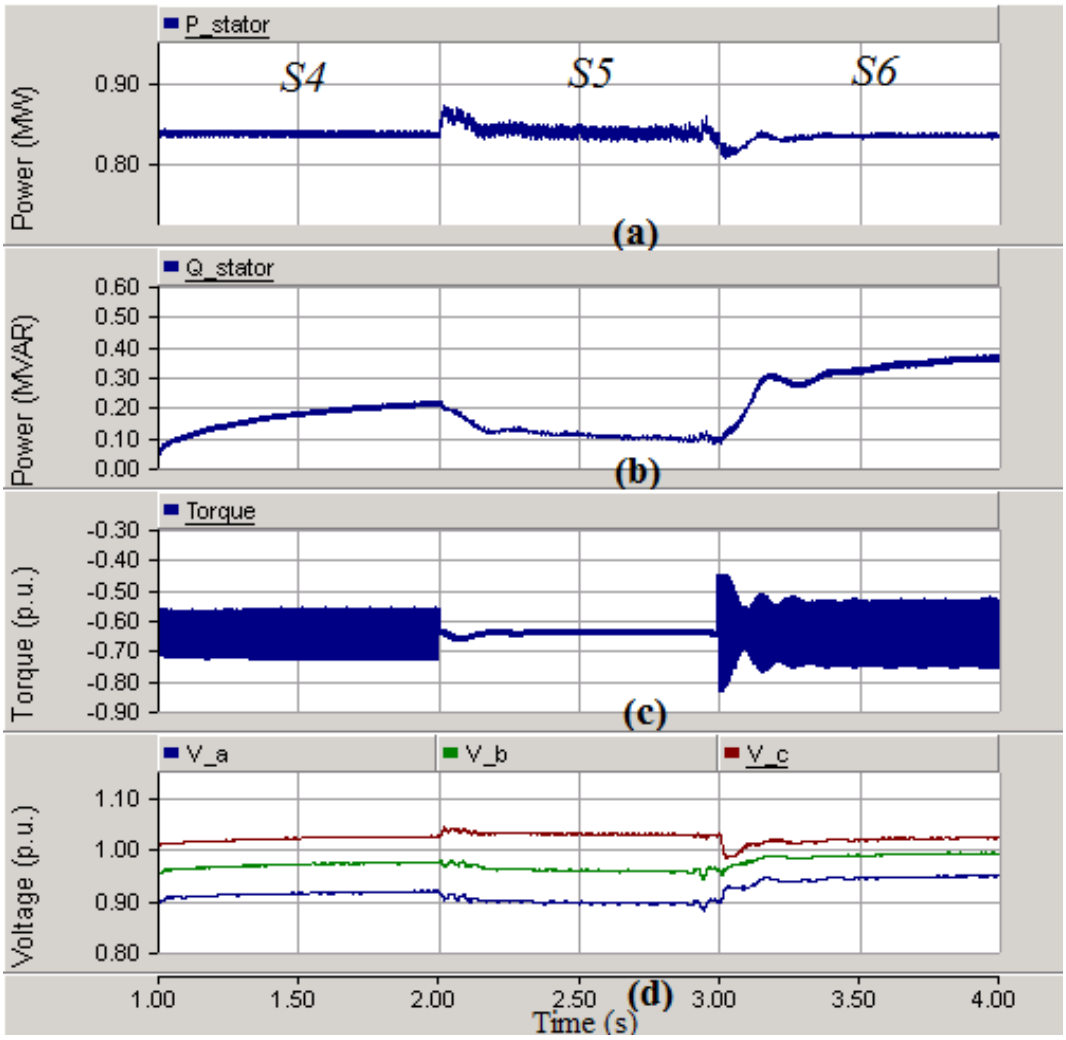

Figure 5.12: Transient behavior of DFIG with various control strategies for voltage control mode with UVS: (a) stator active power; (b) stator reactive power; (c) electrical torque; and (d) voltage magnitude of the load.

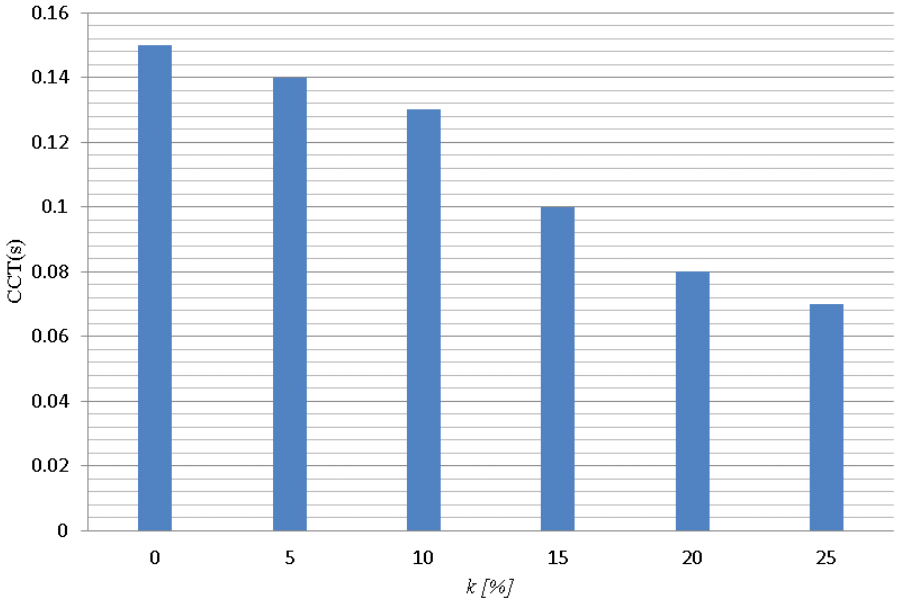

Figure 5.13: CCT of the test system at base load ($l = 1$ p.u.) for a three-phase-to-ground fault.

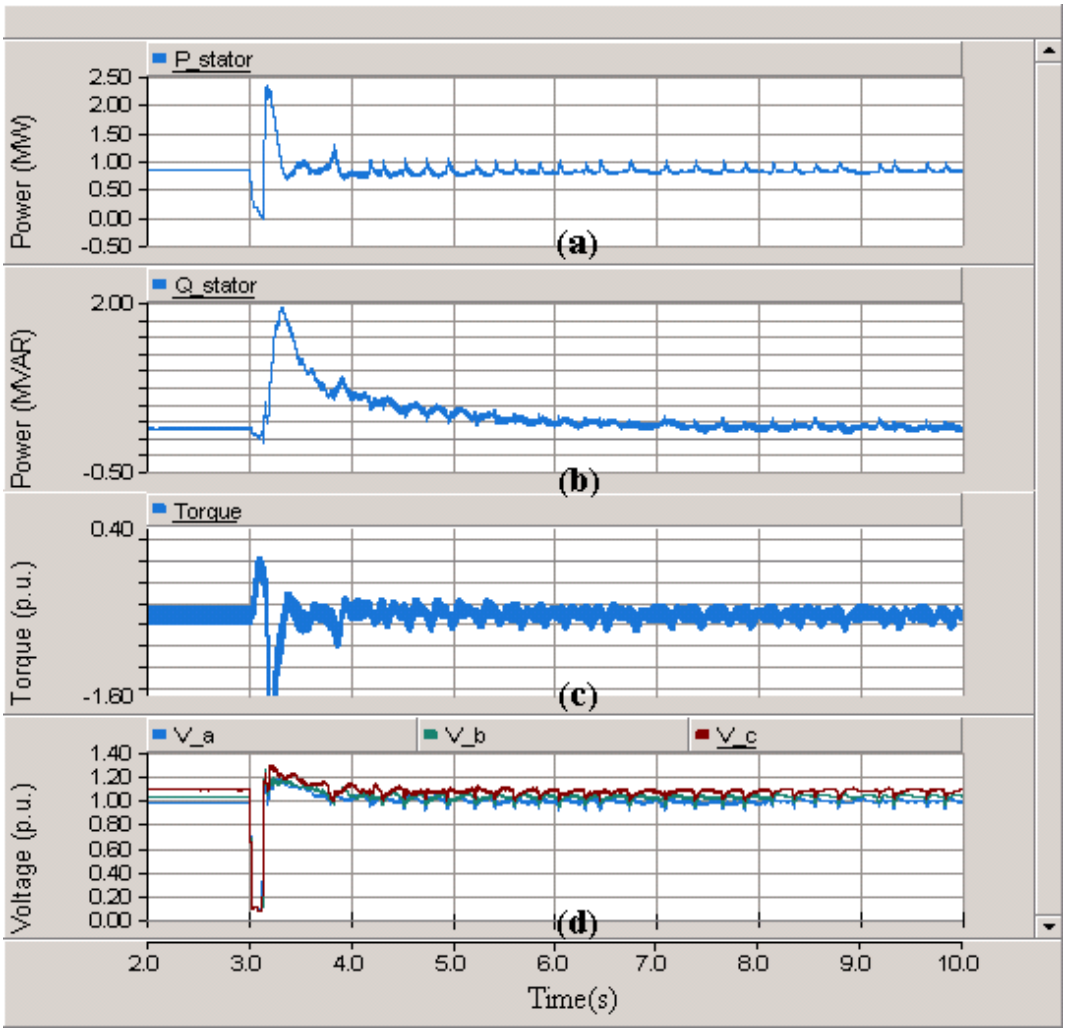

Figure 5.14: Transient behavior of DFIG without UVS at $k = 15\%$ after CCT: (a) stator active power; (b) stator reactive power; (c) electrical torque; and (d) voltage magnitude of the load.

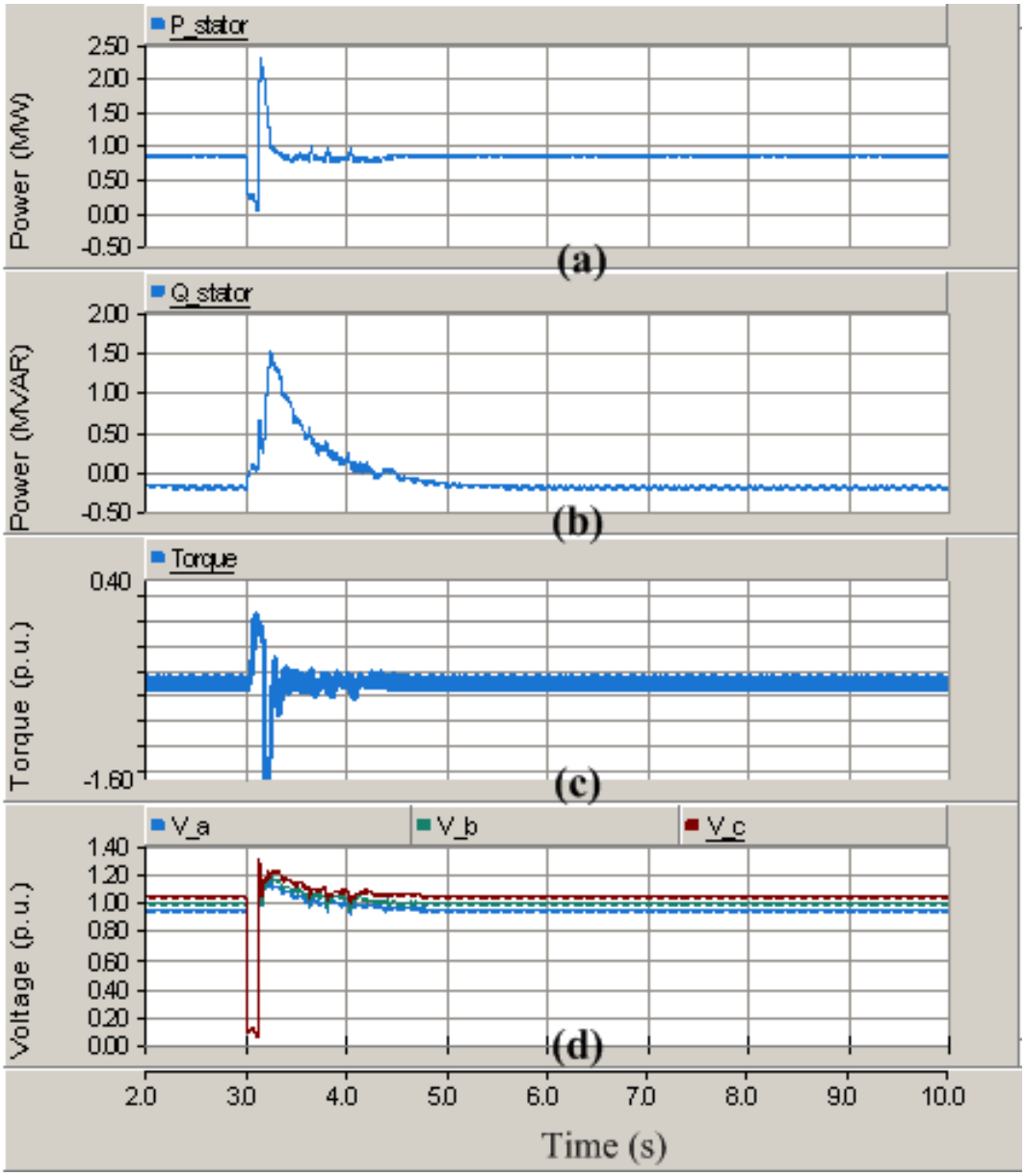

Figure 5.15: Transient behavior of DFIG with UVS at $k = 15\%$ after CCT: (a) stator active power; (b) stator reactive power; (c) electrical torque; and (d) voltage magnitude of the load.

Chapter 6

Conclusions

6.1 Summary

This thesis has concentrated on the modeling, control, and stability analysis of DGs under balanced and unbalanced conditions. Based on existing limited studies in literature of DGs and their effects on distribution systems, which concentrate on the analysis of a few selected DGs, a comprehensive investigation of the effects of different types of DG technologies on voltage, small-perturbation, and transient stability of distribution systems under balanced and unbalanced conditions has been presented in this thesis.

In Chapter 2, power system stability concepts were discussed, along with general models of the power system required for stability studies. The tools for stability studies that would be used in this work were also introduced. Finally, an overview of an MG was presented, including different DG technologies and their interfaces to the grid. The concepts presented in this chapter were used throughout this thesis.

In Chapter 3, the static and the dynamic models of different DGs for stability studies of balanced distribution systems were presented. These models include the dynamic models of the primary governor, generators and their interfaces. The proposed diesel, MT, FC, fixed-speed wind-turbine, BESS, and photovoltaic models were implemented and tested in PSAT. The DG models were tested and compared using two realistic distribution systems with multiple DGs to study their static and dynamic behaviors. The comparison of P-V curves for different static DG models showed , general, that PV control yields more loading margin than PQ and no controls. Thus, fixed-speed wind-turbine DGs proved to be the worst from the point of view of voltage stability. Furthermore, it was observed that the

best DG response in the case of typical load/feeder contingencies is that of inverter-based DGs, in general. The eigenvalue analyses showed that the system may experience LIBs or Hopf bifurcations as loading levels increase.

Chapter 4 concentrated on the stability analyses of SG-based DGs under unbalanced conditions. Voltage stability analyses were performed based on P-V curves obtained from both power flow and dynamic studies; transient stability studies were carried out based on detailed time-domain simulations of contingencies; and small-perturbation stability studies were performed based on identification techniques. The P-V curves showed, in general, that the loadability of the system decreased as unbalancing increased, and from the point of view of transient stability, the time-domain simulations demonstrated that the system was less stable as unbalancing increased. Another interesting result was that, as the system load increased, the critical poles crossed the imaginary axes and the system became unstable as unbalancing increased. A UVS was proposed to improve the stability of the system, demonstrating the effectiveness of the stabilizer by eigenvalue analyses and time-domain simulations.

Chapter 5 concentrated on the stability analyses of DFIG-based DGs under unbalanced conditions. A detailed model and controls of a DFIG under unbalanced conditions were presented and formulated. Voltage stability analyses were performed based on P-V curves obtained from dynamic studies; transient stability studies were carried out based on detailed time-domain simulations of contingencies. The P-V curves showed, in general, that the loadability of the system decreased as unbalancing increased; the time-domain simulations demonstrated that the system was less stable as unbalancing increased. Existing control techniques to compensate the negative impact of unbalanced operation of DFIGs were demonstrated to be ineffective at heavy loading conditions. Hence, a UVS was proposed to improve the stability of the system, demonstrating the effectiveness of the stabilizer with time-domain simulations.

6.2 Contributions

The main contributions of this thesis have been the following:

- Dynamic and static models of different types of DG technologies, both for short- and long-terms stability studies under balanced and unbalanced conditions were developed and implemented in the popular MATLAB-based software tool PSAT, which is an open source simulation package for power system studies.

- An investigation of the effects of DG technologies, in a comprehensive manner, on voltage, small-perturbation, and transient stability of balanced distribution systems was performed.
- Novel static and dynamic voltage stability studies based on three-phase power flows and detailed time-domain simulations were proposed and presented to determine maximum loadabilities of distribution systems with DGs under various unbalanced conditions.
- The application of an identification approach for small-perturbation stability studies of unbalanced systems with DGs was proposed, providing a framework for eigenvalue analysis of unbalanced distribution systems with DGs.
- Existing control techniques to compensate for the negative impact of unbalanced operation of DFIGs were demonstrated to be ineffective at heavily loaded conditions. Furthermore, simple and effective control strategies based on voltage unbalance for both SG- and DFIG-based DGs were proposed to improve the stability of the distribution systems. The simplicity of the proposed UVS makes it practical and relatively easy to implement in real systems.

6.3 Future Work

Further research may be carried out to address the following issues:

- Develop detailed inverter-based DGs models and controls to study stability issues under unbalanced conditions for photovoltaic and FC units.
- Study stability issues for fixed-speed wind-turbines with possible solutions (e.g., BESS) under unbalanced conditions.
- Develop linearized mathematical models of DGs for eigenvalue analyses of distribution systems with multiple DGs under unbalanced conditions.

Appendix

This Appendix provides the data of the test system and DG models which used in this thesis.

Table 1: Line parameters of CIGRE microgrid test system.

Line NO	Bus from-to	R (ohms/km)	X (ohm/km)	Length of line (km)
1	1-2	0.2274	0.341	2.8
2	2-3	0.2274	0.341	4.4
3	3-4	0.2274	0.341	0.6
4	4-5	0.2274	0.341	0.6
5	5-6	0.2274	0.341	1.5
6	6-7	0.2274	0.341	0.2
7	7-8	0.2274	0.341	1.7
8	8-9	0.2274	0.341	0.3
9	9-10	0.2274	0.341	0.8
10	10-11	0.2274	0.341	0.3
11	11-4	0.2274	0.341	0.5
12	3-8	0.2274	0.341	1.3
13	12-13	0.2274	0.341	4.9
14	13-14	0.2274	0.341	3
15	14-8	0.2274	0.341	2

Table 2: Load parameters of CIGRE microgrid test system.

Bus	Voltage (kV)	Power (MVA)	Active power (p.u.)	Reactive power (p.u.)
1	10	20	-	-
2	10	20	-	-
3	10	20	0.0501	0.0208
4	10	20	0.0416	0.0108
5	10	20	0.0727	0.0182
6	10	20	0.0548	0.0137
7	10	20	0.0076	0.0047
8	10	20	0.0586	0.01471
9	10	20	0.0574	0.0356
10	10	20	0.0543	0.0161
11	10	20	0.0330	0.0083
12	10	20	-	-
13	10	20	0.0034	0.00211
14	10	20	0.054	0.0258
15	10	20	-	-

Table 3: Line parameters of Japanese test system.

Voltage (kV)	Power (MVA)	Bus from-to	R (p.u.)	X (p.u.)
6.6	10	1-2	0.003145	0.075207
6.6	10	2-3	0.000330	0.001849
6.6	10	3-4	0.006667	0.030808
6.6	10	3-12	0.027502	0.127043
6.6	10	4-5	0.005785	0.014949
6.6	10	4-7	0.008001	0.036961
6.6	10	5-6	0.014141	0.036547
6.6	10	7-8	0.00899	0.041575
6.6	10	8-9	0.007	0.032346
6.6	10	9-10	0.003666	0.016940
6.6	10	10-11	0.008999	0.041575
6.6	10	12-13	0.031497	0.081405
6.6	10	13-14	0.039653	0.102984
6.6	10	14-15	0.016070	0.004153

Table 4: Load parameters of Japanese test system.

Bus	Voltage (kV)	Power (MVA)	Active power (p.u.)	Reactive power (p.u.)
1	6.6	10	-	-
2	6.6	10	0.0208	0.0021
3	6.6	10	0.0495	0.0051
4	6.6	10	0.0958	0.0098
5	6.6	10	0.0442	0.0045
6	6.6	10	0.0113	0.0012
7	6.6	10	0.0638	0.0066
8	6.6	10	0.0323	0.0033
9	6.6	10	0.0213	0.0022
10	6.6	10	0.0208	0.0029
11	6.6	10	0.2170	0.2200
12	6.6	10	0.0132	0.0014
13	6.6	10	0.0023	0.0003
14	6.6	10	0.0161	0.0016
15	6.6	10	0.0139	0.0014

Table 5: Synchronous machine parameters.

	Japanese test system	CIGRE test system
Power rating (MW)	3.125	0.500
Voltage rating (kV)	2.4	0.416
X_d (p.u.)	1.56	3.45
$X_d^{'}$ (p.u.)	0.296	0.3
$X_d^{''}$ (p.u.)	0.177	0.14
X_q (p.u.)	1.06	1.75
$X_q^{''}$ (p.u.)	0.177	0.16
X_l (p.u.)	0.088	0
$T_{do}^{'}$ (sec)	3.7	1.42
$T_{do}^{''}$ (sec)	0.05	0.014
$T_{qo}^{''}$ (sec)	0.05	0.05
H (sec)	1.0716	0.97

Table 6: AVR type II parameters.

	Chapter 3	Chapter 4
Maximum regulator voltage (p.u.)	6	6
Minimum regulator voltage (p.u.)	0	0
Regulator gain	78	78
Regulator pole (sec)	6	10
Regulator Zero (sec)	3	1
Time constant of the field circuit T_d (sec)	1	1

Table 7: MT parameters.

K_a	1
K_f	1
K_w	16.7
τ_s (sec)	0.05
τ_x (sec)	0.6
τ_y (sec)	1
τ_f (sec)	0.4
τ_{ecr} (sec)	0.01
τ_{cd} (sec)	0.2
T_{min} (p.u.)	1.5
T_{max} (p.u.)	-0.1
W_{min}	0.23

Table 8: Diesel generator parameters.

τ_{d1} (sec)	0.01
τ_{d2} (sec)	0.02
τ_{d3} (sec)	0.2
τ_{d4} (sec)	0.25
τ_{d5}(sec)	0.009
τ_{d6} (sec)	0.0384
τ_{Dd} (sec)	0.024
K_{ds}	8
T_{min}	0
T_{max}	1.1

Table 9: Induction generator parameters.

Power rating (MVA)	2
Voltage rating (kV)	20
X_s (p.u.)	0.10
X_r (p.u.)	0.08
X_m (p.u.)	3
R_r (p.u.)	0.01
R_s (p.u.)	0.01
H_t (sec)	2.5
H_m (sec)	0.5
K_s (p.u.)	0.3

Table 10: FC parameters.

Power rating (MVA)	0.25
Voltage rating (V)	440
τ_{ref} (sec)	2
τ_{st} (sec)	3.37
τ_d (sec)	0.8
R_{in}(ohm)	0.2778
B_{fc}	0.04777
C_{fc}	0.0136
K_m	20
τ_m (sec)	0.1
m_{max}	1.2
m_{min}	0.8
X_t (p.u.)	0.05

Table 11: Photovoltaic generator parameters.

τ_p (sec)	0.015
τ_q (sec)	0.015
K_p	0.04
K_i	20

Table 12: BESS parameters.

Capacity (Ah)	500	τ_{batt} (sec)	7200
K_m	20	E_{m0}	2.18
τ_m (sec)	0.1	K_e	$839 * 10^{-3}$
m_{max}	1.2	R_{00} (m ohm)	$2 * 10^{-3}$
m_{min}	0.8	R_{10} (m ohm)	$0.4 * 10^{-3}$
X_t (p.u.)	0.05	A_0	-0.2
I^*_{batt} (A)	51.5	R_{20} (m ohm)	$15 * 10^{-3}$
C_{0*} (Ah)	317.9	A_{12}	-8
K_c	1.11	A_{22}	-8.45
Θ_f	-40	G_{p0}	2
ϵ	1.19	V_{p0} (V)	0.1
β	1.75	A_p (V)	2

Table 13: Parameters of reduced system used in Chapters 4 and 5.

S_{base}(MVA)	10
Voltage rating (kV)	2.4
Line impedance (Z_1) (p.u.)	0.035 + j 0.21
Line impedance (Z_2) (p.u.)	0.35 + j 2.1

Table 14: DFIG parameters.

Power rating (MVA)	1.717
Voltage rating (kV)	0.69
Stator/rotor turn ratio	0.335
R_s (p.u.)	0.005049
R_r (p.u.)	0.00357
L_s (p.u.)	0.1226
L_r (p.u.)	0.1118
L_m (p.u.)	2.0773
$2H$ (sec)	4.55

Table 15: DFIG PI controllers parameters.

	PI_1	PI_2	PI_3	PI_4	PI_5
Proportional gain	1	0.5	5	10	10
Integral time constant (sec)	0.1	0.2	0.05	0.01	0.01

Table 16: UVS parameters.

	SG	DFIG
K_{UVS}	0.2	1.1
T_{U1} (sec)	0.125	0.125
T_{U2} (sec)	0.030	0.030
V_{UVS}^{max} (p.u.)	0.2	0.2
V_{UVS}^{min} (p.u.)	-0.2	-0.2

References

[1] M. Reza, "Stability analysis of transmission systems with high penetration of distributed generation," Ph.D. dissertation, Delft University of Technology, Delft, Netherlands, 2006.

[2] A. Azmy, "Simulation and management of distributed generating units using intelligent techniques," Ph.D. dissertation, University Duisburg-Essen, Essen, Germany, 2005.

[3] E. Nasr-Azadani, C. Canizares, and K. Bhattacharya, "Modeling and stability analysis of distributed generation," in *Proc. IEEE PES General Meeting*, 2012, pp. 1–8.

[4] W. Freitas, L. C. P. D. Silva, and A. Morelato, "Small-disturbance voltage stability of distribution systems with induction generators," *IEEE Trans. Power Systems*, vol. 20, no. 2, pp. 1653–1654, Aug. 2005.

[5] W. Freitas, J. C. M. Vieira, L. C. P. da Suva, C. M. Affonso, and A. Morelato, "Long-term voltage stability of distribution systems with induction generators," in *Proc. IEEE Power and Energy Society General Meeting*, 2005, pp. 2910–2913.

[6] J. C. Munoz and C. A. Canizares, "Comparative stability analysis of DFIG-based wind farms and conventional synchronous generators," in *Proc. Power Systems Conference and Exposition*, 2011, pp. 1–7.

[7] R. R. Londero, C. M. Affonso, and M. V. A. Nunes, "Impact of distributed generation in steady state, voltage and transient stability- Real case," in *Proc. IEEE PowerTech.*, 2009, pp. 1–6.

[8] R. B. Prada, L. F. Ferreira, and L. C. A. Ferreira, "Limiting distributed generator capacity due to the voltage stability phenomena," in *Proc. Transmission & Distribution Conference and Exposition, Latin America*, 2006, pp. 1–5.

[9] L. Wang, H. Cheung, A. Hamlyn, and R. Cheung, "Network-integrated stability enhancement strategy for power system with distributed generations," in *Proc. IEEE Power and Energy Society General Meeting - Conversion and Delivery of Electrical Energy in the 21st Century*, 2008, pp. 1–7.

[10] L. Wang, A. Hamlyn, H. Cheung, R. Yasin, C. Li, and R. Cheung, "Network-aided strategy and breaker impacts on voltage instability corrective actions for power systems with DGs," in *Proc. IEEE Power and Energy Society General Meeting*, 2009, pp. 1–7.

[11] H. Cheung, L. Wang, A. Hamlyn, and R. Cheung, "Network-assisted corrective actions against short-term and long-term voltage instability in power system with DGs," in *Proc. IEEE Power and Energy Society General Meeting - Conversion and Delivery of Electrical Energy in the 21st Century*, 2008, pp. 1–9.

[12] N. G. A. Hemdan and M. Kurrat, "Distributed generation location and capacity effect on voltage stability of distribution networks," in *Proc. Annual IEEE Conference, Student Paper*, 2008, pp. 1–5.

[13] K. Kumar and M. Selvan, "Planning and operation of distributed generations in distribution systems for improved voltage profile," in *Proc. Power Systems Conference and Exposition*, 2009, pp. 1–7.

[14] X. Tang and G. Tang, "Multi-objective planning for distributed generation in distribution network," in *Proc. Electric Utility Deregulation and Restructuring and Power Technologies*, 2008, pp. 2664–2667.

[15] H. Hedayati, S. A. Nabaviniaki, and A. Akbarimajd, "A new method for placement of DG units in distribution networks," in *Proc. IEEE Power Systems Conference and Exposition*, 2006, pp. 1904–1909.

[16] X. Chen and W. Gao, "Effects of distributed generation on power loss, loadability and stability," in *Proc. IEEE Southeastcon*, 2008, pp. 468–473.

[17] R. S. A. Abri, E. F. El-Saadany, and Y. M. Atwa, "Optimal placement and sizing method to improve the voltage stability margin in a distribution system using distributed generation," *IEEE Trans. Power Systems*, vol. 28, no. 1, pp. 326–334, Feb. 2013.

[18] M. Ettehadi, H. Ghasemi, and S. Vaez-Zadeh, "Voltage stability-based DG placement in distribution networks," *IEEE Trans. Power Delivery*, vol. 28, no. 1, pp. 171–178, Jan. 2013.

[19] J. Slootweg, "Wind power modelling and impact on power system dynamics," Ph.D. dissertation, Delft University of Technology, Delft, Netherlands, 2003.

[20] B. Dong, S. Asgarpoor, and W. Qiao, "Voltage analysis of distribution systems with DFIG wind turbines," in *Proc. IEEE Power Electronics and Machines in Wind Applications*, 2009, pp. 1–5.

[21] Q. Ai, X. Wang, and X. He, "The impact of large-scale distributed generation on power grid and microgrids," *Renewable Energy*, vol. 62, pp. 417–423, Feb. 2014.

[22] C. Abbey and G. Joos, "Supercapacitor energy storage for wind energy applications," *IEEE Trans. Industry Applications*, vol. 43, no. 3, pp. 769–776, Jun. 2007.

[23] T. Kinjo, T. Senjyu, N. Urasaki, and H. Fujita, "Terminal-voltage and output-power regulation of wind-turbine generator by series and parallel compensation using SMES," *Proc. IEE Generation, Transmission and Distribution*, vol. 153, no. 3, pp. 276–282, May 2006.

[24] R. Cardenas, R. Pena, J. Clare, and G. Asher, "Power smoothing in a variable speed wind-diesel system," in *Proc. IEEE Power Electronics Specialist Conference*, 2003, pp. 754–759.

[25] W. Li, G. Joos, and C. Abbey, "Attenuation of wind power fluctuations in wind turbine generators using a dc bus capacitor based filtering control scheme," in *Proc. IEEE Industry Applications Conference, 41st IAS Annual Meeting*, 2006, pp. 216–221.

[26] K. Yoshimoto, T. Nanahara, and G. Koshimizu, "Analysis of data obtained in demonstration test about battery energy storage system to mitigate output fluctuation of wind farm," in *Proc. CIGRE/IEEE PES Joint Symposium, Integration of Wide-Scale Renewable Resources Into the Power Delivery System*, 2009.

[27] S. Teleke, M. E. Baran, A. Q. Huang, S. Bhattacharya, and L. Anderson, "Control strategies for battery energy storage for wind farm dispatching," *IEEE Trans. Energy Conversion*, vol. 24, no. 3, pp. 725–732, Sept. 2009.

[28] A. Abedini and H. Nikkhajoei, "Dynamic model and control of a wind-turbine generator with energy storage," *IET Renewable Power Generation*, vol. 5, no. 1, pp. 67 – 78, Jan. 2011.

[29] S. K. M. Kodsi and C. Canizares, "Application of a stability-constrained optimal power flow to tuning of oscillation controls in competitive electricity markets," *IEEE Trans. Power Systems*, vol. 22, no. 4, pp. 1944–1954, Nov. 2007.

[30] E. Nasr-Azadani, S. H. Hosseinian, P. Hasanpor, and B. Vahidi, "Stability constrained optimal power flow in deregulated power systems," *Electric Power Components and Systems*, vol. 39, no. 8, pp. 713–732, April 2011.

[31] X. Wang and W. Freitas, "Impact of positive-feedback anti-islanding methods on small-signal stability of inverter-based distributed generation," *IEEE Trans. Energy Conversion*, vol. 23, no. 3, pp. 923–931, Sept. 2008.

[32] M. H. Nazari and M. Ilic, "Technical challenges in modernizing distribution electric power systems with large number of distributed generators," in *Proc. IEEE PowerTech*, 2009, pp. 1–8.

[33] W. Freitas, A. Morelato, W. Xu, and F. Sato, "Impacts of ac generators and DSTATCOM devices on the dynamic performance of distribution systems," *IEEE Trans. Power Delivery*, vol. 20, no. 2, pp. 1493–1501, April 2005.

[34] V. Akhmatov, "Analysis of dynamic behaviour of electric power systems with large amount of wind power," Ph.D. dissertation, Technical University of Denmark, Lyngby, Denmark, 2003.

[35] A. P. Grilo, A. d. A. Mota, L. T. M. Mota, and W. Freitas, "An analytical method for analysis of large-disturbance stability of induction generators," *IEEE Trans. Power Systems*, vol. 22, no. 4, pp. 1861–1869, Nov. 2007.

[36] A. Narang, "Impact of large scale distributed generation penetration on power system stability," Natural Resources Canada, CETC-Varennes 2006-089 (TR), CanmetENERGY, Tech. Rep., 2006.

[37] L. Le-Thanh, T. Tran-Quoc, O. Devaux, O. Chilard, C. Kieny, N. Hadjsaid, and J. Sabonnadiere, "Hybrid methods for transient stability assessment and preventive control for distributed generators," in *Proc. IEEE Power and Energy Society General Meeting- Conversion and Delivery of Electrical Energy in the 21st Century*, 2009, pp. 1–6.

[38] I. Xyngi, A. Ishchenko, M. Popov, and L. van der Sluis, "Transient stability analysis of a distribution network with distributed generators," *IEEE Trans. Power Systems*, vol. 24, no. 2, pp. 1102–1104, May 2009.

[39] F. Katiraei, "Dynamic analysis and control of distributed energy resources in a microgrid," Ph.D. dissertation, University of Toronto, Toronto, Canada, 2005.

[40] G. Venkataramanan and M. Illindala, "Small signal dynamics of inverter interfaced distributed generation in a chain-microgrid," in *Proc. IEEE Power Engineering Society General Meeting*, 2007, pp. 1–6.

[41] A. Ishchenko, "Dynamics and stability of distribution networks with dispersed generation," Ph.D. dissertation, Eindhoven University of Technology, Eindhoven, Netherlands, 2008.

[42] G. Quinonez-Varela and A. Cruden, "Development of a small-scale generator set model for local network voltage and frequency stability analysis," *IEEE Trans. Energy Conversion*, vol. 22, no. 2, pp. 368–375, Jun. 2007.

[43] Z. Xu, M. Togeby, and J. Ostergaard, "Demand as frequency controlled reserve - final report of the pso project," Technical University of Denmark, Tech. Rep., 2008.

[44] O. Anaya-Lara, F. M. Hughes, N. Jenkins, and G. Strbac, "Contribution of DFIG-based wind farms to power system short-term frequency regulation," *Proc. IEE Generation, Transmission and Distribution*, vol. 153, no. 2, pp. 164–170, March 2006.

[45] Y. Chen, Z. Xu, and J. Ostergaard, "Control mechanism and security region for intentional islanding transition," in *Proc. IEEE Power and Energy Society General Meeting*, 2009, pp. 1–6.

[46] J. W. Black and M. Ilic, "Demand-based frequency control for distributed generation," in *Proc. IEEE Power Engineering Society Summer Meeting*, 2002, pp. 427–432.

[47] R. H. Lasseter, "Microgrids and distributed generation," *Journal of Energy Engineering*, vol. 133, no. 3, pp. 144–149, Sept. 2007.

[48] F. Katiraei and M. R. Iravani, "Power management strategies for a microgrid with multiple distributed generation units," *IEEE Trans. Power Systems*, vol. 21, no. 4, pp. 1821–1831, Nov. 2006.

[49] J. A. P. Lopes, C. L. Moreira, and A. G. Madureira, "Defining control strategies for microgrids islanded operation," *IEEE Trans. Power Systems*, vol. 21, no. 2, pp. 916–924, May 2006.

[50] Y. Mohamed, "New control algorithms for the distributed generation interface in grid-connected and micro-grid system," Ph.D. dissertation, University of Waterloo, Waterloo, Canada, 2008.

[51] D. Olivares, "An energy management system for isolated microgrids considering uncertainty," Ph.D. dissertation, University of Waterloo, Waterloo, Canada, 2014.

[52] J. M. Guerrero, L. G. de Vicuna, J. Matas, M. Castilla, and J. Miret, "A wireless controller to enhance dynamic performance of parallel inverters in distributed generation systems," *IEEE Trans. Power Electronics*, vol. 19, no. 5, pp. 1205–1213, Sept. 2004.

[53] S. J. Chiang, C. Y. Yen, and K. Chang, "A multimodule parallelable series-connected PWM voltage regulator," *IEEE Trans. Industrial Electronics*, vol. 48, no. 3, pp. 506–516, Jun. 2001.

[54] M. D. Ilic and S. X. Liu, *Hierarchical Power Systems Control.* Londan, UK: Springer, 1996.

[55] J. C. Vasquez, J. M. Guerrero, J. Miret, M. Castilla, and L. de Vicuna, "Hierarchical control of intelligent microgrids," *IEEE Industrial Electronics Magazine*, vol. 4, no. 4, pp. 23–29, Jun. 2010.

[56] A. Mehrizi-Sani and R. Iravani, "Potential-function based control of a microgrid in islanded and grid-connected modes," *IEEE Trans. Power Systems*, vol. 25, no. 4, pp. 1883–1891, Nov. 2010.

[57] A. Yazdani and R. Iravani, "A unified dynamic model and control for the voltage-sourced converter under unbalanced grid conditions," *IEEE Trans. Power Delivery*, vol. 21, no. 3, pp. 1620–1629, Jul. 2006.

[58] E. Pouresmaeil, C. Miguel-Espinar, M. Massot-Campos, D. Montesinos-Miracle, and O. Gomis-Bellmunt, "A control technique for integration of DG units to the electrical networks," *IEEE Trans. Industrial Electronics*, vol. 60, no. 7, pp. 2881–2893, Jul. 2013.

[59] A. Junyent-Ferre, O. Gomis-Bellmunt, T. Green, and D. Soto-Sanchez, "Current control reference calculation issues for the operation of renewable source grid interface VSCs under unbalanced voltage sags," *IEEE Trans. Power Electronics*, vol. 26, no. 12, pp. 3744–3753, Dec. 2011.

[60] X.-P. Zhang, P. Ju, and E. Handschin, "Continuation three-phase power flow: A tool for voltage stability analysis of unbalanced three-phase power systems," *IEEE Trans. Power Systems*, vol. 20, no. 3, pp. 1320–1329, Aug. 2005.

[61] G. Carpinelli, D. Lauria, and P. Varilone, "Voltage stability analysis in unbalanced power systems by optimal power flow," *Proc. IEE Generation, Transmission and Distribution*, vol. 153, no. 3, pp. 261–268, May 2006.

[62] R. H. Salim and R. A. Ramos, "A model-based approach for small-signal stability assessment of unbalanced power systems," *IEEE Trans. Power Systems*, vol. 27, no. 4, pp. 1184–1190, Nov. 2012.

[63] ——, "A framework for analyzing the small-signal dynamic performance of unbalanced power systems," in *Proc. IEEE PES General Meeting*, 2011, pp. 1–8.

[64] R. G. Harley, E. B. Makram, and E. G. Duran, "The effects of unbalanced networks and unbalanced faults on induction motor transient stability," *IEEE Trans. Energy Conversion*, vol. 3, no. 2, pp. 398–403, 1988.

[65] E. B. Makram, V. O. Zambrano, R. G. Harley, and J. C. Balda, "Three-phase modeling for transient stability of large scale unbalanced distribution systems," *IEEE Trans. Power Systems*, vol. 4, no. 2, pp. 487–493, 1989.

[66] R. G. Harley, E. B. Makram, and E. G. Duran, "The effects of unbalanced networks on synchronous and asynchronous machine transient stability," *Elect. Power Syst. Res.*, vol. 13, no. 2, pp. 119–127, 1987.

[67] E. B. Makram, V. O. Zambrano, and R. G. Harley, "Synchronous generator stability due to multiple faults on unbalanced power systems," *Elect. Power Syst. Res.*, vol. 15, no. 1, pp. 31–39, 1988.

[68] P. Ledesma and J. Usaola, "Doubly fed induction generator model for transient stability analysis," *IEEE Trans. Energy Conversion*, vol. 20, no. 2, pp. 388–397, Jun. 2005.

[69] Y. Lei, A. Mullane, G. Lightbody, and R. Yacamini, "Modeling of the wind turbine with a doubly fed induction generator for grid integration studies," *IEEE Trans. Energy Conversion*, vol. 21, no. 1, pp. 257–264, Mar. 2006.

[70] D. Xiang, L. Ran, P. Tavner, and S. Yang, "Control of a doubly fed induction generator in a wind turbine during grid fault ride through," *IEEE Trans. Energy Conversion*, vol. 21, no. 3, pp. 652–662, Sept. 2006.

[71] J. Morren and S. de Haan, "Ride through of wind turbines with doubly fed induction generator during a voltage dip," *IEEE Trans. Energy Conversion*, vol. 20, no. 2, pp. 435–441, Jun. 2008.

[72] ——, "Short-circuit current of wind turbines with doubly fed induction generator," *IEEE Trans. Energy Conversion*, vol. 22, no. 1, pp. 174–180, March 2007.

[73] O. Gomis-Bellmunt, A. Junyent-Ferre, A. Sumper, and J. Bergas-Jan, "Ride-through control of a doubly fed induction generator under unbalanced voltage sags," *IEEE Trans. Energy Conversion*, vol. 23, no. 4, pp. 1036–1045, Dec. 2008.

[74] L. Xu and Y. Wang, "Dynamic modeling and control of DFIG-based wind turbines under unbalanced network conditions," *IEEE Trans. Power Systems*, vol. 22, no. 1, pp. 1320–1329, Feb. 2007.

[75] Y. Zhou, P. Bauer, J. Ferreira, and J. Pierik, "Operation of grid-connected DFIG under unbalanced grid voltage condition," *IEEE Trans. Energy Conversion*, vol. 24, no. 1, pp. 240–246, March 2009.

[76] T. K. A. Brekken and N. Mohan, "Control of a doubly fed induction wind generator under unbalanced grid voltage conditions," *IEEE Trans. Energy Conversion*, vol. 22, no. 1, pp. 129–135, March 2007.

[77] R. Pena, R. Cardenas, E. Escobar, J. Clare, and P. Wheeler, "Control system for unbalanced operation of stand-alone doubly fed induction generators," *IEEE Trans. Energy Conversion*, vol. 22, no. 2, pp. 544–545, Jun. 2007.

[78] L. Yang, Z. Xu, J. stergaard, Z. Y. Dong, K. Wong, and X. Ma, "Oscillatory stability and eigenvalue sensitivity analysis of a DFIG wind turbine system," *IEEE Trans. Energy Conversion*, vol. 26, no. 1, pp. 328–339, March 2011.

[79] P. Kundur, J. Paserba, V. Ajjarapu, G. Andersson, A. Bose, C. Canizares, N. Hatziargyriou, D. Hill, A. Stankovic, C. Taylor, T. V. Cutsem, and V.Vittal, "Definition and

classification of power system stability," *IEEE Trans. Power Systems*, vol. 19, no. 3, pp. 1387–1401, Aug. 2004.

[80] P. Kundur, *Power System Stability and Control*. New York: McGraw-Hill, 1994.

[81] V. Ajjarapu and B. Lee, "Bifurcation theory and its application to nonlinear dynamical phenomena in an electrical power system," *IEEE Trans. Power Delivery*, vol. 17, no. 1, pp. 424–431, Feb. 1992.

[82] C. Canizares and S. Hranilovic, "Transcritical and hopf bifurcation in ac/dc systems," in *Proc. of Bulk Power System Voltage Phenomena-III Seminar*, Aug. 1994, pp. 105–114.

[83] S. Kodsi, "Accounting for the effect of power system controllers and stability on power dispatch and electricity market prices," Ph.D. dissertation, University of Waterloo, Waterloo, Canada, 2005.

[84] C. Canizares(ed.), "Voltage stability assessment : concepts, practices and tools," in *Special Publication of IEEE Power System Stability Subcommittee*, 2002.

[85] V. Ajjarapu and C. Christy, "The continuation power flow: A tool for steady state voltage stability analysis," *IEEE Trans. Power Delivery*, vol. 1, no. 1, pp. 416–423, Feb. 1992.

[86] H. Ghasemi, "On-line monitoring and oscillatory stability margin prediction in power systems based on system identification," Ph.D. dissertation, University of Waterloo, Waterloo, Canada, 2006.

[87] K. Steiglitz and L. E. McBride, "A technique for the identification of linear systems," *IEEE Trans. Automatic Control*, vol. AC-10, pp. 461–464, 1965.

[88] K. Steiglitz and L. McBride, "A technique for the identification of linear systems," *IEEE Trans. Automatic Control*, vol. 10, no. 4, pp. 461–464, Oct. 1965.

[89] F. Milano, *An open source power system analysis toolbox. [Online]. http://www.power.uwaterloo.ca/ fmilano/psat.htm.*

[90] "*PSCAD/EMTDC ver 4.2 Users Manual*", Manitoba HVDC Research Centre Inc., Winnipeg, Manitoba, Canada.

[91] A. G. Exposito, A. J. Conejo, and C. Canizares, *Electric Energy Systems, Analysis and Operation*. Boca Raton: CRC Press, 2009.

[92] "Impact of increasing contribution of dispersed generation on the power system," CIGRE Working Group 37.23, Tech. Rep., Feb. 1999.

[93] "Interconnecting distributed resources with electric power system," *IEEE Std 1547*, 2003.

[94] Y. Zhu and K. Tomsovic, "Development of models for analyzing the load-following performance of microturbines and fuel cells," *Electric Power Systems Research*, vol. 62, no. 1, pp. 1–11, May 2002.

[95] W. I. Rowen, "Simplified mathematical representations of heavy duty gas turbines," *ASME Trans. Journal of Engineering for Power*, vol. 105, no. 4, pp. 865–869, Oct. 1983.

[96] F. Jurado and J. R. Saenz, "Adaptive control of a fuel cell-microturbine hybrid power plant," *IEEE Trans. on Energy Conversion*, vol. 18, no. 2, pp. 342–347, Jun. 2003.

[97] Working Group on Prime Mover and Energy Supply Models for System Dynamic Performance Studies, "Dynamic models for combined cycle plants in power system studies," Tech. Rep. 3, Aug. 1993.

[98] L. N. Hannet and A. Khan, "Combustion turbine dynamic model validation from tests," *IEEE Trans. on Power Systems*, vol. 8, no. 1, pp. 152–158, Feb. 1993.

[99] K. E. Yeager and J. R. Willis, "Modeling of emergency diesel generators in the 800 megawatt nuclear power plant," *IEEE Trans. on Energy Conversion*, vol. 8, no. 3, pp. 433–441, Sept. 1993.

[100] A. D. Hansen and L. H. Hansen, "Wind turbine concept market penetration over 10 years (1995-2004)," *Wind Energy*, vol. 10, no. 1, pp. 81–97, Jan. 2007.

[101] M. D. Lukas, K. Y. Lee, and H. Ghezel-Ayagh, "Development of a stack simulation model for control study on direct reforming molten carbonate fuel cell power plant," *IEEE Trans. on Energy Conversion*, vol. 14, no. 4, pp. 1651–1657, Dec. 1999.

[102] R. Anahara, S. Yokokawa, and M. Sakurai, "Present status and future prospects for fuel cell power systems," in *Proc. IEEE*, vol. 81, 1993, pp. 399–408.

[103] V. Knyazkin, L. Soder, and C. Canizares, "Control challenges of fuel cell-driven distributed generation," in *Proc. IEEE PowerTech*, vol. 2, 2003.

[104] W. Xiao, W. G. Dunford, P. R. Palmer, and A. Capel, "Regulation of photovoltaic voltage," *IEEE Trans. on Industrial Electronics*, vol. 54, no. 3, pp. 1365–1374, Jun. 2007.

[105] B. Tamimi, C. Canizares, and K. Bhattacharya, "Modeling and performance analysis of large solar photo-voltaic generation on voltage stability and inter-area oscillations," in *Proc. IEEE Power and Energy Society General Meeting*, pp. 1–6.

[106] L. M. Hajagos and G. R. Berube, "Utility experience with gas turbine testing and modeling," in *Proc. IEEE Power and Energy Society Winter Meeting*, 2001, pp. 671–677.

[107] M. Ceraolo, "New dynamical models of leadacid batteries," *IEEE Trans. on Power Systems*, vol. 15, no. 14, pp. 1184–1190, Nov. 2000.

[108] S. Barsali and M. Ceraolo, "Dynamical models of leadacid batteries implementation issues," *IEEE Trans. on Energy Conversion*, vol. 17, no. 1, p. 1623, March 2002.

[109] S. Li, K. Tomsovic, and T. Hiyama, "Load following functions using distributed energy resources," in *Proc. IEEE PES Summer Meeting Meeting*, 2000, pp. 1756–1761.

[110] K. Rudion, A. Orths, Z. Styczynski, and K. Strunz, "Design of benchmark of medium voltage distribution network for investigation of DG integration," in *Proc. IEEE Power and Energy Society General Meeting*, 2006, pp. 1–6.

[111] R. H. Salim and R. A. Ramos, "Analyzing the effect of the type of terminal voltage feedback on the small signal dynamic performance of synchronous generators," in *Proc. IREP Symp. Bulk Power System Dynamics and Control*, Aug. 2010.

[112] W. H. Kersting, *Distribution System Modeling and Analysis*. Boca Raton: CRC Press, 2006.

[113] M. Z. Kamh and R. Iravani, "Unbalanced model and power-flow analysis of micro-grids and active distribution systems," *IEEE Trans. Power Delivery*, vol. 25, no. 4, pp. 2851–2858, Oct. 2010.

[114] *MATLAB*, The MathWorks Inc.

[115] R. H. Salim, R. A. Ramos, and N. G. Bretas, "Analysis of the small signal dynamic performance of synchronous generators under unbalanced operating conditions," in *Proc. IEEE PES General Meeting*, 2010.

[116] S. Granville, P. Lino, F. Ralston, L. A. Barroso, and M. Pereira, "Recent advances of sugarcane biomass cogeneration in brazil," in *Proc. IEEE PES General Meeting*, 2009, pp. 1–5.

[117] M. Arriaga, C. A. Canizares, and M. Kazerani, "Renewable energy alternatives for remote communities in northern ontario, canada," *IEEE Trans. Sustainable Energy*, vol. 4, no. 3, pp. 661–670, Jul. 2013.

[118] N. Mohan, T. M. Undeland, and W. Robbins, *Power electronics: converters, applications, and design*. New York: Wiley, 2007.

[119] S. Muller, M. Deicke, and R. W. D. Doncker, "Doubly fed induction generator systems for wind turbines," *IEEE Ind. Appl. Mag.*, vol. 8, no. 3, pp. 26–33, Jun. 2002.

[120] M. Yamamoto and O. Motoyoshi, "Active and reactive power control for doubly-fed wound rotor induction generator," *IEEE Trans. Power Electronics*, vol. 6, no. 4, pp. 624–629, Oct. 1991.

[121] F. Katiraei, M. Iravani, and P. Lehn, "Small-signal dynamic model of a micro-grid including conventional and electronically interfaced distributed resources," *Proc. IEE Generation, Transmission and Distribution*, vol. 1, no. 3, pp. 369–378, May 2007.